NASA SP-199

CASE FILE
COPY

LECTURES IN HIGH-ENERGY ASTROPHYSICS

NATIONAL AERONAUTICS AND SPACE ADMINISTRATION

Cover photo: Milky Way from Aquila to Carina in the infrared.
(Courtesy A. D. Code and T. E. Houck)

NASA SP-199

LECTURES IN HIGH-ENERGY ASTROPHYSICS

EDITED BY
H. ÖGELMAN AND J. R. WAYLAND

PREPARED BY
NASA GODDARD SPACE FLIGHT CENTER

Scientific and Technical Information Division
OFFICE OF TECHNOLOGY UTILIZATION 1969
NATIONAL AERONAUTICS AND SPACE ADMINISTRATION
Washington, D.C.

For sale by the Clearinghouse for Federal Scientific and Technical Information
Springfield, Virginia 22151 – Price $3.00

FOREWORD

The Department of Physics and Astronomy of the University of Maryland and NASA Goddard Space Flight Center jointly organized a lecture series comprising an introductory course in high-energy astrophysics at the graduate level which was presented at the University of Maryland in the summer of 1968. Throughout the lectures, notes were distributed to the students to serve as basic text material for the course. This publication is an expanded and edited version of those notes.

H. Ögelman
Goddard Space Flight Center

J. R. Wayland, Jr.
University of Maryland

Page Intentionally Left Blank

CONTENTS

Page

I. Current Problems of High-Energy Astrophysics
H. Ögelman 1

II. Origin, Composition, and Propagation of the Nuclear Component of Cosmic Rays
C. Fichtel 23

III. Cosmic Ray Electrons and Related Astrophysical Problems
R. Ramaty (Notes taken by M. L. Goldstein) 35

IV. Cosmic Ray Photons
E. Boldt 49

V. Plasma Aspects of Cosmic Rays
D. Wentzel (Notes taken by D. Hall) 85

VI. Relativistic Stochastic Processes
J. R. Wayland 93

VII. Propagation of Solar Cosmic Rays in the Interplanetary Magnetic Field
E. C. Roelof 111

VIII. Interplanetary Medium: Dust, Gas, and Magnetic Fields
L. W. Bandermann 137

I. CURRENT PROBLEMS OF HIGH-ENERGY ASTROPHYSICS

H. Ögelman
NASA Goddard Space Flight Center
Greenbelt, Maryland

INTRODUCTION

If we drop the prefix "astro," high-energy physics may be defined as that branch of physics concerned with the interactions between particles having relative energies in excess of a few hundred MeV, the energy threshold at which the familiar particles of nuclear physics, such as the proton and neutron, start yielding pions, kaons, etc. Since the fundamental interactions that produce these elementary particles seem to be distinct from those observed at lower energies, and since the well-controlled laboratory environment makes it possible to focus attention on a single process, such a categorization is justified; it aids the scientists who can best understand a phenomenon by restricting the scope of their interests.

In astrophysics, however, where the goal is to describe the physics of the universe, the crucial advantage of controlled experimentation is not available. In order to increase our understanding of astrophysics, we must employ information from all available channels; it would be harmful to restrict ourselves to a particular energy band or fundamental process. In defense of specialization, however, it is reasonable to assume that certain physical processes will achieve prominence in certain regions of the universe. Concentrating one's attention on a particular type of process and then relating one's findings to those of colleagues specializing in other types of process can therefore be expected to provide fruitful results.

The field of high-energy astrophysics, consequently, covers processes involving energies of 10^3 eV to 10^{20} eV—17 decades of energy—as compared to the 4 decades of energy covered by present-day high-energy physics (10^7 to 10^{11} eV).

Historically, high-energy astrophysics has developed from cosmic-ray physics. Cosmic rays were discovered over 60 years ago by researchers studying the discharge of carefully insulated electroscopes. When Hess flew an electroscope in a balloon in 1911 and showed that

the discharge rate increased as a function of altitude, it became evident that the cause of the discharge was extraterrestrial. During the past 50 years, extensive work in the field has revealed greatly the astrophysical significance of cosmic rays. The secondaries of cosmic rays were actually the starting point of elementary particle physics; particles such as muons, positrons, pions, kaons, and some hyperons were first discovered in cosmic rays.

With the advances in high-energy accelerators during the past few decades, the aspirations of cosmic-ray studies have shifted from elementary particle physics to astrophysics. However, above 10^{11} eV, cosmic rays are still the only accessible high-energy beam; they are, therefore, still contributing to the field of high-energy physics, in particular to the search for theoretically predicted particles such as quarks, intermediate bosons, and monopoles.

Cosmic-ray energies currently under investigation in high-energy astrophysics range from 10^8 to 10^{20} eV. The universe, however, is a complicated laboratory system in which the beam, the target, and the secondaries produced in the reactions do not always exhibit the patterns with which we are familiar in the laboratory. For example, a seemingly insignificant 10^{-3} eV microwave photon is as potent to a 10^{19} eV cosmic ray proton as a 300 MeV photon produced by an accelerator is to a proton in a hydrogen bubble chamber. In other cases, the cosmic target may be the weak magnetic fields of the galaxy, where an incident electron of 10^{10} eV could, by interacting with the field, produce a radio photon of 10^{-7} eV. The information relevant to the high-energy phenomena could cover the energy interval from 10^{-7} to 10^{20} eV—26 decades of energy!

What types of channels would be able to link us to the rest of the universe and to convey valuable information? Among the discovered elementary particles, we must look for stable ones that will not decay in flight. If a particle has a natural lifetime τ, it can carry information up to a distance R, given by

$$R \simeq \gamma c \tau ,$$

where γ is the Lorentz factor of the particle $\left[1 - (v/c)^2\right]^{-1/2}$, v is the particle velocity, and c is the velocity of light. For the extreme case of 10^{20} eV protons, which is on the verge of present-day detection

schemes, γ is 10^{11}. Assuming that this is a practical limitation on currently observable values, and that we are interested in reaching the limits of our galaxy (i.e., $R \simeq 10^{22}$ cm), this gives

$$\tau \geq 3 \text{ sec} .$$

Among the measured elementary particle lifetimes, the value falls between 10^3 sec for the neutron and 2×10^{-6} sec for the muon, justifying the previous crude argument. Effectively then, we can eliminate the mesons, hyperons, and muons as a part of the incident primary radiation because of their short lifetimes. The rest of the possible primaries are the photon, electron, positron, neutrinos, proton, and, to a certain extent, the neutron. Table 1 summarizes various relevant parameters of these particles.

Table 1. Summary of Relevant Parameters of Photons, Leptons, and Nucleons

Particle	Symbol	Spin	Rest mass (MeV)	Mean life (sec)	Decay mode
Photons	γ	1	0	∞	---
Leptons	e^-, e^+	1/2	0.51	∞	---
	ν_e, $\bar{\nu}_e$	1/2	0	∞	---
	ν_μ, $\bar{\nu}_\mu$	1/2	0	∞	---
Nucleons	p	1/2	938.2	∞	---
	n	1/2	939.5	1000	$n \rightarrow e^- + \bar{\nu}_e + p$

Besides these elementary particles, any stable or quasi-stable (in the sense of the neutron) combination of elementary particles, such as alpha particles or heavy nuclei, should be observable in the primary beam of cosmic rays. Further coalescence of particles to atoms, atoms to molecules, molecules to grains, and so on, is possible and, if spared by destructive collisions, these objects may also be present among the primaries.

Another interesting possible source of information could be the graviton, the stable quantum of the gravitational field. Although no graviton has been observed in a quantum state, its manifestations in the form of gravitational force field are well known. Pioneering astrophysical research in the field of gravitational waves is presently in process (References 1 and 2).

A review of existing information on primary cosmic radiation and a discussion of the general features of our galaxy and the metagalaxy follow.

PRIMARY COSMIC RAYS

The purpose of measuring the primary cosmic-ray flux is to discover the intensity I of each component (proton, electron, photon, etc.) of the flux as a function of energy E, direction θ, ϕ, time t, distance R, and spin $\vec{\sigma}$, (commonly known as polarization). Unfortunately, technological limitations do not allow measurement of all of these quantities. The difficulties arise mainly for the following reasons:

1. The earth's atmosphere is many interaction lengths for the nucleonic component (13 mean free pathlengths for protons) and the high-energy electromagnetic component (25 mean free pathlengths at high energies). This fact forces experimenters to construct apparatus that can be exposed at the top of the atmosphere via balloon, rocket, or satellite, thus limiting the size. These inconveniences currently limit the possible flux measurements to values exceeding 10^{-8} particles per cm^2-sec-sr.

2. The very low flux of certain components relative to the proton component makes it difficult to distinguish them from the secondaries produced in the atmosphere or the apparatus.

3. The solar wind, with its complicated magnetic fields, affects those charged primaries having rigidities below a few GeV and prevents observation of the true galactic distribution.

Despite these difficulties, a wealth of data about primary cosmic rays has been acquired. Some of these data are summarized below.

Protons and Nuclei

The most abundant component of cosmic rays is the proton. Besides the protons, cosmic rays contain 6 percent helium nuclei and 1 percent higher Z nucleons. The direct composition measurements cover the energy range of 10^8 eV per nucleon to about 10^{10} eV per nucleon. Table 1 of Chapter II summarizes the relative intensities of the various cosmic-ray components and gives cosmic abundance estimates. The excess of heavy elements in cosmic rays relative to cosmic abundances is generally interpreted as being caused by accelerating regions, and the excess of light elements as being caused by fragmentation of heavier elements during their passage through ambient gas.

The spectral form of the incident cosmic radiation can be expressed as a power law (Reference 3). In the energy range 10^{10} eV < E < 10^{15} eV, it takes the form

$$I(>E) = KE^{-(\gamma-1)}$$

$$= 10^{-4} \left(\frac{10^{14}}{E}\right)^{1.6} \Big/ \mathrm{m^2\text{-}sec\text{-}sr} ,$$

where E is measured in Ev. In the range 10^{15} eV < E < 10^{16}eV,

$$I(>E) = 2 \times 10^{-10} \left(\frac{10^{17}}{E}\right)^{2.2} \Big/ \mathrm{m^2\text{-}sec\text{-}sr} ,$$

and, for E > 10^{16} eV,

$$I(>E) = 4 \times 10^{-16} \left(\frac{10^{20}}{E}\right)^{1.6} \Big/ \mathrm{m^2\text{-}sec\text{-}sr} ,$$

the total number of particles being 1500/m^2-sec-sr. The primary spectrum is shown in Figure 1. The breaks occurring in the spectrum at 10^{15} and 10^{18} eV are generally interpreted as being caused by the escape of the galactic component and the penetration of the extragalactic component, respectively (Reference 4).

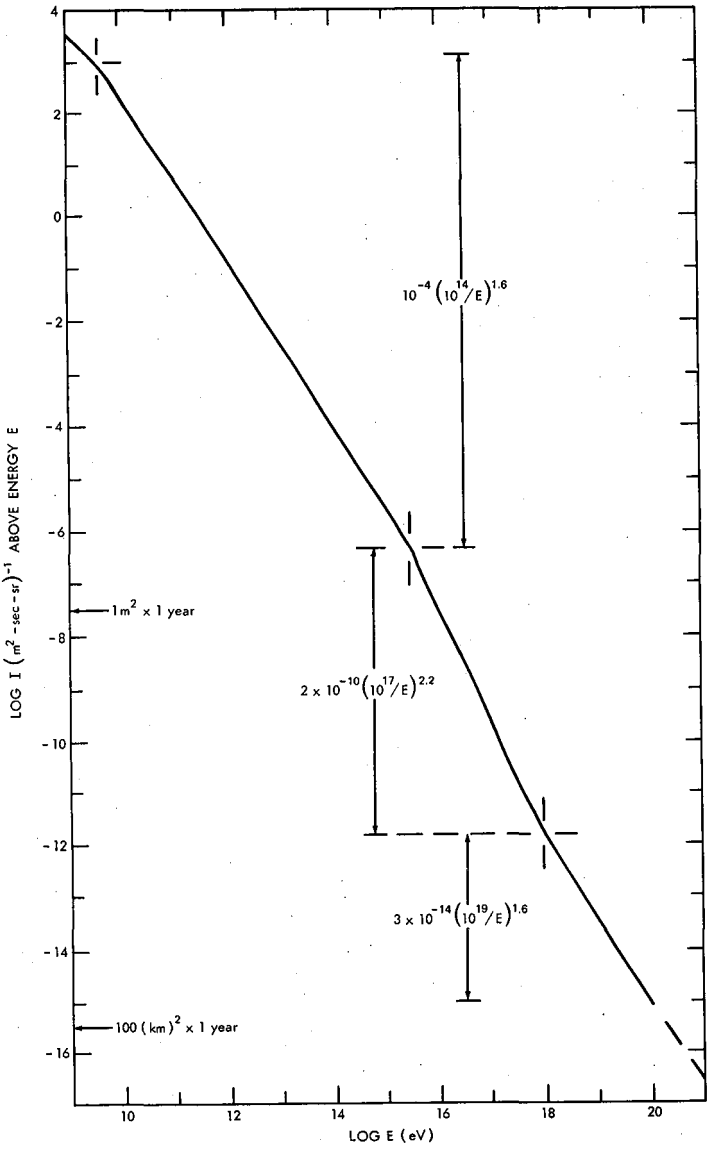

Figure 1—Integral primary energy spectrum (taken from Figure 1 of Reference 4).

Because of the sharp drop in intensity as a function of energy, direct measurements have been carried out only to 10^{14} eV. Above this value, extensive air showers have provided most of the information (Reference 5). At these energies, the atmosphere becomes a part of the detector system and makes it feasible to extend the energy measurements out to 10^{20} eV. Figure 2 shows schematically the development of an extensive air shower in the atmosphere. Typically, the incident nucleon interacts with air molecules and produces pions which in turn decay into electromagnetic channels via the $\pi^{\pm} \rightarrow \mu^{\pm} \rightarrow e^{\pm}$ or the $\pi^{\circ} \rightarrow 2\gamma$ processes. Progressively, as the average energy per particle decreases, their numbers increase, reach a maximum, and then die out. During this development, the particles form a coherent front recognizable by detectors placed on the ground.

Two advantages of the atmosphere as a detector are evident. One is its extensive depth, which allows even 10^{20} eV showers to develop well within the atmosphere; the other is its low density, which allows the spreading of the shower particles, enabling a small number of detectors to cover effectively a large area. A primary proton of 10^{19} eV produces an easily detectable flux of secondaries 1 km from its impact point. Since a single detector would not be able to distinguish the difference between a large shower far away and a smaller one

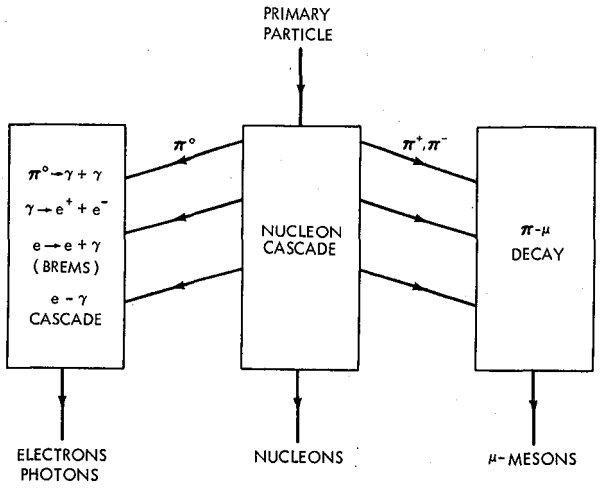

Figure 2–Schematic diagram of the propagation of an extensive air shower (Wolfendale, 1963).

close by, the technique used is to distribute a number of detectors over an area of 10 or more square kilometers and look for coincident pulses. Moreover, the relative timing of the pulses in the shower front allows the determination of the primary direction. The density of particles at various detectors allows estimation of the total number of secondaries N which can then be related to the energy of the primary particle by theoretical arguments.

The penalty paid for the convenience of air-shower detection is the loss of some information regarding the nature of the primary. Still, some signature of the primary is retained. For example, showers with relatively small numbers of muons could be attributed to an incident electron or photon (References 7 and 8) since, in such a shower, electromagnetic cascade development would be enhanced relative to nuclear cascade development. A shower initiated by a multi-nucleon particle might show separated peaks of electron density near its core because of individual showers developed by each nucleon (Reference 9).

The results of air-shower measurements have indicated the plausibility of a significant flux of protons and high-Z primaries of around 10^{14} to 10^{15} eV total energies; however, the interpretation of the data is complex, and the results are not well confirmed.

The isotropy of cosmic rays in the energy ranges discussed has been remarkable. The usual definition of isotropy δ is

$$\delta = \frac{I_{max} - I_{min}}{I_{max} + I_{min}} .$$

The conservative upper limits of δ at various energies E are (Reference 10):

$$\delta \leq 0.1\% , \qquad E < 10^{14} \text{ eV} ;$$

$$\delta \leq 1\% , \qquad E \sim 10^{16} \text{ eV} ;$$

$$\delta \leq 3\% , \qquad E \sim 10^{17} \text{ eV} .$$

However, there are some indications that around 10^{12} eV there is a small anisotropy, of fractions of a percent in amplitude, from the direction of the galactic center. When one considers that, in the weak magnetic fields of about 3×10^{-6} gauss present in our galaxy, the radius of curvature of a primary with energy 10^{19} eV is the same order of magnitude as the size of our galaxy, the difficulty of acceleration and confining these particles within our galaxy becomes understandable.

Another topic under investigation is the long-time scale variation of cosmic radiation. The basic measurements have been conducted on meteorites which have been traveling in space for long periods of time. If one measures the induced radioactivity for different elements having various decay lifetimes, it is possible to interpret the concentration as induced by cosmic-ray bombardment. Measurements of decay half-lives from 12.5 years to 10^9 years indicate that cosmic rays have been bombarding the solar system at about their present rate for over a billion years.

For a more complete discussion of this whole area, see Chapter II, "Origin, Composition, and Propagation of the Nuclear Component of Cosmic Rays," by C. Fichtel.

Electrons

Significant measurements have been made during the past several years, resulting in the determination of the primary electron spectrum in the energy range 10^6 to 10^{11} eV (References 11, 12, and 13). It is generally agreed that the flux below a few GeV is dominated by solar effects. The higher energy flux, believed to be galactic in origin, can be represented by a power law:

$$I(E) = 10^2 \left(\frac{E}{10^9}\right)^{-2.3 \pm 0.2} \text{ electrons m}^{-2}\text{-sec}^{-1}\text{-sr}^{-1}\text{-GeV}^{-1} .$$

Figure 3 shows the measured spectrum on top of the atmosphere.

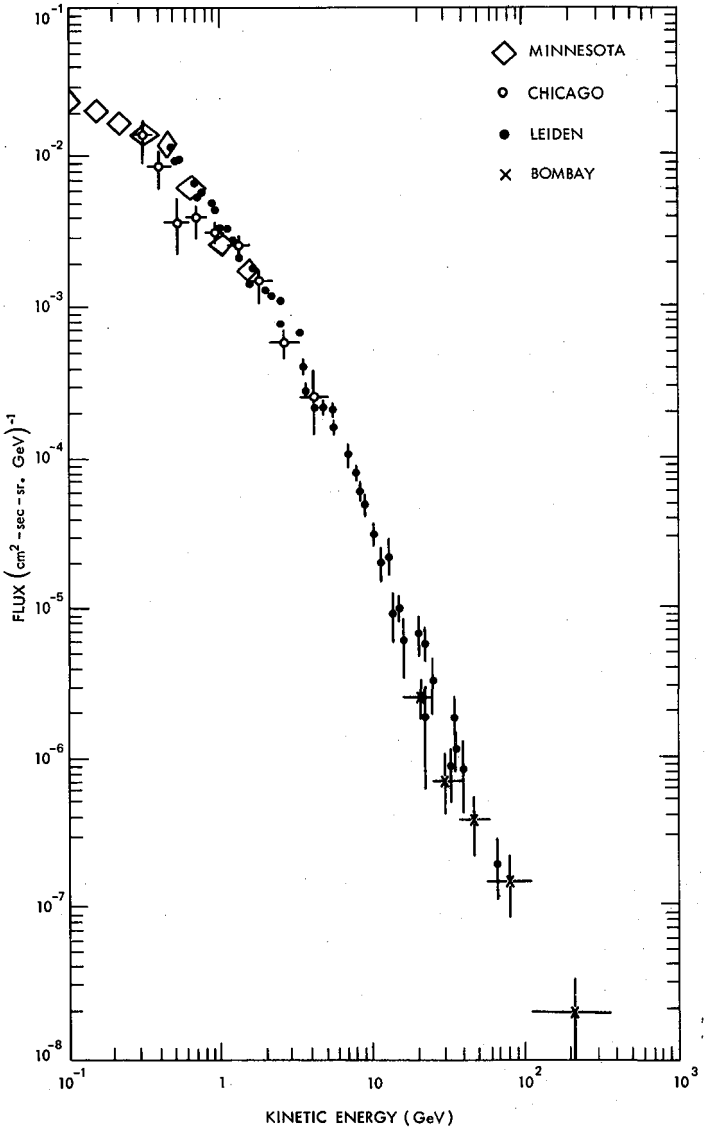

Figure 3–The differential energy spectrum of primary electrons. Results of experiments are indicated; Minnesota (Webber and Chotkowski 1966), Chicago (L'Heureux 1968); Leiden (Blecker et al. 1967); and Bombay (Daniel and Stephens 1966). Taken from Scheepmaher and Tanaka, 1968.

The electron-to-positron ratios have also been measured at various energies; Table 2 (from Reference 14) summarizes these measurements.

Table 2. Summary of Measurements of Electron-to-Positron Ratios

Electron energy (eV)	$e^+/(e^+ + e^-)$
1.75×10^8	0.43 ± 0.21
6×10^8	0.30 ± 0.14
2×10^9	0.33 ± 0.16

Independent measurements on the electron spectrum can be made from radio astronomy data by interpreting the galactic background noise as being caused by electron synchrotron radiation. Presently, a consistent picture is emerging, yielding information on the lifetimes of these electrons in the galaxy and on their production mechanisms. For a more detailed treatment of this subject, see Chapter III: "Cosmic-Ray Electrons and Related Astrophysical Problems," by R. Ramaty.

Photons

In contrast to the charged particles, which are deflected by interstellar magnetic fields, photons travel in straight lines and can thus be traced to their origin. The visible photons are very anisotropic, exhibiting their points of origin (stars, nebulae, galaxies, etc.). The radio-frequency photons exhibit similar anisotrophy. Since the atmosphere is transparent to electromagnetic radiation between 10^{-8} and 10^{-3} eV and around 1 eV, ground-based astronomy, both optical and radio, has yielded much information. There are several outstanding features of this low-energy photon information that are related to high-energy astrophysics. The measurement of the anisotropic radio waves and their interpretation as synchrotron radiation emitted by high-energy electrons in the weak magnetic fields of the sources has been one of the most significant achievements

of high-energy astrophysics. The rate of energy emission by an electron of energy E in a magnetic field H is given by

$$\frac{dE}{dt} = -3.8 \times 10^{-6} H^2 \text{(gauss)} E^2 \text{(GeV)} 10^9 \text{ eV/sec} ,$$

and the frequency of emission is strongly peaked around:

$$\nu_c \simeq 1.6 \times 10^{13} H(\text{gauss}) E^2 \text{(GeV)} \text{Hz} .$$

Historically, it was the Crab Nebula, a supernova remnant over 900 years old, to which these measurements and theoretical calculations were first applied. Indirect arguments concerning the energy balance of the gas and the magnetic pressure lead to magnetic fields of 10^{-3} to 10^{-4} gauss. These values of H imply that 10^9 eV electrons emit the radio noise and that 10^{11} to 10^{12} eV electrons emit the blue continium light received from the Crab Nebula. The synchrotron emission mechanism is identified primarily by the polarization of the radiation. Experimental measurements of this polarization have confirmed the synchrotron radiation theory.

The same type of measurements, applied to other discrete radio-frequency emitting regions exhibiting nonthermal spectra, proved the existence of high-energy electrons in various other localities in our galaxy and in other galaxies. Up to the present time, radio measurements have been the only means of localizing the sources of high-energy particles. However, radio emission, being a secondary effect, is connected with important parameters such as the energy distribution of the electrons through the uncertain estimates of local magnetic field strengths. It is, of first rate importance to observe the high-energy flux itself and to associate it with the sources. Recent measurements of gamma rays above 100 MeV by the OSO-III satellite-borne detector indicate a strong anisotropy towards the galactic center, thereby constituting the first clear detection of high-energy photons (Reference 15).

Another recent discovery having an important bearing on high-energy particle interactions is the existence of 3°K black body

radiation, where the peak of the radiation is at about 7×10^{-4} eV (Reference 16). This black body radiation is generally interpreted as being universal and a consequence of the decoupling of matter and radiation at an early epoch of the universe (Reference 17). Because of its high photon density ($600/cm^3$), this radiation renders the universe opaque to particles with which it has resonant interactions (Reference 18).

The diffuse photons of lower energy pervading the universe are shown in Figure 4. In our galaxy, the optical and lower frequency radio noise is enhanced relative to the microwave noise. However, the photon spectrum is still divided into four distinct energy regions, namely nonthermal radio, microwave, optical, and X-rays. For a detailed treatment of this topic see Chapter IV, "Cosmic-Ray Photons," by E. Boldt.

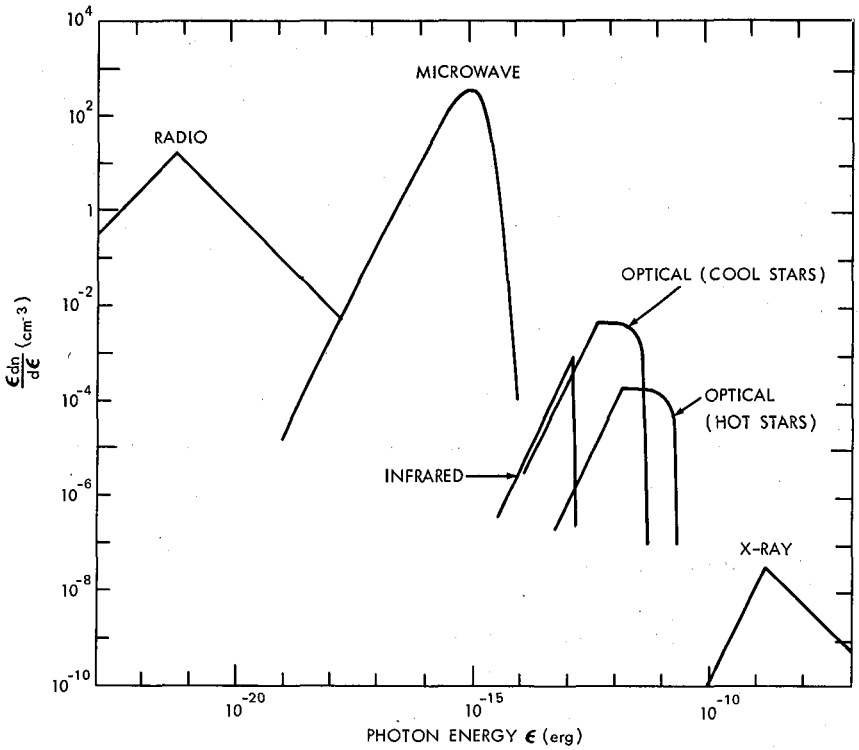

Figure 4—Power spectrum of metagalactic photons as assessed by Gould and Schreder, 1967.

Neutrinos

Being a neutral particle, the neutrino should offer the same directional advantages as the photon. However, it exhibits weak interactions only. The total charged-particle production cross-sections are of the order 10^{-38} E_ν cm^2 per neutrino, where E_ν is the neutrino energy in GeV (Reference 5). This is the theoretical cross-section inferred from Fermi's universal weak interaction theory and is valid for energies in excess of 1 GeV; at lower energies, the cross-section is proportional to E_ν^2. The magnitude of the problem is obvious; kiloton detectors would be necessary to detect such particles. The estimates of the neutrino flux from interstellar space at energies above 1 GeV are similar to those of gamma rays, amounting to 10^{-4} neutrinos cm^{-2}-sec^{-1}-sr^{-1}. However, the atmospheric secondaries should be as intense as 10^{-1} neutrino cm^{-2}-sec^{-1}-sr^{-1}. In view of this difficulty, high-energy neutrino astronomy could only bear fruit if kiloton detectors could be assembled in space or on the moon. High-energy neutrinos have been observed over a mile underground, but, these are generally considered to be atmospheric secondaries (Reference 20).

Low-energy solar neutrinos that are produced by the ordinary nuclear reactions involved in hydrogen burning have been a topic of recent interest (Reference 21). Detectors have been built that could detect the Ar^{37} formed by the reaction

$$Cl^{37} + \nu \rightarrow Ar^{37} + e^-$$

The negative results of these experiments challenge the theoretical predictions (Reference 22).

THE ASTRONOMICAL SETTING

Our sun, with the parameters

$$M_\odot = 2 \times 10^{33} \text{ g},$$

$$\mathcal{L}_\odot = 4 \times 10^{33} \text{ ergs/sec},$$

and

$$R_{\odot} = 7 \times 10^{10} \text{ cm},$$

is one of the 10^{11} stars filling our galaxy. A schematic drawing of the galaxy, indicating its dimensions and shape, is shown in Figure 5. The star distribution in the galaxy is concentrated in a disk about 300 pc thick (1 pc = 3.1×10^{18} cm) with an average density of 0.1 star/pc^3. The density of the stars in the nucleus seems to increase to 100 stars/pc^3. Most of the stars in the disk and the nucleus belong to population I, which is the younger type of star. A small fraction of the stars form globular clusters which are located away from the disk. These stars are generally of population II, i.e., older stars.

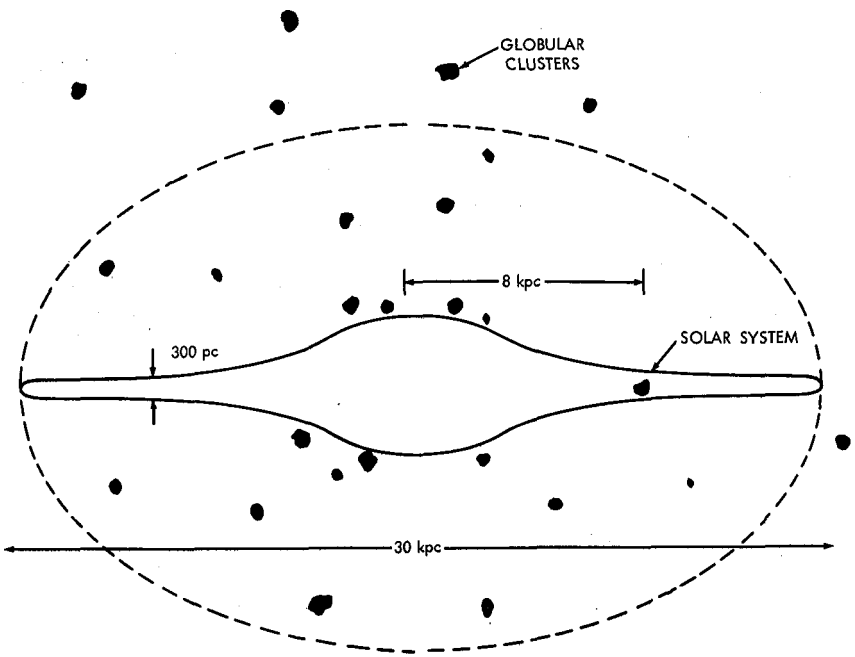

Figure 5–Schematic representation of our galaxy (dotted lines show the extent of proposed halo).

The spiral-arm structure of our galaxy is more evident when one examines the interstellar gas distribution. Studies of the gas distribution became possible after the discovery of the monochromatic 21-cm hyperfine transition line emitted by the neutral hydrogen atom. Figure 6 shows the profiles of the 21-cm hydrogen line. Interpreting the shift in frequency as caused by galactic rotation, one can determine from the shape of the observed emission the neutral hydrogen density at that direction and distance. The resulting picture is shown in Figure 7, clearly indicating the spiral structure of our galaxy. These regions of neutral hydrogen, called H_I clouds, have average densities of 10 atoms/cm^3 and are at a temperature of 100°K. The random cloud velocities are of the order of 10 km/sec. The clouds seem to be lumpy with scales of 10 pc. The neutral hydrogen occupies about 10 percent of the volume of the disc, the other 90 percent being ionized hydrogen clouds called H_{II} regions. In these H_{II} regions, the density is estimated to be ~0.2 ion/cm^3, and the temperature to be ~10^4°K. The existence of the molecular hydrogen is still an open question. Published estimates vary from 10 percent of the atomic hydrogen concentration to 10 times this concentration. If low-energy cosmic rays (~100 MeV) pervade the galaxy, it is extremely difficult to understand how the molecules could be preserved against the disruptive ionizing effects of the radiation (Reference 25).

The other constituent of the interstellar medium is the grains or macromolecules which cause the observed interstellar reddening. The average density of these is estimated to be less than 10^{-25} gm/cm^3.

The existence of a spherical halo surrounding our galaxy was first suspected as a consequence of the slow decrease of radio intensity in directions away from the disk. Although some of the other spiral galaxies exhibit such a halo, others do not. At the present, it is regarded as a theoretically attractive characteristic of our galaxy although experimental evidence is inconclusive. The plausible shape and size of the halo is a spheroid with a major radius of 15 kpc and a minor radius of 8 kpc. The density of hydrogen outside the disk is estimated to be 10^{-26} gm/cm^3 or less.

The nucleus of the galaxy has a diameter of approximately 8 pc as measured by thermal radio emission of ionized hydrogen, the concentration of which may be as high as 10^3 atoms per cubic centimeter.

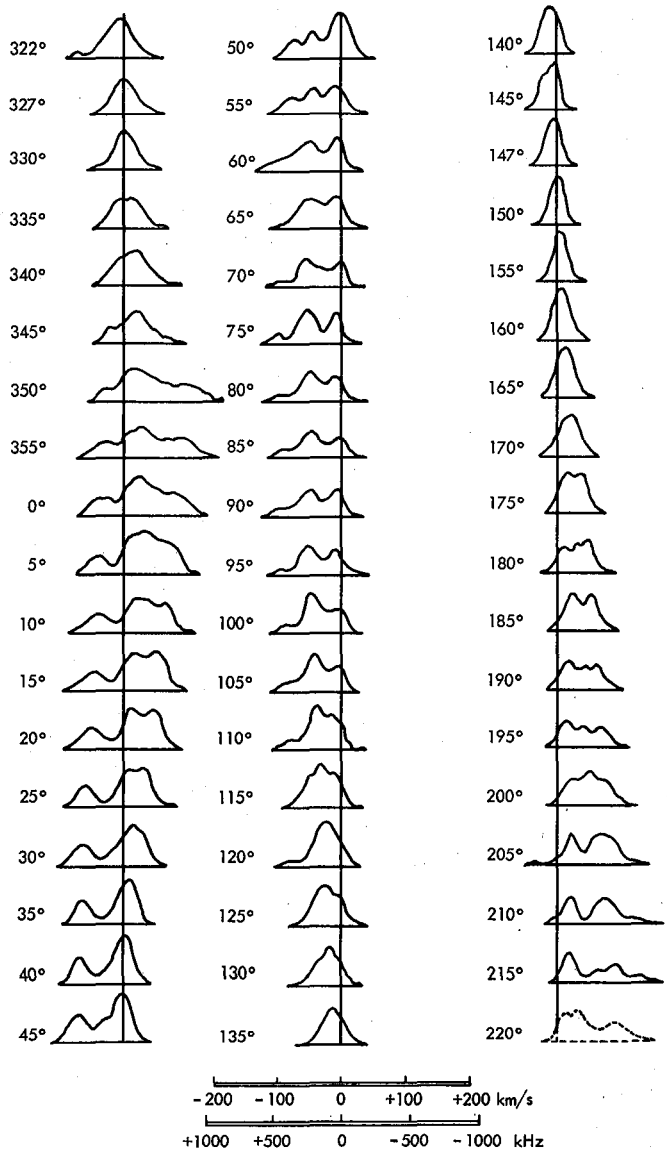

Figure 6—Profiles of the 21-cm hydrogen radio line at 54 longitudes (Reference 23).

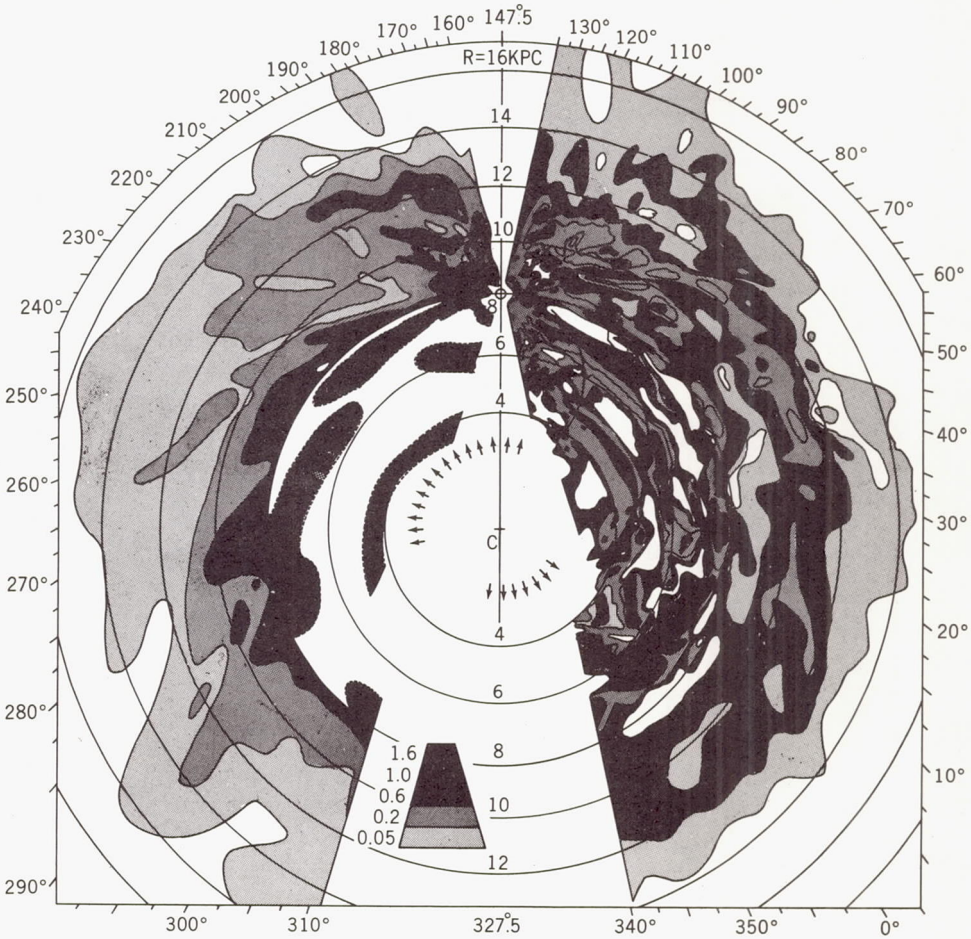

Figure 7—Contour map of neutral-hydrogen density in the galactic system (Reference 24).

Magnetic fields in the galaxy were first postulated by Fermi in 1949 to explain the isotropy of cosmic rays (Reference 26). Today we have independent evidence in the polarization of distant starlight, interpreted as the preferential absorption of grains oriented by the magnetic fields, and nonthermal radio emission, interpreted as synchrotron radiation of high-energy electrons in galactic magnetic fields. Measurements of these quantities and theoretical energy balance arguments seem to favor an average field of 3×10^{-6} gauss, with field lines running in the plane of the galaxy. It seems plausible that, in the spiral arms, the field strength may go up to 10^{-5} gauss.

The photon densities in our galaxy can be listed in the radio, microwave, and optical regions. In the disk, optical photons have a density of 0.2 photon/cm^3; radio photons, about 0.1 photon/cm^3. In the halo, these densities may be less by a factor of 3. Microwave radiation, being universal, pervades the entire galaxy at a density of 600 photons/cm^3.

In the vicinity of our galaxy, we find 15 other galaxies, forming with ours what is termed the local group, including the Magellanic Clouds and the well known Andromeda nebula. The size of this system is approximately 1 megaparsec. The average separation of these galaxies is approximately 50 times their diameter.

Other clusters of galaxies, such as Virgo, have been observed to contain as many as 1000 galaxies. The other observed galaxies seem to recede from us at a rate V proportional to their distance R:

$$V = HR ,$$

where H is the Hubble constant, 10^8 cm/sec-Mpc. Extrapolating this relationship to a velocity equal to that of light gives 10^{28} cm as the observable limit to the universe. The galaxies observed within this volume show a variety of different properties and power outputs. For example, it is believed that quasars are distant, relatively small galaxies with energy outputs of 10^{52} ergs/sec as compared with an average galaxy's output of 10^{45} ergs/sec. It is generally believed that, in these peculiar galaxies, high-energy processes much more intense than those encountered in our own galaxy are dominant.

REFERENCES

1. Weber, J., Phys. Today 21(4):34, 1968.

2. Weber, J., Phys. Rev. Letters 20:1307, 1968.

3. Greisen, K., Proceedings of the Ninth International Conference on Cosmic Rays, 609, London: 1965.

4. Peters, B., Proceedings of the Moscow Cosmic Ray Conference, III: 157, Moscow: 1960.

5. Greisen, K., Annual Rev. of Nuclear Sci. 10:63, 1960.

6. Wolfendale, A. W., "Cosmic Rays," New York: Philosophical Library Inc., 1963.

7. Suga, K. et al., Proceedings of International Conference on Cosmic Rays, Jaipur, India: 1963.

8. Firkowski, R., Gaum, J., Zawadski, A., and Maze, R., J. Phys. Soc. Japan 17, Suppl. AIII: 123, 1962.

9. Bray, A. D. et al., Nuovo Cim. Ser. X, 32:827, 1964.

10. Ginzburg, V. L., and Syrovatskii, S. I., "The Origin of Cosmic Rays," New York: Pergamon Press, MacMillan Co., 1964.

11. Daniel, R. R., and Stephens, S. A., Phys. Rev. Letters 17:935, 1966.

12. L'Heureux, J., and Meyer, P., Can. J. Phys. 46:892, 1968.

13. Bleeker, J. A. M. et al., Can. J. Phys. 46:S523, 1968.

14. Hartman, R. C., Meyer, P., and Hidebrand, R. H., J. Geophys. Res. 70:2713, 1965.

15. Clark, G. W., Garmire, G. P., and Kraushaar, W. L., Ap. J. Letters 153:L205, September 1968.

16. Penzias, A. A., and Wilson, R. W., Ap. J. 142:419, 1965.

17. Dicke, R. H., Peebles, P. J. E., Roll, P. G., and Wilkinson, D. T., Ap. J. 142:414, 1965.

18. Greisen, K., Phys. Rev. Letters 16:748, 1966.

19. Gould, R. J., and Schreder, G. P., Phys. Rev. 155:1408, 1967.

20. Reines, F., Proc. Roy. Soc. A.301:125, 1967.

21. Bachall, J. N., and Shaviv, G., Ap. J. 153, 1968.

22. Davis, Harmer, and Hoffman, Phys. Rev. Letters 20:1205, 1968.

23. Van de Hulst, H. C., Mueller, C. A., and Oort, J. H., B.A.N. 12:117, 1954.

24. Oort, J. H., Kerr, F. T., and Westerhout, G., Monthly Notices 118:379, 1958.

25. Balasubrahmanyan, V. K., Boldt, E., Palmiera, R. A. R., and Sandri, G., Can. J. Phys. 46:633, 1968.

26. Fermi, E., Phys. Rev. 75:1169, 1949.

Page Intentionally Left Blank

II. ORIGIN, COMPOSITION, AND PROPAGATION OF THE NUCLEAR COMPONENT OF COSMIC RAYS

C. Fichtel
NASA Goddard Space Flight Center
Greenbelt, Maryland

NUCLEAR COMPOSITION

In studying the origin and propagation of the cosmic radiation, it is valuable to begin by reviewing the composition of the nucleonic component. Table 1 gives the relative abundances of some of the nuclear components of interest here, as well as some relevant ratios.

Table 1. Relative Abundances of Indicated Nuclear Components With a Base of 100 for He; and Ratios of Some Nuclear Groups

Nucleus	High energy cosmic rays	Universal abundances
Protons	$(1.5 \pm 0.2) \times 10^3$	$(0.7 \text{ to } 1.3) \times 10^3$
He	100	100 ± 10
Li, Be, B	1.6 ± 0.3	10^{-5}
C, N, O, F	6.7 ± 1.6	1.0
$H(Z \geq 10)$	2.5 ± 0.3	(0.1 to 0.4)
$VH(Z \geq 20)$	0.7 ± 0.2	(0.005 to 0.02)
$He^3/(He^3 + He^4)$	~ 0.2	-
Carbon/Oxygen	1.1 ± 0.1	(0.1 to 0.4)
$(Z > 30)/(Z \geq 20)$	$\sim 0.4 \times 10^{-3}$	$(0.4 \text{ to } 1.3) \times 10^{-3}$
$(Z > 40)/(Z \geq 20)$	$\sim 0.3 \times 10^{-4}$	$(0.5 \text{ to } 3) \times 10^{-4}$

The Li, Be, B, and He^3 in the cosmic radiation are thought to be secondaries formed in interactions between cosmic ray nuclei and interstellar material (presumably mostly hydrogen). Although there

are some difficulties in explaining the amount of these nuclei as a function of energy, which will be discussed in the last part of this lecture, the abundances of these secondary nuclei can be explained in general terms by assuming that on the average the cosmic radiation has gone through about 4 ± 1 g/cm^2 of material. This somewhat unusual unit, i.e. "g/cm^2," arises because it is the product of a length times a density, a quantity that determines the degree to which the heavier cosmic ray nuclei break up in interactions. With this figure and the current best estimate of the density of interstellar material in the galactic disk—about 1 atom/cm^3—the average lifetime of the cosmic radiation in the disk is found to be a few million years. This number, together with our knowledge of the cosmic ray energy spectrum and flux, will tell us the rate at which cosmic rays must be supplied. If the cosmic radiation pervades the whole galaxy and not just the disk, it still has to be supplied at about the same rate because its lifetime is larger by approximately the same factor as the volume. The subject of the region of containment of the cosmic rays will be discussed later in this chapter.

The volume of the disk will be taken as

$$\pi\left(1.5 \times 10^4 \times 3 \times 10^{18}\right)^2 \times \left(400 \times 3 \times 10^{18}\right) = 8 \times 10^{66}\ \mathrm{cm}^3 .$$

If there are 2×10^{-10} cosmic rays per cubic centimeter, the total number of cosmic rays in the disk is a little more than 10^{57} and their energy is 8×10^{66} eV or about 10^{55} ergs. Using the lifetime derived above, the rate at which cosmic rays must be supplied is about 2×10^{43}/sec, and the rate at which energy must be supplied is about 10^{41} ergs/sec.

The numbers quoted in the last paragraph refer to cosmic rays with energies above about 0.3 GeV/nucleon. At lower energies the cosmic radiation is strongly modulated by the outward flowing hot solar plasma called the "solar wind." This is a problem in itself and will not be pursued here. The degree of modulation is the subject of considerable controversy, and estimates of the number of low energy cosmic rays outside the solar system vary by more than an order of magnitude. Fortunately, because their energy is so much lower than the average cosmic ray energy, the total cosmic ray energy is probably not increased by more than a factor of two even under the most extreme assumptions, and probably less.

Before leaving the subject of secondaries in the cosmic radiation, which is what led to the discussion just completed, a few other features will be mentioned. A significant fraction of the nuclei with charges just below iron are probably also secondaries on the basis of their unusual abundances. Many of the odd nuclei from $Z = 7$ to 19 would also be expected to be secondaries, and the carbon-to-oxygen ratio should be enhanced, as indeed it appears to be.

The excess of heavy nuclei in the cosmic radiation, relative to universal abundances, is seen to increase generally from the medium nuclei (where the excess relative to helium is about a factor of 6) to the iron group (where it is about a factor of 100). This increase is usually attributed to the character of the source region. The nuclei with charges greater than iron also show an excess relative to helium in the cosmic radiation, but the ratios of nuclei with $Z \geq 30$ and $Z \geq 40$ relative to the iron group appear to be the same as the universal abundances. This feature is also thought to be a characteristic of the source region, and theoretical attempts to explain this composition are a subject of considerable current interest.

Another feature of the nuclear component which enters the picture is that, except for small variations, the relative abundances of the various nuclei seem to vary little with energy from energies as low as 0.05 GeV/nucleon up to at least 50 GeV/nucleon, and there is some evidence that the relative abundances of the major groups do not change substantially even up to energies as high as 10^6 GeV/nucleon.

ORIGIN

Region of Containment

There are basically three major regions in which the cosmic rays could be contained and be presumed to originate: a small region surrounding the solar system; our own galaxy; and the universe.

The solar system can be rejected for numerous reasons, including the following:

1. The magnetic fields of the solar system cannot contain the highest energy particles, that is those above about 10^2 GeV/nucleon.

2. The cosmic rays are most intense when the sun is least active.

3. The composition of the cosmic radiation differs greatly from that of the sun and that of energetic solar particles (average energy between a few and tens of MeV/nucleon) which the sun is known to emit in association with some big solar flares.

4. The energy of the particles in the solar particle events is very small compared to the average cosmic ray energy, and there is no known way that the sun could create such high energy particles and retain its present characteristics. Even if the sun could emit the higher energy particles, they would be highly anisotropic, since they would be virtually undeflected by the magnetic fields in the solar system.

The universe as a whole seems unlikely as the region in which cosmic rays are localized for several reasons.

Gamma-ray studies indicate that the density in interstellar space would have to be less than 10^{-7} atom/cm^3 if the cosmic ray intensity were the same as in the vicinity of the solar system. This density seems too small to be consistent with x-ray measurements and other considerations but the question is not finally resolved. If cosmic rays are extragalactic in origin, the galactic magnetic field must connect to the metagalactic region to let cosmic rays into the galaxy and out again in about 10^6 years; but the nature of this connection is difficult to visualize since the galaxy has rotated about twenty-five times in the life of the universe. There is also the question of finding a source or sources to supply the needed energy.

These and similar difficulties are strong objections, but they do not absolutely eliminate the universe or some local region of it—most probably the region in which the highest energy cosmic rays ($E \gtrsim 3 \times 10^{18}$ eV/nucleon) are contained. For the present discussion, however, the universe will also be rejected as the region of containment for the majority of cosmic rays.

Turning again to the galaxy, two basic conditions must be satisfied. First, the cosmic rays must be produced at the desired rate with the necessary characteristics; and secondly they must be confined satisfactorily to the galaxy. With regard to the second condition, we may assume that the maximum rigidity that a particle can have and still

be contained easily in the galaxy is one which is an order of magnitude smaller than that corresponding to a radius of gyration equal to the radius of the galaxy. This rigidity is

$$R = \left\{300\, r_{gal.}\,(\mathrm{cm})\, H_{gal.}\,(\mathrm{gauss})\right\} \cdot \left\{\frac{1}{10}\right\}$$

Using $r_{gal.} = 1.5 \times 10^4$ parsecs and $H_{gal.} = 3 \times 10^{-6}$ gauss (this number is very poorly known), gives a rigidity of 5×10^{18} eV; thus, all but particles with the very highest rigidity could be contained in the galaxy. Similar arguments would indicate that a particle with rigidity equal to about 3×10^{16} eV or less could be contained in the disk.

In examining the problem of containing cosmic rays in the disk, the various contributing pressures for expansion must be considered and their resultant gradient balanced against ρg, the local density times the local value for the acceleration of gravity. The expansive pressures are those due to the cosmic ray gas, to the magnetic field, and to the kinetic motion of the interstellar particles. Parker has shown that for a magnetic field of (3 to 5) $\times 10^{-6}$ gauss (estimated from Faraday rotation measurements and polarization measurements, assuming graphite grains are primarily responsible for the polarization), a balance occurs for an interstellar density of 1 to 2 hydrogen atoms/cm^3. This is in good agreement with current estimates. If a similar calculation is made for the galactic halo, the relatively low density of material thought to exist there implies that the cosmic ray density is quite low; so, in effect, cosmic rays are not stored there if current ideas are correct.

The magnetic field configuration in the disk is actually unstable and forms humps from which the cosmic rays can escape more easily. The cosmic rays must escape somehow, because they are being supplied continually and yet their average energy density remains constant. The unstable motion of the magnetic fields in the disk implies a filamentary structure for the galactic field, and there is some evidence to support that hypothesis. It is thought that the diffusion of cosmic rays in this field is rather slow, and that as a result the cosmic rays are a relatively local phenomenon. It is possible that the cosmic rays seen near the earth come mostly from sources in the galactic spiral arm segment in which our sun is located. The cosmic ray

bulk motion perpendicular to the disk is very slow in this picture, since the main component of the field is parallel to the plane of the disk, and the net motion is due as much to the pressure balance mentioned above as to the result of scattering and spiraling in the magnetic field.

Source

Assuming then that the cosmic rays can be contained in the galaxy, what is their source? Current theories seem to favor supernovae because they seem to be the only objects capable of supplying the necessary energy. From the theory of supernovae and from the radio observations interpreted in terms of synchrotron emission of relativistic electrons, it seems reasonable that each supernova will supply from 10^{49} to 10^{52} ergs to cosmic rays. Assuming a supernovae occurs once every 50 years in our galaxy, supernovae would be able to supply cosmic ray energy at the rate of about 10^{40} to 10^{43} ergs/sec on the average. The energy supply rate calculated earlier in this chapter, 10^{41} ergs/sec, is within this range. Supernovae are also believed to be rich in heavy elements, and this is consistent with cosmic ray composition. In order to proceed further, and in particular to consider both the problems of energy spectra and of the maximum energy, it is necessary to examine specific models for supernovae.

Present theories of supernovae are based on the concept that a supernova explosion is initiated by a dynamic implosion of a massive star. This implosion results from the gravitational instability of the star, at the end of nuclear synthesis, wherein there is thermal decomposition of iron back into helium. Although there is some debate, the most popular current view is that the gravitational instability occurs because the neutrinos emitted in the electron capture process leading to neutron-rich material remove energy faster than quasi-static contraction can supply it. As a result, a dramatic implosion occurs and continues in virtual free-fall until the pressure of the Fermi gas neutrons in the core becomes high enough to stop it.

A large gravitational energy is thus freed and transferred to the neutrinos. The neutrinos, whose mean free paths are smaller than the radius of the star, deposit their energy inside the star, and a shock wave is formed. The velocity of this shock wave increases towards the surface and becomes relativistic for a small fraction of

the outer envelope, which is then converted into cosmic rays. To discuss this process in detail is far beyond the scope of this lecture, but the results predict a power law spectrum in energy similar to that actually observed, and it is supposedly possible to obtain the highest energies by this process. The excess of heavy nuclei can also be explained by this model, but there is some question as to whether it predicts the correct composition in detail.

One consequence of the hydromagnetic shock wave theory of supernova origin is a definite prediction regarding an energetic electromagnetic pulse being emitted from the surface layer during this layer's ejection and subsequent adiabatic expansion. The detection of such a pulse and identification of it with an optically observed supernova is an important test of this theory of the origin of cosmic rays.

An alternative—and less well defined—picture of cosmic ray acceleration in a supernova is that the cosmic rays are accelerated by the moving magnetic fields in the general turbulence following the explosion. General arguments can be made to explain how the energy spectrum might be obtained. There remains the problem of explaining how the highest energies could be obtained in this case, and there are also other detailed aspects, such as the electron acceleration and degree of energy loss, which have not been satisfactorily resolved. No intense, high energy gamma ray pulse similar to that of the shock wave acceleration theory is predicted in this case.

PROPAGATION

The cosmic ray energy spectra which are observed at the earth represent the source spectra after they have passed through interstellar matter and have been modulated within the solar system. Whereas presumably the solar system modulation is primarily the result of electromagnetic fields, interstellar space is believed to contain enough material along the path of the particle to change appreciably the particle energy as well as the intensity of the radiation. In the interstellar medium, it is normally assumed that the intensity in an energy interval is changed significantly only by fragmentation in interactions and by ionization energy loss, and not by acceleration nor by the complicated time-dependent magnetic effects which probably cause the intensity variation in the solar system.

If the acceleration in interstellar space is negligible, it is possible to calculate the energy dependence of the relative abundances of various particle groups outside the solar system, assuming various source spectra, provided that the collision cross sections in interstellar space and the amount of material traversed are sufficiently well known. The exact nature of the solar modulation is not yet known, but the general belief is that it probably depends only on the velocity and charge-to-mass ratio of the particle. Therefore, although nuclei with the same charge-to-mass ratio but different charges will lose energy at different rates in interstellar space, the fluxes of these particles will be modulated in the same way, thereby permitting the separation of modulation effects from interstellar energy loss and fragmentation effects.

In making a calculation, a particular set of simplifying assumptions is often made. These are:

1. The source energy per nucleon spectra of all multiply charged nuclei have the same shape, at least above 100 MeV/nucleon. (Note that this effectively permits the spectra to be both velocity and rigidity dependent, since all of the multiply charged nuclei of interest at the source have nearly the same charge-to-mass ratio.)

2. The abundances of both He^3 and light nuclei ($3 \leq Z \leq 5$) at the source are negligible compared to He^4 and medium nuclei respectively.

3. The average interstellar mean free path is independent of the energy per nucleon of the particles.

Before outlining the general procedure, these assumptions will be discussed.

The similarity in source spectral shape, at least for particles of the same charge-to-mass ratio, is suggested by the predictions of the basic acceleration mechanisms, such as the simple Fermi theory, the principle of equipartition of energy, and the shock-wave theory of acceleration by supernovae. Some of the more complicated variations of these theories can lead to predictions of differences in the energy spectra of different charge-to-mass ratios, but this point will not be pursued here. Further support to the choice of spectra of the same

shape for particles of the same charge-to-mass ratio is obtained from the study of solar particles.

With respect to the composition, the only important assumption is that light nuclei and He^3 are essentially absent in the source. For the light nuclei, this assumption is based on the fact that light nuclei are very rare in the universe (about 10^{-5} of the abundance of medium nuclei) because they are unstable at the high temperatures of most stars. The justification for assuming there is virtually no He^3 at the source is similar.

Finally, the assumption that the average mean free path is independent of energy is based on simplicity and the fact that in a simple steady state situation, the path length does not vary with velocity. A rigidity dependent average path length is possible if, for example, high rigidity particles escape more easily; and this alternative possibility has been considered in the literature. It is sometimes assumed that the cosmic radiation may pass through part of the material in the source region itself. However, only relatively minor differences result from the different natures of the material in the source and in interstellar space. It is expected that there will be a distribution in path lengths about an average path length. Again, for most path length distributions, the results to be considered here do not differ much from the results of assuming that all cosmic rays pass through the same amount of material.

As has already been mentioned, the material in interstellar space affects the cosmic ray particles by causing energy loss and fragmentation. In order to take both of these phenomena into account, it is necessary to begin with the appropriate transport equation. The fundamental equation can be written in the form

$$\frac{d}{dx}\left[w_i(E)\, j_i(E, x)\right] = w_i(E)\, H_i(E, x)\,, \qquad (1)$$

where x is the position along the particle path; $w_i = (dE/dx)_i$; i refers to the particular nuclear species; j_i is the differential directional intensity per unit energy per nucleon E, for particles of type i; and H_i is the number of particles added or subtracted per unit volume, time, solid angle, and energy per nucleon.

In the case under consideration H_i consists of two parts, the source term S_i and the loss term due to collisions. Hence,

$$H_i\,(E, x) = S_i\,(E, x) - j_i\,(E, x)/\Lambda_i\,(E)\,. \tag{2}$$

Here, Λ_i is the loss mean free path, which is related to the interaction mean free path λ_i by the equation

$$1/\Lambda_i = \left(1 - P_{ii}\right)\lambda_i\,, \tag{3}$$

where P_{ii} is the average number of particles of type i formed in the interaction of a type i nucleus. In turn, S_i is given by

$$S_i\,(E, x) = \sum_{k>i} j_k\,(E, x)/\Lambda_{ki}\,(E)\,, \tag{4}$$

where Λ_{ki} is the mean free path for production of i-type particles from k-type particles. The sum in (4) can be restricted to particles heavier than i, because the lighter ones will not contribute to i nuclei in an interaction, and the i-to-i type interaction is already included in the last term of (2).

Substituting (2) into (1) and rearranging terms yields

$$\frac{d}{dx}\left[w_i\, j_i\right] + w_i\, j_i\left(1/\Lambda_i\right) = w_i\, S_i\,. \tag{5}$$

Multiplying (5) by the integrating factor $\exp(x/\Lambda)$ and rewriting the left-hand side yields

$$\frac{d}{dx}\left[\exp\left(x/\Lambda_i\right) j_i\, w_i\right] = \exp\left(x/\Lambda_i\right) w_i\, S_i\,. \tag{6}$$

Then (6) may be used to propagate the particle energy spectra at the source, $j_i\,(E, 0)$, through interstellar matter in small steps. The

step size must be sufficiently small that the variations in terms such as w_i (E) and Λ_i (E) introduce only a negligible error into the calculation.

The results of such a calculation show that it is not possible to obtain full agreement between the calculated abundance ratios of various nuclear species as a function of energy/nucleon and the observed values. Possible explanations which have been suggested recently include a very strong rigidity effect in the solar modulation; a rigidity dependent path length; fragmentation at the source before most of the acceleration; and two-source models. Only the last seems not to have strong objections. One suggested two-source model includes a contribution at low energies from celestial objects less active than supernovae, and another suggests a recent close supernova burst to be added to the general cosmic radiation. At present the problem is not finally resolved, but it still appears that the interstellar medium probably plays the general role described above and also is responsible for the light nuclei and other presumed secondary products observed in the cosmic rays.

BIBLIOGRAPHY

Universal Abundances

Suess, H. E. and Urey, H. C., Reviews of Modern Physics 28:53 (1956)

Cameron, A. G. W., Astrophys. J. 129:676 (1959)

Cosmic Ray Nuclear Composition

Balasubrahmanyan, V. K., Hagge, D. E., Ludwig, G. H., and McDonald, F. B., J. Geophys. Res. 71:1771 (1966)

Webber, W. R., and Ormes, J. F., J. Geophys. Res. 72:5957 (1967)

Comstock, G. M., Fan, C. Y., and Simpson, J. A., Astrophys. J. 146:51 (1966)

Origin

Colgate, S. A., and Johnson, H. J., Phys. Rev. Letters 5:235 (1960)

Ginzburg, V. L., and Syrovatskii, S. I., "The Origin of Cosmic Rays," Pergamon Press, MacMillan Co. (1964)

Colgate, S. A., and White, R. H., Astrophys. J. 143:626 (1966)

Propagation

Fichtel, C. E., and Reames, D. V., Phys. Rev. 149:995 (1966)

Kaplon, M. F., and Skadron, G., Rev. Geophys. 4:177 (1966)

Fichtel, C. E., and Reames, D. V., Phys. Rev. 175:1564 (1968)

General

For a fairly complete study of the status of cosmic ray research as of the summer of 1967, see the Proceedings of the Tenth International Conference on Cosmic Rays, published as a supplement to the May 1968, Canadian Journal of Physics, particularly the papers in the OG (origin) and MOD (modulation) section.

III. COSMIC-RAY ELECTRONS AND RELATED ASTROPHYSICAL PROBLEMS*

R. Ramaty
NASA Goddard Space Flight Center
Greenbelt, Maryland

INTRODUCTION

Various quantities which are relevant to our understanding of cosmic-ray electrons can be measured at the earth. Among these are

a. The energy spectrum and intensity of the electron flux (the latter quantity is measured in such units as electrons/m^2-sec-sr-BeV);

b. The charge composition, i.e., the relative numbers of electrons and positrons; and

c. Time variations.

The effects of solar modulation, so evident in the proton spectrum, have not yet been detected in the electron component. However, the upper limits which have been established are consistent with some of the theoretical predictions. Other measurements which are indirectly useful in understanding the electron component include the nonthermal radio background and the spectrum of high-energy photons (X and gamma radiation). It is hoped that such measurements will further our understanding of some of the outstanding problems in high-energy astrophysics. Some of these problems are discussed below and include the origin of cosmic rays, solar modulation, galactic propagation, the connection with electromagnetic radiation, and the problem of energy loss, which is discussed first.

Since the charge-to-mass ratio of electrons is so much greater than that of protons and other heavy nuclei, the electrons lose energy at a proportionately higher rate. This energy loss results in X, gamma, and radio radiation. The primary interactions which give

*Notes taken by M. L. Goldstein.

rise to these photons are the synchrotron, bremsstrahlung, and inverse Compton processes.

SYNCHROTRON RADIATION

Consider an electron moving in a static, uniform magnetic field **B**. The pitch angle of the electron is ϕ, and the angle made by the field direction and the observation direction is θ (Figure 1).

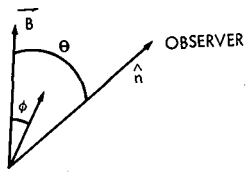

Figure 1–Relationship of electron pitch angle and angle made by field direction and observer direction.

The power radiated by such an electron into solid angle $d\Omega$ per unit frequency interval $d\omega$ is

$$\frac{d^2 P}{d\Omega\, d\omega} = \sum_{s=1}^{\infty} \frac{\omega^2 e^2}{2\pi c}\, \delta\left(\omega - P_s\right) \left[\beta_1^2 J_s'^{\,2}(x) + \left(\frac{s\omega_B}{\gamma\omega} \cot\theta - \sin\theta\beta_2\right) J_2^2(x)\right] \frac{\text{erg}}{\text{sec-sr-Hz}} \cdot \quad (1)$$

This expression is independent of azimuth. In Equation 1,

$$P_s = \frac{s\omega_B}{\gamma} + \beta_2\, \omega \cos\theta \ , \quad (2)$$

$$\gamma = E/mc^2, \text{ E being the electron energy} , \quad (3)$$

β_1 is the magnitude of the component of electron velocity ($\div$ c) which is orthogonal to **B**, β_2 is the component of electron velocity ($\div$ c) which is parallel to **B**,

$$\omega_B = eB/mc \ , \quad (4)$$

and

$$x = \frac{s\beta \sin\theta \sin\phi}{1 - \beta \cos\theta \cos\phi} . \tag{5}$$

When the electron becomes relativistic ($\gamma >> 1$), one can show that no appreciable power is emitted by the electron unless $(\theta - \phi) \simeq 1/\gamma$.

If one were to integrate

$$\frac{d^2 P}{d\Omega \, d\omega}$$

over all solid angles, the result would be equivalent to the emission from a region of tangled magnetic field. This integral can be done for electrons moving in circular orbits to yield

$$\int \frac{d^2 P}{d\Omega \, d\nu} \, d\Omega = \frac{dP}{d\nu} , \tag{6}$$

where

$$\frac{dP}{d\nu} = \frac{\sqrt{3}}{2\pi} \frac{e^4 B^2}{m^2 c^3} \frac{1}{\gamma} \sum_s F\left(\frac{\nu}{\nu_c}\right) \delta\left(\nu - \frac{S\nu_B}{\gamma}\right) , \tag{7}$$

$$F\left(\frac{\nu}{\nu_c}\right) = \frac{4\pi}{\sqrt{3}} \frac{1}{\gamma\beta} \left[S\beta^2 J'_{2s} (2s\beta) - s^2 \left(1 - \beta^2\right) \int_0^\beta J_{2s} (2sx) \, dx \right] , \tag{8}$$

and

$$\nu_c = \frac{3}{2} \nu_B \gamma^2 ; \tag{9}$$

$F(\nu/\nu_c)$ is plotted as a function of ν/ν_c in Figure 2 for electrons of various values of γ.

As γ increases, the harmonics lie progressively closer together. The curve $\gamma = \infty$ is commonly used in synchrotron calculations. It can be shown that as $\gamma \to \infty$,

$$F\left(\frac{\nu}{\nu_c}\right) \to \frac{\nu}{\nu_c} \int_{\nu/\nu_c}^{\infty} K_{5/3}(y)\, dy$$

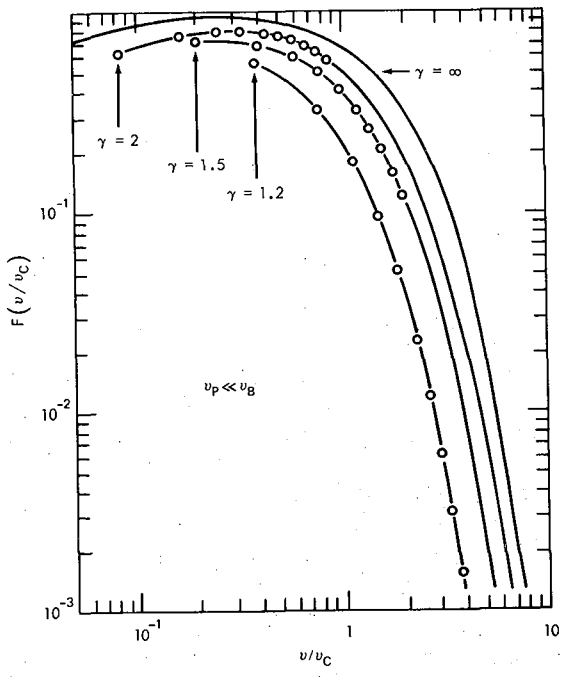

Figure 2–$F(\nu/\nu_c)$ versus ν/ν_c for various values of γ.

The peak in $F(\nu/\nu_c)$ is at $\nu/\nu_c \approx 0.3$. If there is a plasma present with dielectric constant $n^2 = \left(1 - \omega_p^2/\omega^2\right)^{1/2}$, where ω_p is the plasma frequency $\left(4\pi Ne^2/m\right)^{1/2}$, and N is the electron number density, the curves of $F(\nu/\nu_c)$ bend over at low frequencies. The effect of the ambient plasma, therefore, leads to a low-frequency cutoff of synchrotron radiation. The total power radiated by an electron in a vacuum is obtained by integrating $dP/d\nu$ over all frequencies and is given by

$$\int \frac{dP}{d\nu}\, d\nu = \dot{E} = \frac{2}{3}\, c r_0^2 B^2 \beta^2 \gamma^2 , \tag{10}$$

where r_0 is the classical radius of the electron, e^2/mc^2.

INVERSE COMPTON EFFECT

e	$+$	γ	$\rightarrow$	e	$+$	γ
high-energy electron		low-energy photon		scattered electron		high-energy photon

If we let ϵ be the energy of the incident low-energy photon and ϵ' be that of the scattered photon, then neglecting angular terms, one can easily show from the kinematics of the interaction that

$$\epsilon' = \frac{4}{3}\gamma^2 \epsilon .$$

The rate of energy loss is just the energy lost per collision multiplied by the number of collisions per second. Thus, the total radiated power is given by

$$\dot{E} = \left(\frac{4}{3}\gamma^2 \epsilon\right)\left(\frac{\sigma_c\, cW_{ph}}{\epsilon}\right) = \frac{4}{3}\sigma_c\, cW_{ph}\, \gamma^2 \qquad \text{for} \qquad \gamma \lesssim 5\times 10^4, \tag{11}$$

where the restriction in γ values requires that classical Thomson scattering occurs so that $\gamma\epsilon/mc^2 << 1$, and

$$\sigma_c = \frac{8}{3}\pi r_0^2 .$$

Thus synchrotron and Compton energy losses are both proportional to the energy density of the ambient fields. This result can be derived more directly and exactly by starting with the formula for instantaneous power radiated by an electron in an arbitrary electromagnetic field (References 1 and 2), which is

$$P = \frac{2e^4}{3m^2 c^3}\left[\frac{(\mathbf{E} + \mathbf{B}\times\mathbf{H})^2 - (\mathbf{B} - \mathbf{E})^2}{1 - \beta^2}\right] . \tag{12}$$

Using the fact that for any energy flow which is isotropic, $\langle\beta - (\mathbf{E}\times\mathbf{H})\rangle = 0$, and that for unpolarized fields

$$\langle(\beta\times\mathbf{E})^2\rangle_{AV} = \frac{2}{3}\beta^2 , \qquad \langle(\beta\times\mathbf{H})^2\rangle_{AV} = \frac{2}{3}\beta^2 H^2 ,$$

we have

$$\langle P\rangle_{AV} = \frac{8}{3}\pi r_0^2\left(\frac{cE^2}{4\pi}\right) + 3.555\cdots\pi r_0^2\left[\frac{(E^2 + H^2)}{8\pi}\right]\left(\frac{P}{mc}\right)^2 . \tag{13}$$

In the situation in which the only **E** fields present are radiation fields, the energy flux incident on the electron is $(8/3)\pi r_0^2(cE^2/4\pi)$. Thus the average rate of change of energy is

$$-\langle d\epsilon/dt\rangle_{AV} = 3.555\cdots\pi r_0^2 c\left[\frac{(E^2 + H^2)}{8\pi}\right]\left(\frac{P}{mc}\right)^2 , \tag{14}$$

where $E^2/8\pi$ is just ω_{ph} in the Compton process, and $(P/mc^2)^2 = \gamma^2 \beta^2$. However, in this derivation, we have included static magnetic fields as well and therefore have included synchrotron losses.

PRODUCTION OF POSITRONS AND NEGATONS IN COSMIC-RAY INTERACTIONS IN INTERSTELLAR SPACE

Cosmic-ray protons undergo various interactions with interstellar hydrogen. Among these interactions are

$$p + p \rightarrow p + p + a(\pi^+ + \pi^-) + b\pi^\circ$$

$$\underbrace{p + n}_{d} + \pi^+ + a(\pi^+ + \pi^-) + b\pi^\circ$$

$$2n + 2\pi^+ + a(\pi^+ + \pi^-) + b\pi^\circ$$

The threshold for pion production in the lab system is 287 MeV. As the incident energy is increased above threshold, the first reaction to occur is $pp \rightarrow pn\pi^+$. At low energies, therefore, the ratio of π^+ to π^- is greater than unity. At high energies, this ratio tends toward unity. If we call $q_\pi(T_\pi)$ the rate of production of pions per unit volume per unit energy of the pion (T_π), then

$$q_\pi(T_\pi) = 4\pi \int dT_p \; j(T_p)\, \sigma(T_p)\, Nf(T_p, T_\pi) \; . \tag{15}$$

The units of the right-hand side are, reading from left to right, (4π) = steradians, $[j(T_p)]$ = protons/cm^2-sec-sr-energy interval, $[\sigma(T_p)]$ = cm^2, [N] = number of hydrogen atoms per cm^3, $[f(T_p, T_\pi)]$ = proton energy/pion energy. Cosmic-ray experiments directly

measure $j(T_p)$, while N is derived from 21-cm radio data; f and $\sigma(T_p)$ are measured in the laboratory.

We are interested in pion production because charged pions decay first into muons and finally into electrons via

$$\pi^{\pm} \rightarrow \mu^{\pm} + \nu$$

$$\mu^{\pm} \rightarrow e^{\pm} + \nu + \bar{\nu} .$$

The decay energies of the two-body decay are uniquely determined from energy-momentum conservation although this is not true of the three-body decay, and thus the electrons and neutrinos are produced with a continuum of energies. If we let $P(\gamma_e^*, \cos\theta^*)\, d\gamma_e^*\, d\cos\theta^*$ be the probability that an electron is produced with energy γ_e in the direction θ^* (where * indicates the muon's rest system), then

$$q(\gamma_\mu)\, d\gamma_\mu\, P(\gamma_e^*, \cos\theta^*)\, d\gamma_e^*\, d\cos\theta^* = d\gamma_e\, d\gamma_e^*\, d\gamma_\mu\, q(\gamma_e, \gamma_e^*, \gamma_\mu) , \quad (16)$$

where $q(\gamma_\mu)$ is the number of muons of energy γ_μ produced per cm^3 per second per unit γ_μ, and

$$\gamma_e = \gamma_\mu \gamma_e^* + \sqrt{\gamma_\mu^2 - 1}\sqrt{\gamma_e^{*2} - 1}\cos\theta^* . \quad (17)$$

Since we are not interested in γ_e^* and γ_μ, we define

$$Q(\gamma_e) = \iint q(\gamma_e; \gamma_e^*, \gamma_\mu)\, d\gamma_e^*\, d\gamma_\mu$$

$$= \iint d\gamma_e^*\, d\gamma_\mu\, q_\mu(\gamma_\mu)\, P(\gamma_e^*, \cos\theta^*)\, \frac{d(\cos\theta^*)}{d\gamma_e} , \quad (18)$$

where

$$\frac{d(\cos\theta^*)}{d\gamma_e} = \frac{1}{\sqrt{\gamma_\mu^2 - 1}\sqrt{\gamma_e^{*2} - 1}} \cdot \tag{19}$$

One assumes that pion decay is not very sensitive to angles. Because the π, μ mass difference is small, one can show that $q_\mu(\gamma_\mu) \approx q_\pi(\gamma_\pi)$. Analogous simplifications are difficult to make for muon decay because the μ, e mass difference is large (~200), and the decay is sensitive to the angle of emission of the electrons, positrons, and neutrinos. The equilibrium flux of electrons in interstellar space can be obtained by solving a diffusion-energy loss equation. This is discussed later.

The measurements of the spectrum and charge composition of cosmic-ray electrons at the earth are shown in Figure 3. The curves of e_s and e_s^+ correspond to the calculated fluxes in interstellar space of total secondary electrons and positrons respectively. The curves e_s^+ (Mod I) and e_s^+ (Mod II) represent the modulated positron fluxes at the earth, using either one of the modulating functions given in the figure. As can be seen, the existing positron data are consistent with both models, but measurements of positrons below 100 MeV could easily determine the amount of electron modulation at these energies.

The modulation of electrons and their extrapolated interstellar spectrum were discussed by Ramaty and Lingenfelter (Reference 3).

PROPAGATION OF ELECTRONS IN INTERSTELLAR SPACE

Let $Q(E, \mathbf{r}, t)$ be the number of electrons produced at $\mathbf{r}$ with energy E per unit volume per second. While losing energy, particles diffuse away from this source region. The equation which describes this is

$$\frac{\partial u}{\partial t} - \nabla \cdot (D\nabla u) + \frac{\partial}{\partial t}(\dot{E}u) = Q(E, \mathbf{r}) , \tag{20}$$

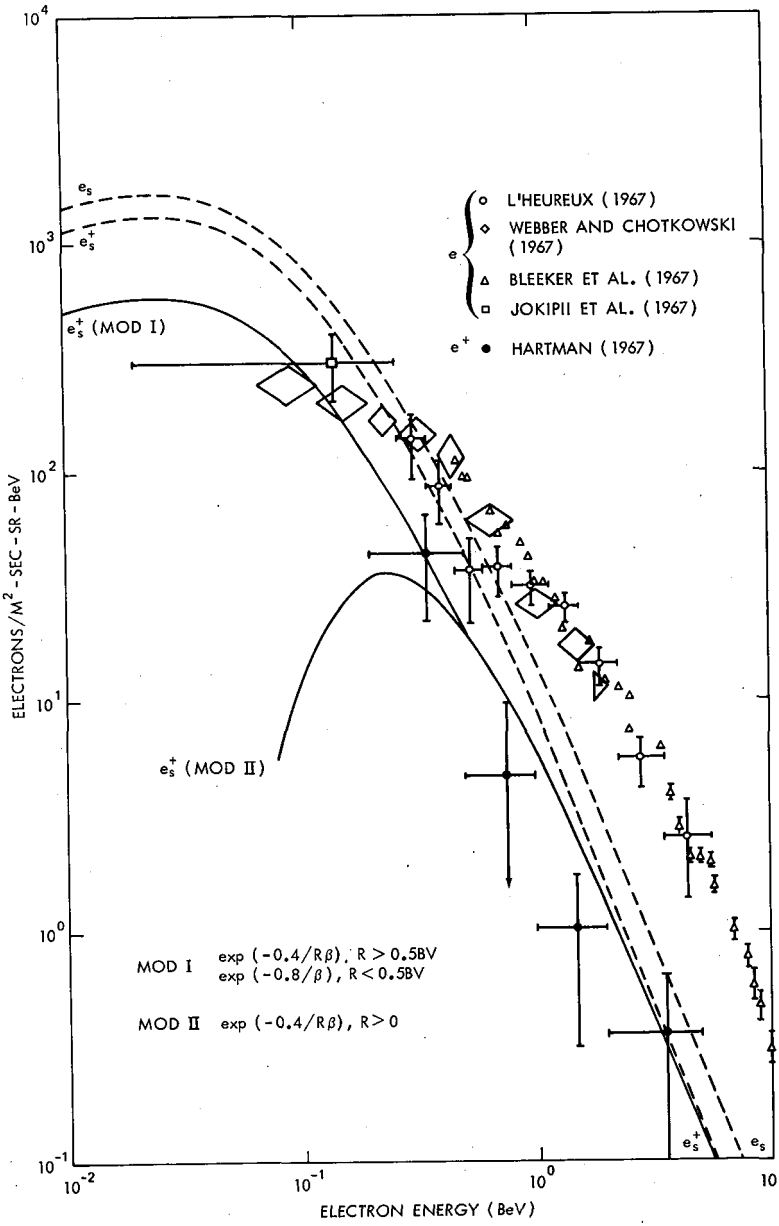

Figure 3—Earth measurements of the spectrum and charge composition of cosmic-ray electrons.

where u is the electron density, D the diffusion coefficient, and $\dot{E}(E)$ is the rate of energy loss caused by ionization, bremsstrahlung, synchrotron, and inverse Compton losses. Furthermore, we restrict ourselves to the example of an infinite volume. The solution is

$$u(E, \mathbf{r}) = \frac{1}{|\dot{E}|} \int_E^\infty dE' \int d^3 r' \frac{e^{-|\mathbf{r}-\mathbf{r}'|^2/4D\tau}}{(4\pi D\tau)^{3/2}} Q(E', \mathbf{r}') \; ; \quad (21)$$

$$\tau \equiv \int_E^{E'} \frac{dE''}{\dot{E}(E'')} \; . \quad (22)$$

We assume

$$Q(E, \mathbf{r}) = q(E)\,\rho(\mathbf{r}) \; , \quad (23)$$

so that

$$u(E, \mathbf{r}) = \frac{1}{\dot{E}} \int dE'\, q(E')\, f(\xi, \mathbf{r}) \; , \quad (24)$$

where

$$f(\xi, \mathbf{r}) = \int d^3 r' \frac{e^{-|\mathbf{r}-\mathbf{r}'|^2/4D\tau}}{(4\pi D\tau)^{3/2}} \rho(\mathbf{r}') \; , \quad (25)$$

and

$$\xi = \frac{\tau}{a^2/2D},$$

where a is the radius of the diffusing region (e.g., the galaxy).

A simplified result which at least qualitatively illustrates some features of the more exact solutions may be obtained by setting

$$\nabla \cdot (D\nabla u) = u/T .$$

In this case, $f(\xi) = e^{-\xi}$, and T is the time required for a cosmic ray to diffuse out of the galaxy. If ρ is the density of matter in interstellar space measured in gm/cm^2, we can define a path length $x = \rho cT$. Synchrotron and Compton energy losses can be combined by setting

$$\frac{d\gamma}{dt} = \kappa\gamma^2 .$$

The characteristic time for energy loss is then

$$\left(\frac{1}{\gamma}\frac{d\gamma}{dt}\right)^{-1} = (\kappa\gamma)^{-1} .$$

The solution of the diffusion equation now tells us that after a time T all electrons having energies greater than γ_0, where $\kappa\gamma_0 = 1/T$, will have lost a significant fraction of their energy. For the special case in which $Q \propto \gamma^{-n}$, the solution is illustrated in Figure 4.

The fact that no break in the measured electron spectrum is seen up to about 300 BeV indicates that $T \gtrsim 10^6$ years. Combining this information with estimates of the path length X determined from studies of the isotopes H^2 and He^3 as well as the nuclei Li, Be, and B, one

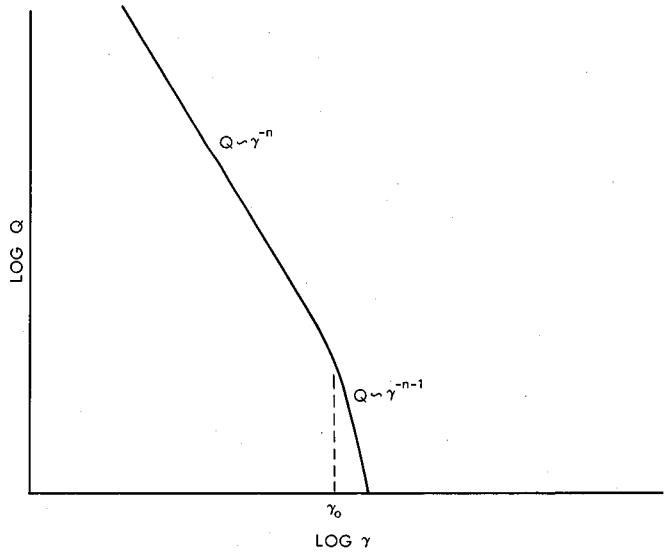

Figure 4–Solution to special case $Q \propto r^{-n}$.

finds that $\rho \approx 1 g/cm^2$. This indicates that the high-energy electrons must be confined in the galactic disk. Parker (Reference 4) arrived at a similar conclusion for the majority of cosmic rays from dynamical considerations of the cosmic rays and the interstellar gas and magnetic fields.

Other questions of astrophysical interest related to cosmic-ray electrons are the origin of the nonthermal radio background and the diffuse components of X- and gamma rays. These questions were not discussed in this lecture and the reader is referred to the references cited.

REFERENCES

1. Landau, L. D., and Lifshitz, E., "Classical Theory of Fields," Reading Mass.: Addison-Wesley, 1959.

2. Jones, F. C., "Inverse Compton Scattering of Cosmic Ray Electrons," Phys. Rev. 137:B1306, March 1965.

3. Ramaty, R., and Lingenfelter, R. E., "Solar Modulation and the Galactic Intensity of Cosmic-Ray Positrons and Negatrons," Phys. Rev. Letters 20:120, January 1968.

4. Parker, E. N., "The Dynamical State of the Interstellar Gas and Field," Astrophys. J. 154:57, 1968. (This article may be consulted for other works by Parker on Cosmic rays and the galaxy.)

BIBLIOGRAPHY

Felten, J. E., and Morrison, P., "Omnidirectional Inverse Compton and Synchrotron Radiation from Cosmic Distributions of Fast Electrons and Thermal Photons," Astrophys. J. 146:686, December 1966.

Ginzburg, V. L., and Syrovatskii, S. I., "The Origin of Cosmic Rays," New York: Pergamon Press, MacMillan Co., 1964.

Jackson, J. D., "Classical Electrodynamics," New York: Wiley and Sons, 1962.

Ramaty, R., and Lingenfelter, R. E., "Galactic Cosmic-Ray Electrons," J. Geophys. Res. 71(15):3687, August 1966.

Schott, G. A., "Electromagnetic Radiation and the Mechanical Reactions Arising from It," Cambridge: University Press, 1912.

Schwinger, J., "On the Classical Radiation of Accelerated Electrons," Phys. Rev. 75:1912, June 1949.

Takakura, J., and Keizo, K., "Spectra of Solar Radio Type IV Bursts," Publ. Astron. Soc. Japan 13:94, 1961.

Verma, S., "High Energy Electrons and Emission of the Omnidirectional Synchrotron Radiation in Radio-Frequency and X-Ray Regions," Astrophys. J. 152:537, May 1968.

IV. COSMIC-RAY PHOTONS

E. Boldt
NASA Goddard Space Flight Center
Greenbelt, Maryland

THERMAL SOURCES

Unlike laboratory situations in physics observations, photon astrophysics is limited to remote observations without the experimental capability of controlling and perturbing the physical conditions being investigated. Hence, we shall attempt to interpret the production and propagation of the photons of astronomy in terms of processes already examined in the laboratory (e.g., synchrontron, bremsstrahlung, and black-body radiation; Compton scattering, photoelectric absorption, etc.).

The source of the most intense flux of cosmic photons observed at the earth is the sun. For wavelengths from $\sim 10^3$Å to 1 cm, this source appears as a black body of $T \approx 6 \times 10^3$°K. The spectrum peaks in the visible region, where the earth's atmosphere is relatively transparent. For radio waves exceeding ~1 cm wavelength, the intensity exceeds that of a black body at 6×10^3°K and approaches that of a black body at 10^6°K for very long wavelengths (greater than ~1m). The emission in the ultraviolet ($\lesssim 10^3$Å) and X-ray regions ($< 10^2$Å) also exceeds that of a black body at 6×10^3°K but does not, in fact, follow a black-body spectrum at an elevated temperature. The X-ray emission from the quiet sun indicates a hot ($\gtrsim 10^6$°K), transparent thermal electron plasma; solar flares emit hard X-rays ($\gtrsim$10 keV). In no instances have solar gamma rays ($\gtrsim$MeV photons) yet been observed.

Since thermal radiation appears to be an important astrophysical phenomenon, it is useful to relate observations to the black-body model. The number of photons N per degree of freedom within a volume Γ of phase space is given by

$$N = \int_{\Gamma} \frac{f(\mathbf{p}, \mathbf{x})\, d^3\mathbf{p}\, d^3\mathbf{x}}{h^3}, \tag{1}$$

where **p** and **x** are the photon momentum and position vectors, respectively, and h is Planck's constant. The function f(**p**, **x**) is the distribution function for the photons of a disordered (e.g., thermal) radiation field, obeying Bose statistics. There are two degrees of freedom, one for each of the two spin states available to a photon. If we consider a small region Γ in the vicinity of (**p**, **x**) and measure N in several temporally separate, independent observations, we obtain

$$\frac{\left\langle \left(N - \langle N \rangle \right)^2 \right\rangle}{\langle (N) \rangle} = 1 + f(\mathbf{p}, \mathbf{x}) \ . \tag{2}$$

From Equation 2 we note that thermal photon fluctuations are somewhat similar to what would be expected from the classical statistics associated with particle counting but are in fact always greater by an amount given by f. This dual behavior for the statistics of photons, whereby they behave somewhat as particles on one hand, but yet exhibit the "bunching" characteristic of wave interference on the other hand, was first noted by Einstein for the black-body distribution function, viz:

$$f_B = \frac{1}{\left[\exp\left(h\nu/kT \right) - 1 \right]} \ . \tag{3}$$

For this black-body distribution function, the photon bunching (Equation 2) exhibits two interesting limits as follows:

$$\frac{\left\langle \left(N - \langle N \rangle \right)^2 \right\rangle}{\langle N \rangle} \to 1 \qquad \left(\text{for} \left[\frac{h\nu}{kT} \right] \gg 1 \right) , \tag{4a}$$

$$\frac{\left\langle \left(N - \langle N \rangle \right)^2 \right\rangle}{\langle N \rangle} \to \frac{kT}{h\nu} \qquad \left(\text{for} \left[\frac{h\nu}{kT} \right] \ll 1 \right) . \tag{4b}$$

Table 1 summarizes the amount of photon bunching at various characteristic wavelengths for several important astronomical sources ranging from the 3°K universal microwave background radiation to the 10^6 °K radio emission of the sun. For this range, there is appreciable bunching for $\lambda > 1$ cm and almost none at shorter wavelengths (e.g.,

Table 1. Photon Bunching, $\left\langle \left(N - \langle N \rangle \right)^2 \right\rangle \Big/ \langle N \rangle$

Radiation field	kT (eV)	Wavelength				
		5×10^3 Å	10^{-2} cm	1 cm	21 cm	1 m
Universal microwave (3°K)	3×10^{-4}		(1)	(3)	(40)	
Interstellar hydrogen (100°K) (21 cm)	9×10^{-3}				(10^3)	
Optical sun (6×10^3°K)	5×10^{-1}	(1.01)		(4×10^3)		
Optical B-star (14×10^3°K)	1	(1.2)		(10^4)		
Radio sun (10^6°K)	90					(9×10^7)
Photon energy		3 eV	10^{-2} eV	10^{-4} eV	6×10^{-6} eV	10^{-6} eV

optical). Thus, there is a rather clear separation here between (1) radio astronomy as a carrier of wave information about the radiation field observed, and (2) optical and X-ray astronomy as a carrier of particle-type information, in the sense that each observed quantum is statistically independent of all others. For a nonequilibrium radiation field, the photon bunching may be very different from that for a thermal field. As an example of a nonequilibrium field, consider an ideal laser and note that in this extreme case we recover classical particle behavior in the sense that

$$\frac{\left\langle \left(N - \langle N \rangle \right)^2 \right\rangle}{\langle N \rangle} = 1 , \tag{5}$$

even though the number of photons within a single cell $\left(h^3\right)$ of phase space could be $>10^{10}$.

From Equation 1, we may construct the photon intensity of a radiation field as

$$\frac{dJ}{d|\mathbf{p}|} = \frac{2cp^2 f}{h^3} \text{ photons/(area-time-solid angle-unit } |\mathbf{p}|) . \tag{6}$$

The spectral intensity is then obtained as

$$I_\nu = (h\nu) \frac{dJ}{d\nu} = \frac{2h\nu^3 f}{c^2} . \tag{7}$$

For a black body (Equation 3), the spectral intensity (Equation 7) becomes

$$I_\nu = \frac{2h\nu^3}{c^2} \Big/ \left[\exp\left(+h\nu/kT\right) - 1 \right] , \tag{8a}$$

$$I_\nu \approx \left(\frac{2h\nu^3}{c^2} \right) \exp\left(-h\nu/kT\right) \qquad \left(\text{as } \frac{h\nu}{kT} \to \infty \right) , \tag{8b}$$

$$I_\nu \approx \left(\frac{2h\nu^3}{c^2}\right)\frac{kT}{h\nu} = \frac{2kT}{\lambda^2} \qquad \left(\text{as } \frac{h\nu}{kT} \to 0\right) . \tag{8c}$$

Equation 8c is the Rayleigh-Jeans limit. The "brightness" temperature (T_B) to be associated with an observed spectral intensity I_ν is given via Equation 8 as

$$kT_B = \frac{h\nu}{\ln\left(\frac{2\,h\nu^3}{c^2\,I_\nu} + 1\right)} \qquad (\text{all } h\nu) , \tag{9a}$$

$$kT_B \approx \frac{I_\nu}{2}\lambda^2 \qquad \left(\text{for } \frac{h\nu^3}{c^2\,I_\nu} \ll 1\right) . \tag{9b}$$

If in fact the observed source is thermal and the observations are in the regime $(kT/h\nu) \gg 1$, then Equation 9b is an appropriate approximation, the one usually used in radio astronomy, and there should be an appreciable bunching of photons given via Equation 4b as

$$\frac{\left\langle\left(N - \langle N\rangle\right)^2\right\rangle}{\langle N\rangle} = \frac{kT}{h\nu} = \frac{c^2\,I_\nu}{2\,h\nu^3} . \tag{10}$$

In the other extreme, if one inadvertently attributes a brightness temperature to a laser source, then the lack of photon bunching would indicate a nonequilibrium aspect of the source. Thus, for the radio astronomy regime $\left(c^2\,I_\nu \gg h\nu^3\right)$, we can identify a thermal source by observing over a narrow band at ν and comparing the measures of photon bunching and I_ν with the relation fixed by Equation 10. For the optical and X-ray regime, this thermal identification at a spectral point is unavailable in most instances.

For a black-body source, the measured brightness temperature is of course independent of the observed wavelength. For the observed extended sources of radio-emission (e.g., Galaxy, M31, Cas A, Cent A), the brightness temperature generally decreases as the observed wavelength decreases. Two notable exceptions to this are (1) the universal microwave background, which exhibits an apparently constant brightness

temperature of ~3°K over almost two decades of wavelength, and (2) the sun, which gives a rather constant 10^6°K for wavelengths longer than 1 meter.

What is the brightness temperature of the Crab Nebula in the X-ray region? To evaluate this, we use the recently obtained X-ray information that

$$I_\nu \simeq \frac{10^{11}}{\nu} \frac{\text{eV}}{\left(\text{Hz - cm}^2\text{-sec-sr}\right)} \tag{11}$$

over a solid angle $\approx 10^{-7}$ sr.

Using Equation 11 in Equation 9a, we obtain for the Crab Nebula

$$\frac{h\nu}{kT} = \approx 60 \qquad (\text{at } \lambda \approx 1\text{Å}) \ . \tag{12}$$

If the Crab is a thermal source of X-rays then, from Equation 12, we note that it is definitely in the particle (i.e., nonbunching photons) regime at a high brightness temperature ($T \gtrsim 10^6$°K). As we shall discuss later, the X-ray spectrum of the Crab (Equation 11) is not of the form expected for an isothermal source, be it a black body or a transparent, hot plasma radiating via the bremsstrahlung mechanism.

The sun and Sco X-1, the brightest X-ray star yet observed, both exhibit X-ray spectra consistent with that expected from hot thermal plasmas at $\gtrsim 10^6$°K and $\gtrsim 10^7$°K, respectively. The photon distribution function f inferred from Equation 7 is definitely much less than unity for the solar X-rays, indicating that even for a clearly thermal source the X-rays are again in the particle regime; the corresponding analysis for Sco X-1 still lacks the information required on the lower limit to the angular size.

For a black body, the isotropic intensity I of energy is

$$I = \frac{\sigma T^4}{\pi} , \tag{13}$$

where σ = Stefan-Boltzmann constant.

Table 2 shows the total output for several objects of interest. For black-body radiation, Equation 13 was used to evaluate $(2\pi r)^2 I$ for the total optical output of the sun, with r as the solar radius, and for the total microwave power exchanged by the galaxy over the spherical halo ($r \simeq 10^{23}$ cm). Although at only 3°K, the galactic microwave power equals the optical power output for $\sim 10^{11}$ suns at a black-body temperature of 6×10^3°K. The sun and Sco X-1 are probably both thermal X-ray sources, but the output of Sco X-1 equals that of $\sim 10^{13}$ suns as far as X-rays are concerned. These comparisons illustrate the wide range of thermal situations that obtain in astrophysics.

Table 2. Source Strengths

Source	Output (ergs/sec)
X-ray sun (Thermal plasma $\gtrsim 10^6$°K)	10^{23}
Optical sun (Black body, 6×10^3°K)	4×10^{33}
Sco X-1 (Optical, blue star)	$\sim 10^{33}$
Sco X-1 (X-rays, thermal plasma, $\gtrsim 10^7$°K)	$\sim 10^{36}$
Crab Nebula (Radio and optical, synchrotron radiation)	$\sim 10^{36}$
Crab Nebula (X-rays)	$\sim 10^{37}$
Galactic microwave (3°K black body)	6×10^{44}

The observed apparent brightness temperature of the Crab ($T_B \gtrsim 10^6$°K for X-rays) may be used to calculate I, via Equation 13. Comparing the integrated X-ray flux from the Crab (see Table 2) with

$(2\pi r)^2 I$ fixes the radius r to be associated with a black-body source as $r \approx 10^8$ cm (i.e., smaller than the earth) whereas X-ray observations clearly indicate a size comparable to a light year. This rules out black-body emission for the bulk of the X-rays from the Crab Nebula.

The black-body photons of the microwave background and starlight constitute scatterers for high-energy charged particles, as we shall describe later. The scattered photons may then become energetic enough to be called X-rays. We shall find it useful to relate the energy of the photons of the black-body target with the temperature by noting that

$$\langle h\nu \rangle = 2.7 \text{ kT} \tag{14}$$

and, from Wien's Displacement Law, that the maximum I_ν occurs at

$$\left(I_\nu\right)_m = 2.8 \text{ kT} . \tag{15}$$

It is also important, in considering the black body as a target, to specify the spatial number density n of photons, given by

$$n = \frac{4\pi I}{\langle h\nu \rangle c} \sim 20 \cdot T^3 , \tag{16}$$

where n is in cm^{-3}, and T is in °K. Values of photon density for the microwave background, visible light, and X-rays in various astronomical regions of interest are listed in Table 3.

Table 3. Photon Density (cm^{-3})

Radiation field	Galaxy	Crab Nebula	Sun
Microwave background (3°K black body)	5×10^2	5×10^2	5×10^2
Optical	1	10^2	4×10^{12}
X-rays	10^{-8}	10^{-1}	1

NONEQUILIBRIUM RADIATION PROCESSES

The photon source function q at $h\nu$ for radiating charged particles in space is

$$q\left(\text{photons/cm}^3\text{-sec-erg}\right) = \frac{1}{(h\nu)}\int\left[\frac{d}{dh\nu}\left(\frac{dW}{dt}\right)\right]\left[\frac{d}{dW}\left(\frac{d^3N}{dx^3}\right)\right]dW \quad , \tag{17}$$

where W is the kinetic energy of the radiating particle, and N is the number of radiating particles.

The observed photon flux is

$$J\left(\text{photons/cm}^2\text{-sec-sr-erg}\right) = \frac{1}{4\pi}\int_0^\infty q\,dr \quad , \tag{18}$$

where r is the radial distance from the observer in the direction of the observed flux.

The central problem then is to define the charged-particle population and the radiation losses. The interaction of an electron with its electromagnetic environment causes radiation loss as follows:

$$\frac{-dW}{dt} = v\sigma_0\, n_\nu \left\langle h\nu \right\rangle \quad , \tag{19}$$

where $\langle h\nu \rangle$ is the mean energy of radiated photons, v is the electron velocity, σ_0 is the Thompson cross-section, and n_ν is the number density of effective target quanta in the ambient electromagnetic environment.

The starting point of this analysis is the relativistic classical radiation law (e.g., Reference 1, Equation 9-72), viz:

$$\frac{-dW}{dt} = \frac{2}{3}\, r_e^2\left[\left(\mathbf{E} + \frac{\mathbf{v}}{c}\times\mathbf{H}\right)^2 - \frac{1}{c^2}\,(\mathbf{E}\cdot\mathbf{v})^2\right]\gamma^2 c \quad , \tag{20}$$

where r_e is the classical electron radius, and $\gamma^{-2} = 1 - (v/c)^2$.

An environment of plane electromagnetic waves corresponds to

$$\mathbf{H} = \mathbf{n} \times \mathbf{E} , \tag{21a}$$

$$\mathbf{n} \cdot \mathbf{E} = 0 , \tag{21b}$$

$$E^2 = H^2 , \tag{21c}$$

where $\mathbf{n}$ is a unit vector along $\mathbf{E} \times \mathbf{H}$.

We consider the case where the vectors ($\mathbf{n}$) are randomly oriented, for which we have

$$\langle \mathbf{n} \cdot \mathbf{v} \rangle = 0 . \tag{22}$$

This prescription (Equations 21 and 22) allows an evaluation of Equation 20 as

$$\left(\frac{-dW}{dt}\right)_{EH} = \sigma_0 \, c(\rho)_{EH} \left(1 + \frac{\beta^2}{3}\right) \gamma^2 , \tag{23}$$

where

$$(\rho)_{EH} = \frac{H^2 + E^2}{8\pi} = \frac{E^2}{4\pi} = \frac{H^2}{4\pi} .$$

In the relativistic limit, we have

$$\left(\frac{-dW}{dt}\right)_{EH} \rightarrow \frac{4}{3} \sigma_0 \, c(\rho)_{EH} \gamma^2 . \tag{24}$$

For a radiation field environment consisting of quanta of average energy $\epsilon \equiv (\rho/n_\nu)$, a comparison of Equation 24 with Equation 19 shows

that, in the relativistic limit,

$$\langle h\nu \rangle = \frac{4}{3} \gamma^2 \epsilon \ . \tag{25}$$

This relation, between the mean energy of the radiated photon and that of the quanta of the medium, describes what is known as inverse Compton scattering. The soft quanta of the environment are typically optical starlight and radio waves; these serve as targets for high-energy electrons.

Another case of great astrophysical importance corresponds to a finite H field and no E field (i.e., E = 0); this is the condition for magnetic bremsstrahlung ("synchrontron radiation"). We obtain, from Equation 20,

$$\left(\frac{-dW}{dt}\right)_H = \frac{2}{3} r_e^{\,2} c\beta^2 \gamma^2 H^2 \ , \tag{26}$$

where

$$(H_\perp)^2 \equiv \frac{(\mathbf{v} \times \mathbf{H})^2}{v^2} \ .$$

For the situation of random field orientations, we use

$$H_\perp^2 = \frac{2}{3} H^2 \ . \tag{27}$$

We note that

$$\rho_H = H^2/8\pi \ . \tag{28}$$

Then, from Equations 26, 27, and 28, we obtain

$$\left(\frac{-dW}{dt}\right)_H = \frac{4}{3}\sigma_0 c(\rho)_H \gamma^2 \beta^2 , \tag{29a}$$

$$\left(\frac{-dW}{dt}\right)_H \rightarrow \frac{4}{3}\sigma_0 c(\rho)_H \gamma^2 \qquad \text{as } \beta \rightarrow 1 . \tag{29b}$$

It is important to recognize that this radiation loss formula (Equation 29b) for synchrotron emission is identical to that for inverse Compton losses (Equation 24) in the ultrarelativistic regime, when we exchange $(\rho)_H$ and $(\rho)_{EH}$.

From Equations 19 and 29a, we identify

$$\langle h\nu \rangle = \frac{4}{3}\gamma^2 \beta \epsilon , \tag{30}$$

where $\epsilon \equiv (\rho)_H / n_\nu$.

In the nonrelativistic limit, for cyclotron radiation, the radiated photon energy is

$$\langle h\nu \rangle = h\nu = \hbar \frac{e}{mc} H_\perp . \tag{31}$$

Using Equations 31 and 30 for $\gamma \rightarrow 1$ prescribes ϵ, as

$$\epsilon = \frac{3}{4} \frac{\left(\hbar \frac{e}{mc} H_\perp\right)}{\beta} . \tag{32}$$

Inserting Equation 32 into Equation 30 yields a general expression for the mean radiated photon energy as

$$\langle h\nu \rangle = \gamma^2 \hbar \frac{e}{m} H_\perp . \tag{33}$$

For the ultrarelativistic situation, the photon energy at the peak of intensity is $\sim 0.3 \langle h\nu \rangle$ (see Reference 2).

For an electric field alone (H = 0), we have the condition for bremsstrahlung radiation, and Equation 20 gives

$$\left(\frac{dW}{dt}\right)_E = 2\sigma_0 \, c(\rho)_E \left(1 - \frac{\beta^2}{3}\right)\gamma^2 , \tag{34}$$

where we have again considered a randomly oriented field for which

$$\langle \cos^2 \theta \rangle = \frac{1}{3} ,$$

where θ is the angle defined by **E** and **v**.

We consider that the electric field arises from a number density n_0 of discrete charges Ze that may be localized to within an impact parameter b. Therefore, we construct the electrostatic energy density ρ_E required for Equation 34 as follows:

$$\rho_E = n_0 \left(\int_b^\infty \frac{\left(Ze/r^2\right)^2}{8\pi} \, 4\pi r^2 \, dr \right) . \tag{35}$$

The smallest impact parameter b, for localization of the charge, is given by wave mechanics according to the prescription

$$b = \lambda/4 , \tag{36}$$

where $\lambda = h/(mv)$. Insertion of Equation 36 into Equation 35 yields

$$\rho_E = \frac{\alpha Z^2}{\pi} \, mc^2 \beta n_0 , \tag{37}$$

where $\alpha \equiv e^2/\hbar c = 1/137$. Using ρ_E in the nonrelativistic limit ($\beta \to 0$, $\gamma \to 1$) of Equation 34 yields

$$\left(\frac{-dW}{dt}\right)_E = \frac{16}{3}\,\alpha Z^2\, r_e^{\,2}\left(m_0\, c^2\right)\beta\, c n_0 \;. \qquad \text{NR} \tag{38}$$

This is the same as the nonrelativistic (NR) expression given by Heitler (Reference 3); the extreme-relativistic (ER) expression is given by Heitler as

$$\left(\frac{-dW}{dt}\right)_E = 4\alpha Z^2\, r_e^{\,2}\left(m_0\, c^2\right)\gamma\, c n_0\left[\ell n\left(183\, Z^{-1/3}\right) + \frac{1}{18}\right]. \qquad \text{ER} \tag{39}$$

The conventional approximation to $\langle h\nu \rangle$ is

$$\langle h\nu \rangle \doteq \frac{1}{2}\, W \;. \tag{40}$$

Comparing Equation 38 with Equation 19, using the identification (Equation 40) for $\langle h\nu \rangle$, gives

$$n_\nu = \frac{8\alpha}{\pi}\frac{n_0}{\beta^2} \;. \tag{41}$$

Table 4 summarizes the relevant parameters for electron radiation losses by synchrotron emission, inverse Compton scattering, and bremsstrahlung radiation, as described earlier. The numerical values for these parameters for two important extended regions, the Crab Nebula and the galaxy, are listed in Table 5. The equivalent kinetic temperature T_k and black-body temperature T_B are defined also in Table 5 for each of the electromagnetic states described for the environment. For all the astronomical situations enumerated in Table 5, the equivalent black-body temperature is always the order of 10°K, whereas the equivalent kinetic temperature varies by more than 17 orders of magnitude. The electromagnetic state listed as "Coulomb"

Table 4. Review of Some Radiation Mechanisms

$\left[\text{Radiation Loss Formulation: } -(dW/dt) = v\sigma_0(\rho/\epsilon)\langle h\nu\rangle.\right]$

Parameter	Synchrotron (ultrarelativistic)	Inverse Compton (ultrarelativistic; for black body)	Bremsstrahlung (nonrelativistic)
$\langle h\nu\rangle$	$\frac{4}{3}\gamma^2\epsilon$	$\frac{4}{3}\gamma^2\epsilon$	$\frac{1}{2}W$
ϵ	$\frac{3}{4}\hbar\frac{e}{mc}H_\perp$	$2.7\ kT$	$\frac{\beta}{4}W$
ρ	$H^2/8\pi$	$4\sigma T^4/c$	$\frac{(\alpha Z^2)\beta n_0}{\pi}(m_0c^2)$
$\Lambda \equiv \frac{-(dW/dt)}{W}$	$\frac{4}{3}\sigma_0 c\gamma\left(\frac{\rho_H}{m_0c^2}\right)$	$\frac{4}{3}\sigma_0 c\gamma\left(\frac{\rho_{EH}}{m_0c^2}\right)$	$\frac{4}{\pi}\sigma_0 c\frac{(\alpha Z^2)}{\beta}n_0$

refers to the electrostatic fields generated by the indicated astronomical proton gas, which constitutes the bremsstrahlung target.

The decay constants Λ for the various radiation-loss mechanisms that occur for electrons are presented in Table 4, and the numerical values for the corresponding lifetimes (i.e., Λ^{-1}) are listed for many situations of interest along with the value of γ required in each instance to obtain radiation in the X-ray region (i.e., $\sim$1Å).

The favored process for radiative loss in the Crab Nebula is obtained from inspection of Table 6, which indicates that the lifetime of a 10^{13} eV electron for synchrotron X-ray emission is only about 1 year. As indicated in Table 6, the lifetime is proportional to γ^{-1}. Hence, for a lifetime comparable to the age of the Crab Nebula ($\sim 10^3$ years), it is necessary for an electron to have an energy $\leq 10^{10}$ eV. Since the average energy of a synchrotron-radiated photon is proportional to γ^2, an electron of 10^{10} eV corresponds to photons in the far infrared. This is the region where the observed electromagnetic spectrum of the Crab Nebula exhibits a change in spectral index. Hence, the break in the

Table 5. Some Astronomical Photon Gases and Fields

Electromagnetic state	Quanta			Kinetic temp. (equivalent) $T_k = \epsilon/2.7k$ (°K)	Black body temp. (equivalent) $T_B = (\rho c/4\sigma)^{1/4}$ (°K)
	ϵ (eV/photon)	ρ (eV/cm^3)	$n_\nu = (\rho/\epsilon)$ (photon/cm^3)		
X-ray photons (~1Å)					
Galaxy	10^4	10^{-5}	10^{-9}	4×10^7	0.2
Crab	10^4	10^3	10^{-1}	4×10^7	20
Magnetic					
Galaxy (5×10^{-6} G)	5×10^{-14}	1	10^{13}	10^{-10}	3
Crab (10^{-3} G)	10^{-11}	4×10^4	10^{15}	10^{-8}	40
Optical photons (~6×10^3Å)					
Galaxy	2	1	0.5	10^4	3
Crab	2	10^2	50	10^4	10
Microwave background					
Universal (3°K)	7×10^{-4}	1	10^3	3	3
Coulomb					
Galaxy ($n_0 \approx 1/\text{cm}^3$)	$\beta W/4$	$10^3\beta$	$4 \times 10^3/W$	$\beta W/(11k)$	$\sim 20\beta^{1/4}$
Crab ($n_0 \approx 1/\text{cm}^3$)	$\beta W/4$	$10^3\beta$	$4 \times 10^3/W$	$\beta W/(11k)$	$\sim 20\beta^{1/4}$

Table 6. Conditions Required for X-ray (~1Å) Production Mechanisms in Extended Sources, and Associated Lifetimes

Extended source	Synchrotron			Inverse Compton						Bremsstrahlung		
				Optical field			Microwave field					
	Required electron		$1/\Lambda_H$ (years)	Required electron		$1/\Lambda_{EH}$ (years)	Required electron		$1/\Lambda_{EH}$ (years)	Required electron		$1/\Lambda_E$ (years)
	γ	n_e (cm^{-3})		γ	n_e (cm^{-3})		γ	n_e (cm^{-3})		β	n_e (cm^{-3})	
Crab Nebula (~10^{18} cm)	10^7	10^{-10}	1	10^2	10^3	10^7	10^4	10^{-6}	10^7	0.3	10^7	10^3
Galaxy (~10^{23} cm)	10^8	10^{-21}	10^4	10^2	10^{-8}	10^9	10^4	10^{-11}	10^7	0.3	10^{-6}	10^3

spectrum appears to be consistent with the synchrotron picture, but the extremely short lifetime for X-ray synchrotron emission would require much continuous activity within the remnant, persisting $\sim 10^3$ years after the supernova.

We consider now the spatial density n_x of X-rays generated by electrons of density n_e within a spherical region (radius R) of space, interacting with the environmental field quanta (density n_ν) of that region. From Equations 17, 18, and 20, we obtain that at the origin

$$n_x = \left(\frac{4\pi}{c}\right) \int_0^R \frac{(h\nu)\, J d\,(h\nu)}{\langle h\nu \rangle} \approx \sigma_0 R \left(\langle n_e n_\nu \rangle\right) \beta \,, \tag{42}$$

where

$$\langle n_e n_\nu \rangle \equiv R^{-1} \left(\int_0^R n_e n_\nu \, dr \right) .$$

Taking $R \approx 10^{18}$ cm for the Crab Nebula and $R \approx 10^{23}$ cm for the galaxy, the electron concentration n_e that is required for the observed diffuse X-ray density within each of these source regions may be calculated by using Equation 42 with the n_ν appropriate to the radiation interaction considered (see Table 5 for numerical values of n_ν). As shown in Table 5, the X-ray photon densities n_x within the Crab Nebula and the galaxy are $\sim 10^{-1}/\text{cm}^3$ and $10^{-9}/\text{cm}^3$, respectively; these are the numbers used in Equation 42 for evaluating the magnitudes of n_e listed in Table 6.

By inspecting Table 6, we infer that the energy density for electrons of $\sim 10^{13}$ eV in the Crab Nebula which would be responsible for X-ray emission by synchrotron radiation amounts to ~ 1 percent of the energy density in the magnetic field itself. The energy density for the electrons of $\sim 10^{10}$ eV required for X-ray production by inverse Compton scattering of the microwave background is ~ 10 percent of the energy density of the magnetic field confining the electrons. However, such a density of $\sim 10^{10}$ eV electrons would synchrotron-radiate more photons in the radio band than observed. The electron number density

required for bremsstrahlung generation of the X-rays of the Crab Nebula is prohibitively high for such an extended source. Although it appears from this analysis that synchrotron radiation is likely, probably the only unambiguous way to establish synchrotron radiation as the dominant X-ray-generating mechanism of the Crab Nebula is through a definitive measurement of the X-ray polarization.

For the galaxy, Table 6 indicates that electrons of $\sim 10^{14}$ eV at an energy density of $\sim 10^{-7}$ eV/cm^3 would give sufficient radiation by the synchrotron process; this density is higher than direct cosmic-ray electron measurements at lower energies would suggest. Inverse Compton scattering by the microwave background would require electrons of $\sim 10^{10}$ eV at $\sim 10^{-1}$ eV/cm^3—again too high. Inverse Compton scattering by starlight would require electrons of $\sim 10^8$ eV at an energy density of ~ 1 eV/cm^3—too high again. Electrons of $\sim 10^4$ eV would generate sufficient galactic X-rays by bremsstrahlung for an electron energy density of $\sim 10^{-2}$ eV/cm^3, comparable to the kinetic energy density for the interstellar hydrogen gas. The effect of X-ray generation in the metagalaxy has not been considered here, but could be important.

SPECTRA

The spectral representations for the radiation-loss mechanisms of bremsstrahlung, inverse Compton scattering, and synchrotron emission are approximated as follows:

Bremsstrahlung:

$$\frac{d}{dh\nu}\left(\frac{dW}{dt}\right)_E \approx \left(\frac{dW}{dt}\right)_E \Big/ W \ . \tag{43}$$

Inverse Compton:

$$\frac{d}{dh\nu}\left(\frac{dW}{dt}\right)_{EH} \approx \left(\frac{dW}{dt}\right)_E \left[\delta\left(h\nu - \frac{4}{3}\gamma^2 \epsilon\right)\right] \ . \tag{44}$$

Synchrotron:

$$\frac{d}{dh\nu}\left(\frac{dW}{dt}\right)_H \approx \left(\frac{dW}{dt}\right)_H \left[\delta\left(h\nu - 0.3\gamma^2 \epsilon\right)\right] \ . \tag{45}$$

(For a discussion of the approximation given by Equation 45, see Reference 2.)

We may now construct the photon source functions for bremsstrahlung, inverse Compton, and synchrotron radiation by evaluating Equation 17 for Equations 43, 44, and 45, respectively, using the basic radiation loss formula (Equation 19):

$$q_E = \frac{c\,\sigma_0 \langle h\nu \rangle}{h\nu} \int_{h\nu}^{\infty} n_\nu \frac{d}{dW}\left(\frac{d^3 N}{dx^3}\right) \frac{dW}{W} , \tag{46}$$

where $\langle h\nu \rangle = W/2$ (see Equation 40) and $n_\nu = 8\alpha/\pi \left(n_0/\beta^2\right)$ (see Equation 41);

$$q_{EH} = c\,\sigma_0\, n_\nu \left(\frac{dW}{dh\nu}\right) \frac{d}{dW}\left(\frac{d^3 N}{dx^3}\right) , \tag{47}$$

where

$$\gamma^2 = \frac{3}{4}\,(h\nu/\epsilon) \;;$$

and

$$q_H = c\,\sigma_0\, n_\nu \left(\frac{dW}{dh\nu}\right) \frac{d}{dW}\left(\frac{d^3 N}{dx^3}\right) , \tag{48}$$

where

$$\gamma^2 \approx 3(h\nu/\epsilon) \quad \text{and} \quad \epsilon = \frac{3}{4}\,\hbar\,\frac{e}{m}\,H_\perp \,.$$

We examine here the functional dependence of q on photon energy for the case of a power-law electron distribution:

$$\frac{d}{W}\left(\frac{d^3 N}{dx^3}\right) \propto W^{-n} \quad . \tag{49}$$

Using Equation 49 for q as given by Equations 46, 47, and 48 gives

$$q_E \propto (h\nu)^{-n} \quad , \tag{50}$$

$$q_{EH} \propto (h\nu)^{-(n+1)/2} \quad , \tag{51}$$

$$q_H \propto (h\nu)^{-(n+1)/2} \quad . \tag{52}$$

It is interesting to note that the power law index for relativistic, charged cosmic rays is observed to be $n \approx 5/2$, and the diffuse cosmic photon spectrum exhibits a power law above 10^4 eV of index ~ 2. These observations are then spectrally consistent with the emission mechanisms of synchrotron radiation and inverse Compton scattering as indicated in Equations 51 and 52 where $(n + 1)/2 \approx 2$, for $n \gtrsim 5/2$. The X-ray spectrum of the Crab Nebula also exhibits a power law spectrum of index 2.

Another electron spectrum of astrophysical interest is that for a thermal gas, viz:

$$\frac{d}{dW}\left(\frac{d^3 N}{dx^3}\right) \propto (W)^{1/2} \exp(-W/kT) \quad , \tag{53}$$

where T is the kinetic temperature for the Maxwellian distribution. These hot electrons will radiate by bremsstrahlung collisions with the atoms and positive ions of the gas. If one uses the Maxwellian

distribution for electrons in evaluating q_E, then

$$q_E = \frac{2}{\sqrt{\pi}} (n_e)(n_0) \alpha Z^2 \left[\frac{c \sigma_0 g}{h\nu} \left(\frac{m_0 c^2}{\frac{3}{2} kT} \right) \exp\left(-\frac{h\nu}{kT}\right) \right], \tag{54}$$

where n_e and n_0 are the number densities of electrons and ions (charge Ze), respectively.

The quantity g in Equation 54 is the free-free Gaunt factor, which is about unity for most atoms, and which is given explicitly for hydrogen by

$$g = \frac{\sqrt{3}}{\pi} \left[\exp(h\nu/2kT)\right] K_0(h\nu/2kT) , \tag{55}$$

where $K_0(x)$ is the modified Bessel function of second kind (Drummond, 1961). The total power radiated per unit volume by thermal bremsstrahlung is obtained by integrating q_E as given by Equation 54 over all photon energies and yields

$$\int_0^\infty (h\nu)\, q_E\, dh\nu = 14 \times 10^{-24}\, n_e\, n_0\, g \left(\frac{T}{10^8}\right)^{1/2} \frac{\text{ergs}}{\text{cm}^3\ \text{sec}} , \tag{56}$$

where T is in °K.

As an example of a thermal source, consider the X-ray star Sco X-1, which exhibits a spectrum of the form (Equation 54) to be expected from a transparent thermal plasma at $T \lesssim 10^8$°K. The total output in X-rays is estimated as $\sim 10^{36}$ ergs/sec. If we take the volume as comparable to the sun ($\sim 10^{33}$ cm^3), we may use Equation 56 to evaluate $(n_e n_0)$ as $\sim 10^{26}$ cm^{-6}. For the case $n_e = n_0$, the number density of electrons and ions in this hot gas is $\sim 10^{13}$ cm^{-3}.

Now that the thermal state of Sco X-1 has been specified, we may test if the associated hot plasma is indeed transparent. To do this, we

need the absorption cross-section (σ_a), which may be obtained from Kirchhoff's law:

$$q_E = c\,\sigma_2\, n_e\, B_\nu \ , \tag{57}$$

where B_ν is the number of photons per unit volume per unit photon energy interval for a black body at temperature T.

From Equations 1 and 3,

$$B_\nu = \frac{4\pi\,(h\nu)^2}{(hc)^3\left[\exp(h\nu/kT) - 1\right]} \ . \tag{58}$$

We may now evaluate the absorption mean free path $\left[\lambda \equiv (n\,\sigma_a)^{-1}\right]$ from Equations 54, 57, and 58 and obtain, for $h\nu \gtrsim kT$,

$$\lambda = \frac{4 \times 10^{38}}{gZ^2\, n_e\, n_0}\left(\frac{T}{10^8}\right)^{1/2}(h\nu)^3 \ , \tag{59}$$

where λ is in cm, $h\nu$ is in eV, n is in cm^{-3}, and T is in °K.

For X-ray emission (~1Å) from Sco X-1, we use Equation 59 to determine that $\lambda \gtrsim 10^{24}$ cm, which is larger than the galaxy. Hence, the plasma of Sco X-1 is transparent, and our picture remains consistent.

The dominant mechanism for X-ray absorption is the photoelectric effect. For light elements ($Z < 10$), the absorption length at the energy of the K-edge ($\lesssim$1 keV) is $\lesssim 10^{18}$ atoms/cm^2. For unit atom number density, this absorption length corresponds to 1 light year. Hence, photoelectric absorption by the interstellar medium causes an appreciable attenuation of stellar X-rays for energies less than 1 keV.

COSMIC PHOTONS FROM PROTON INTERACTIONS

X-Rays

In ionizing the atomic hydrogen of the interstellar gas, a cosmic-ray proton sometimes imparts appreciable energy to the ejected

electron; in such a case, the electron is called a "knock-on electron." This electron undergoes the acceleration required for attaining its exit velocity during the collision and therefore radiates through the bremsstrahlung mechanism, which in this instance is called "inner bremsstrahlung" (Reference 5). For nonrelativistic collisions, the energy imparted to an electron by a proton of kinetic energy U is limited by

$$W \leq 4\left(\frac{m_0}{M_0}\right)U \ , \tag{60}$$

where m_0 is the electron rest mass, and M_0 is the proton rest mass.

The source function for inner bremsstrahlung (q_I) is obtained from

$$h\nu\, q_I = n_0 \left\{ \int_{U=1/4(M_0/m_0)(h\nu)}^{\infty} dU \left(\frac{dn}{dU}\right) \beta_p\, c \left[\int_{W=h\nu}^{W=4(m_0/M_0)U} \left(\frac{dW}{dh\nu}\right)\left(\frac{d\sigma}{dW}\right) dW \right] \right\}, \tag{61}$$

where $dW/dh\nu$ gives the spectral energy radiation of the knock-on electron as

$$\frac{dW}{dh\nu} = \frac{2}{3}\frac{\alpha}{\pi}\left(\beta_e\right)^2 \ , \tag{62}$$

and $d\sigma/dW$ is the differential cross-section for producing a knock-on electron of kinetic energy W (velocity β_e) with a proton of kinetic energy U (velocity β_p); thus

$$\frac{d\sigma}{dW} = \frac{4\pi\left(r_e\right)^2}{\left(\beta_e\right)^2\left(\beta_p\right)^2 W} \ . \tag{63}$$

In Equation 61 dn/dU is the spatial spectral density of cosmic-ray protons at U, ionizing hydrogen gas of n_0 atoms per unit volume.

The inner integral of Equation 61 may be evaluated with Equations 62 and 63 as

$$\int_{W=h\nu}^{W=4(m_0/M_0)U} \left(\frac{dW}{dh\nu}\right)\left(\frac{d\sigma}{dW}\right) dW = \frac{\alpha}{\pi} \frac{\sigma_0 \ln\left(\frac{2m_0 c^2}{h\nu} \beta_p^2\right)}{(\beta_p)^2} . \tag{64}$$

This is similar in form to the expression for the ionization loss per unit path length dU/dx, given by

$$\frac{dU}{dx} = \frac{3}{2} n_0 \frac{\sigma_0 (m_0 c^2) \ln\left(\frac{2m_0 c^2}{I} \beta_p^2\right)}{(\beta_p)^2} , \tag{65}$$

where I is the ionization potential for the atom.

Using Equation 65 in Equation 61, via Equation 64, we obtain

$$(h\nu)\, q_I = \frac{8}{3} \frac{\alpha}{(m_0 c^2)} \left[\int_{U=(M_0/4m_0)h\nu}^{\infty} \frac{\ln\left(\frac{2m_0 c^2 \beta_p^2}{h\nu}\right)}{\ln\left(\frac{2m_0 c^2 \beta_p^2}{I}\right)} \frac{dJ}{dU} \frac{dU}{dx} dU \right] , \tag{66a}$$

$$(h\nu)\, q_I \approx \frac{8}{3} \frac{\alpha}{m_0 c^2} \left[\int_{U=(M_0/4m_0)h\nu}^{\infty} \left(\frac{dJ}{dU}\right)\left(\frac{dU}{dx}\right) dU \right] , \tag{66b}$$

where (dJ/dU) is the spectral intensity of cosmic-ray protons/(cm^2-sr-sec-eV).

This simple form (Equation 66b) for the inner bremsstrahlung source function allows us to make a comparison with the ionization energy dissipated per second per unit volume of the interstellar hydrogen

gas by all charged cosmic rays above energy U, defined by

$$Q = 4\pi \left[\int_U^\infty \left(\frac{dJ}{dU}\right)\left(\frac{dU}{dx}\right) dU \right] . \tag{67}$$

The Q required to keep the interstellar gas heated to the observed temperature of 100°K is $Q \approx 5 \times 10^{-14}$ eV/cm^3-sec, for a hydrogen density of 1 atom/cm^3. This heating is likely to arise from low-energy cosmic rays ($U \gtrsim 15$ MeV). (See Reference 6.)

We may write the source function for inner bremsstrahlung in terms of Q as follows:

$$(h\nu)\, q_I \approx \frac{2}{3}\frac{\alpha}{\pi}\frac{Q}{(m_0 c^2)} \quad \text{for} \quad h\nu \le \left(\frac{4m_0}{M_0}\right) U_0 , \tag{68}$$

where U_0 is the lowest cosmic-ray proton energy that makes an appreciable contribution to Q. Using $U_0 = 15 \times 10^6$ eV and $Q = 5 \times 10^{-14}$ eV/cm^3-sec, we obtain from Equation 68 that inner bremsstrahlung generation is $(h\nu\, q_I) \approx 10^{-22}$ eV/eV-cm^2-sec, for $h\nu \le (4m_0/M_0)\, U_0$ ($= 3 \times 10^4$ eV). For a direction that intercepts a depth ℓ of interstellar gas, the corresponding inner bremsstrahlung X-ray intensity I would be

$$I = \frac{\ell}{4\pi}\,(h\nu\, q_I)\,\frac{\text{eV}}{\text{eV cm}^2\text{-sec-sr}} . \tag{69}$$

For $\ell = 10^{23}$ cm, the diameter of the galactic disk, we get $I \approx 1$ eV/cm^2-sec-eV. This is comparable to the observed background flux at $h\nu \sim 30$ keV. If charged cosmic rays of $U \gtrsim 15$ MeV are indeed responsible for the heating of the interstellar gas, then we should be able to track the interstellar gas distribution with a significant component of the observed diffuse X-ray flux at ~30 keV. The spectral shape of this X-ray emission is an integral measure (Equation 66b) of the low-energy, charged cosmic-ray spectrum. Because of the drastic solar modulation of such low-energy cosmic rays, the inner bremsstrahlung

X-rays generated in interstellar hydrogen might provide the only available means for such spectroscopy.

Consider an interstellar charged, cosmic-ray spectrum of the form

$$\frac{dJ}{dU} \sim U^{-n} \quad . \tag{70}$$

Using Equations 70 and 65 in Equation 66b gives

$$(h\nu)\, q_I \sim (h\nu)^{-n} \quad . \tag{71}$$

These expressions (Equations 70 and 71) indicate the basic aspect of interstellar inner bremsstrahlung spectroscopy for charged cosmic rays at low energy.

Gamma Rays

At $U \gtrsim 1$ GeV, cosmic-ray protons produce pions via nuclear interactions with the hydrogen of the interstellar medium. The neutral pion decays into two photons with energies in the range

$$\frac{M_\pi c^2}{2}\left(\frac{1+\beta_\pi}{1\cdot\beta_\pi}\right)^{1/2} > h\nu > \frac{M_\pi c^2}{2}\left(\frac{1-\beta_\pi}{1+\beta_\pi}\right)^{1/2} , \tag{72}$$

where β_π = velocity of the pion (mass M_π) in units of c and $M_\pi c^2 \approx 140$ MeV. The mean and most probable energy for each photon is $E_\pi/2$, where E_π is the total pion energy. Near pion-production threshold,

$$E_\pi \approx \left(\frac{E_p}{Mc^2}\right) M_\pi c^2 \quad , \tag{73}$$

where E_p is the total cosmic-ray proton energy, and M is the proton rest mass.

For an ultrarelativistic case,

$$E_\pi \approx \left(\frac{E_p}{Mc^2}\right)^2 M_\pi c^2 \ . \tag{74}$$

The source function for pion-produced photons is obtained from

$$h\nu\left(q_p\right) =$$

$$n_0\left\{\int_{E_p=Mc^2\left(h\nu/M_\pi c^2\right)}^{\infty} dE_p \left[\int_{E_\pi=h\nu}^{E_\pi=\left(E_p/Mc^2\right)M_\pi c^2} \left(\frac{dE_\pi}{dh\nu}\right)\left(c\beta_p\right)\left(\frac{d\sigma}{dE_\pi}\right)\left(\frac{dn}{dE_p}\right)dE_\pi\right]\right\} \tag{75}$$

where $\left(dn/dE_p\right)$ is the cosmic-ray proton spectral density.

We use the approximations

$$\frac{dE_\pi}{dh\nu} \approx 2h\nu\ \delta\left(E_\pi - 2h\nu\right) \ , \tag{76}$$

$$\frac{d\sigma}{dE_\pi} \approx \sigma_\pi\ \delta\left(E_p - \frac{M}{M_\pi}\ E_\pi\right) \ , \tag{77}$$

where σ_π is the total neutral pion-production cross-section just above threshold ($\sim 10^{-26}$ cm^2 at 1 GeV).

These approximations (Equations 76 and 77) and Equation 75 give, at $h\nu = 1/2\left(M_\pi/M\right)E_p$,

$$q_p \approx 16\pi\, n_0\, \sigma_\pi \left(\frac{M}{M_\pi}\right)\left(\frac{dJ}{dE_p}\right) \ , \tag{78}$$

where dJ/dE_p is the spectral intensity of cosmic-ray protons (protons/eV-cm^2-sec-sr). From Equation 78, note that the number spectrum of cosmic pion-generated gamma rays at $h\nu$ measures the cosmic-ray proton spectrum at $\sim 14\ (h\nu)$, which is $\gtrsim 1$ GeV.

Recent observations by Clark, Garmire, and Kraushaar (Reference 7) with a gamma-ray detector aboard OSO-III indicate that there is an appreciable flux of gamma rays $\gtrsim 10^2$ MeV associated with the galactic gas disk. The intensity of these gamma rays is about an order of magnitude higher than that which would be expected from the pions produced by a cosmic-ray proton beam at several GeV that is similar to the one observed near the earth. One possible explanation of the apparently excessive gamma-ray flux would be to attribute an enhanced cosmic-ray intensity to some regions of interstellar space relative to what we actually observe near the earth at ~1 to 10 GeV.

STELLAR STATISTICS FOR X-RAY SOURCES

In observational stellar statistics, we are concerned with the number N^* of stars, their apparent intensities I, and the distribution function g defined by

$$g \equiv \frac{d}{dI}\left(\frac{dN^*}{d\Omega}\right), \tag{79}$$

where Ω denotes solid angle. Spatial statistical models again concern the number N^* of stars; however, here we refer to their intrinsic luminosities L and the distribution function ρ^* in space defined by

$$\rho^* = \frac{d}{dL}\left(\frac{d^3 N^*}{d^3 \mathbf{x}}\right), \tag{80}$$

where $\mathbf{x}$ is the vector stellar position. The two distribution functions of stellar statistics are related by

$$\int_{\Omega}\int_{I} g(I, \Omega)\, dI\, d\Omega = \int_{\Omega}\int_{R}\int_{L} \rho^*(L, R, \Omega)\, R^2\, dL\, dR\, d\Omega, \tag{81}$$

where R is the distance from the source to the observer and $d^3\mathbf{x} = R^2\, dR d\Omega$. The parameters L and I are related by the "point source" condition

$$L = 4\pi R^2 I. \tag{82}$$

From Equations 81 and 82, one may obtain the relation between g and ρ^* as

$$g(I, \Omega) = \frac{\int L^{3/2} \rho^* \left(L, \sqrt{L/4\pi I}, \Omega\right) dL}{2(4\pi)^{3/2} I^{2.5}} . \tag{83}$$

For the situation where ρ^* is independent of $R \left(= \sqrt{L/4\pi I}\right)$, the numerator of Equation 83 is independent of I, and the expression assumes the simple form

$$g(I, \Omega) \propto I^{-2.5} . \tag{84}$$

Consider the total number of stars N_R^* within a field $\Delta\Omega$ and within a distance R. For this case, we have

$$N_R^* = \bar{n}_x \left(\frac{R^3}{3} \Delta\Omega\right) , \tag{85}$$

where $\bar{n}_x$ is the mean spatial number density of stars within the region observed. For the case of a finite R and a lower bound to L, there exists a minimum observable intensity I_0 defined by

$$N_R^* = \Delta\Omega \int_{I_0}^{\infty} g \, dI . \tag{86}$$

This total number of stars within the examined region N_R^* is to be compared with the number of stars N_I^* for which the observed intensity exceeds I:

$$N_I^* = \Delta\Omega \int_{I}^{\infty} g \, dI . \tag{87}$$

The integrated stellar intensity of all photons $I_{\Delta\Omega}$ observed within $\Delta\Omega$ is given by

$$I_{\Delta\Omega} = \Delta\Omega \int_{I_0}^{\infty} gI \, dI \; . \tag{88}$$

From Equations 84, 87, and 88, we obtain the relations

$$\left(I_0\right)^{1/2} = \frac{3\left(I^{3/2} N_I^*\right)}{I_{\Delta\Omega}} \; , \tag{89}$$

$$\left(N_R^*\right)^{1/3} = \frac{I_{\Delta\Omega}}{3I\left(N_I^*\right)^{2/3}} \; . \tag{90}$$

From Equations 85 and 90, we get an expression for $\bar{n}_*$ as

$$\bar{n}_* = \frac{3\left(I_{\Delta\Omega}\right)^3}{(\Delta\Omega)\, R^3 \left(I^3 N_I^*\right)} \; . \tag{91}$$

In summary, from the observables N_I^*, I, and $I_{\Delta\Omega}$, we can obtain I_0 and N_R^* directly from Equations 89 and 90, respectively. With some additional information for estimating R, we can utilize Equation 91 to estimate the spatial density of those stars which are defined by the direction of observation and which substantially contribute to the observed photon flux within the bandwidth utilized.

We use the X-ray data of Friedman et al. (Reference 8) to obtain I_0, N_R^* and $\bar{n}_*$ for two regions of importance to X-ray astronomy, Cygnus and Sagittarius.

For Cygnus,

$N_I^* = 8$, for $I = 0.15$ photon/cm^2-sec,
$I_{\Delta\Omega} = 5$ photons/cm^2-sec, for $\Delta\Omega = 0.23$ sr.

Using Equations 89 and 90 for these Cygnus observations gives

$$I_0 = 0.08 \text{ photon/cm}^2\text{-sec}; N_R^* \approx 21.$$

From the angular disposition of the X-ray sources in Cygnus with respect to the galactic stellar distribution, Friedman et al. conclude that $R \approx 4 \times 10^{21}$ cm for this complex of sources. Using this estimate, we use Equation 91 to evaluate $\bar{n}_x \simeq 5 \times 10^{-63}/\text{cm}^3$ for the X-ray stars in Cygnus.

For Sagittarius,

$$N_I^* = 15, \text{ for } I = 0.3 \text{ photon/cm}^2\text{-sec},$$
$$I_{\Delta\Omega} = 18, \text{ for } \Delta\Omega \approx 0.18 \text{ sr}.$$

Friedman et al. estimate that $R \approx 8 \times 10^{21}$ cm for the Sagittarius sources. Using Equation 91, this yields $\bar{n}_x \simeq 3 \times 10^{-63}/\text{cm}^3$ for the number density of X-ray stars in this region.

The X-ray star densities for Cygnus and Sagittarius appear to be quite comparable. In general, this analysis indicates that the number density of X-ray stars within the galaxy is $\lesssim 10^{-6}$ of the number density of optical stars. This implies $\lesssim 10^5$ X-ray stars within the entire galaxy.

This discussion on stellar statistics for X-ray sources is the outgrowth of some ideas suggested by Professor W. Kraushaar of the University of Wisconsin.

REFERENCES

1. Landau, L., and Lifshitz, E., "Classical Theory of Fields," Reading, Mass.: Addison-Wesley, 1951.

2. Ginzburg, V. L., and Syrovatsky, S. I., "The Origin of Cosmic Rays," New York: Pergamon Press, MacMillan Co., 1964.

3. Heitler, W., "Quantum Theory of Radiation," Third edition, Oxford: Clarendon Press, 1954.

4. Drummond, J. E., "Plasma Physics," New York: McGraw-Hill Book Co., Inc., 1961.

5. Hayakawa, S., and Matsuoka, M., Progress Th. Physics, Supplement 30:204, (Japan) 1964.

6. Balasubrahmanyan, V. K., Boldt, E., Palmeira, R. A. R., Sandri, G., "The Electromagnetic Radiation Associated with Energy Dissipated by Cosmic Rays in Interstellar Hydrogen," Canadian J. Phys. 46:S 633, 1968.

7. Clark, G. W., Garmire, G. P., and Kraushaar, W. L., "Observation of High Energy Cosmic Gamma Rays," Astrophys. J. 153: L 203, 1968.

8. Friedman, H., Byram, E. T., and Chubb, T. A., "Distribution and Variability of Cosmic X-Ray Sources," Sci. 67:156, 374, April 1967.

BIBLIOGRAPHY

Balasubrahmanyan, V. K., Boldt, E., Palmeira, R. A. R., Sandri, G., "The Electromagnetic Radiation Associated with the Energy Dissipated by Cosmic Rays in Interstellar Hydrogen," Canadian J. Phys. 46:S 633, 1968.

Boldt, E., "X-Ray Sources (Astronomy)," McGraw-Hill Yearbook of Science and Technology, New York: McGraw-Hill Book Co., Inc., 1968.

Boyd, R., "Techniques for the Measurement of Extra-Terrestrial Soft X-Radiation," Space Sci. Rev. 4(35), February 1965.

Clark, G. W., Garmire, G. P., and Kraushaar, W. L., "Observation of High Energy Cosmic Gamma Rays," Astrophys. J. 153:L 203, 1968.

Drummond, J. E., "Plasma Physics," New York: McGraw-Hill Book Co., Inc., 1961.

Fazio, G., "Gamma Radiation from Celestial Objects," Annual Review of Astron. and Astrophys. 5:481, 1967.

Fichtel, C., "Gamma Ray Astronomy," Sky and Telescope 35(1), February 1968.

Friedman, H., Byram, E. T., and Chubb, T. A., "Distribution and Variability of Cosmic X-Ray Sources," Sci. 67:156, 374, April 1967.

Garmire, G., and Kraushaar, W., "High Energy Cosmic Gamma Rays," Space Sci. Rev. 4:123, February 1965.

Ginzburg, V. L., and Syrovatsky, S. I., "The Origin of Cosmic Rays," New York: Pergamon Press, MacMillan Co., 1964.

Gould, R. J., "Origin of Cosmic X-Rays," Am. J. Phys. 35:376, February 1967.

Greisen, K., "Experimental Gamma Ray Astronomy," in: "Perspectives in Modern Science," R. Marshak, ed., New York: Interscience, 1966.

Hayakawa, S., and Matsuoka, M., Progress Th. Physics, Supplement 30:204, (Japan) 1964.

Heitler, W., "Quantum Theory of Radiation," Third Edition, Oxford: Clarendon Press, 1954.

Landau, L., and Lifshitz, E., "Classical Theory of Fields," Reading, Mass.: Addison-Wesley, 1951.

Morrison, P., "Extra Solar X-Ray Sources," Annual Review of Astron. and Astrophys. 5:325, 1967.

Tucker, W., "Cosmic X-Ray Sources," Astrophys. J. (148):745, July 1967.

Appendix A

USEFUL CONSTANTS

Electromagnetic Interactions:

$$r_e = \frac{e^2}{mc^2} = 3 \times 10^{-13} \text{ cm} \quad \text{(Classical Electron Radius)}$$

$$\sigma_0 = \frac{8}{3}\pi\left(r_e\right)^2 = 7 \times 10^{-25} \text{ cm}^2 \quad \text{(Thompson Cross-section)}$$

Quantum Localization of Charge:

$$\alpha = \frac{e^2}{\hbar c} = \frac{1}{137} \quad \text{(Fine Structure Constant)}$$

Thermal:

Boltzmann

$$k = 8.6 \times 10^{-5} \text{ eV/°K}$$

$$\left(1.4 \times 10^{-16} \text{ ergs/°K}\right)$$

Stefan

$$\sigma = 5.7 \times 10^{-5} \text{ ergs/cm}^2 \text{ sec } (°\text{K})^4$$

Photon Energy:

$$h\nu\,(\text{eV}) = 12.4 \times 10^{-7}/\lambda \text{ (meters)}$$

Page Intentionally Left Blank

V. PLASMA ASPECTS OF COSMIC RAYS*

D. Wentzel
University of Maryland
College Park, Maryland

From the point of view of plasma physics, the cosmic rays constitute an extremely hot and tenuous plasma which coexists in space with the "interstellar gas." This concept, which has been stressed by E. N. Parker, leads to several interesting consequences. Of particular interest here is the dynamic role of cosmic rays in determining certain properties of the galaxy. We begin with a very simple picture of a plane-stratified galactic disk, symmetric about the central plane ($z = 0$) with all physical quantities approaching zero as $|z| \to \infty$. A gravitational attraction toward $z = 0$ is provided by the stars in the disk, and opposing forces which keep the interstellar gas above the disk (to a scale height of order 100 pc $= 10^{20.5}$ cm) are provided by its own pressure, by the pressure $B^2/8\pi$ of the magnetic field, and by the cosmic rays. The field B is thought of for the moment as being parallel to the galactic disk and provides a coupling whereby the gas and the cosmic rays may interact. The pressures (or energy densities) of the gas, the cosmic rays, and the magnetic field are all typically of order 1 eV/cm^3.

The interstellar gas is observed to be largely condensed into "clouds," and it is easy to picture an instability that would cause this. If one part of a magnetic field line dips slightly in toward the galactic plane, the ionized gas tends to flow "downhill" into this region (Figure 1). The added weight then further depresses this part of the line,

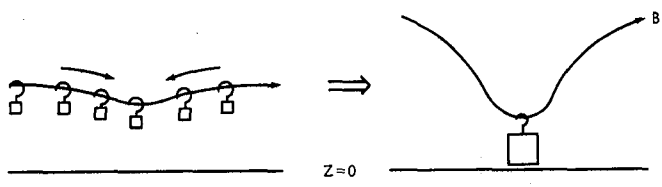

Figure 1–Distortion of the magnetic field.

*Notes taken by D. Hall.

while the nearby higher parts now have been unloaded and thus released, except for their ends, which are anchored in the gas clouds. These "loops" of unloaded field extend well above the galactic plane. Now, since the cosmic-ray "gas" has a "sound speed" comparable to the speed of light, and gravitational attraction of this "gas" toward $z = 0$ is completely negligible, one would expect it to fill up the magnetic field loops very quickly until a uniform pressure is reached. But some of the loops must extend so high that their field strength at the top is insufficient to contain this cosmic-ray pressure. These loops are thus "inflated" indefinitely, providing escape routes through which cosmic rays can leave the galaxy. In this case there would exist a gradient of cosmic-ray pressure directly related to the time scale of the escape process. At any rate, the galactic disk cannot be in a state of hydrostatic equilibrium.

An attractive feature of this picture is that it provides a regulating mechanism to keep cosmic-ray and magnetic pressures comparable in the disk: too few cosmic rays will be unable to inflate the field very well, and will collect; too many will inflate the field rapidly, and let themselves out.

It is now clearly important to investigate how fast the cosmic rays escape. First, observational evidence (the abundances of light nuclei) indicates that those we see have been in the disk for an average of about 10^6 years. Searches for sidereal diurnal variation have found anisotropies $\lesssim 1$ percent even at high energies ($\sim 10^6$ GeV), indicating a net streaming velocity less than 600 km/sec and, therefore, a distance from source to escape of only $\sim$600 pc. This has been a puzzle: on the one hand, the observed field seems to lie along the spiral arm, and escape along the spiral arm would mean paths $\gg$600 pc; on the other hand it is difficult to understand how the particles could diffuse across the field so efficiently as to reach the surface of the disk before traveling 600 pc. However, J. R. Jokipii and E. N. Parker now propose that the observations of mean fields parallel to the galactic plane are compatible with a model using "stochastic lines of force" (References 1 and 2). They believe that with reasonable step sizes in the random walk a typical line of force anywhere in the galaxy could reach the surface somewhere within about 600 pc of its course along the spiral arm.

Now we are faced with a paradox: the magnetic field line on which we lie should be connected to a cosmic-ray escape route only about

2000 light years away, and cosmic rays should be escaping by blowing up the inflated fields at speed c; this fact should be communicated to us with a time lag of only 2000 years, so that we should observe the cosmic rays streaming toward their exit. But we do not. The reason is probably that the streaming is limited to a speed much less than c by some sort of dynamical friction, and the remainder of this chapter concerns the question of how this friction may arise.

The interstellar medium constitutes a magnetized plasma which will support hydromagnetic waves; the Alfvén velocity characterizing these waves is $v_A \sim 10^{-4}$ c. Of particular interest are those waves that propagate in the direction very nearly along the undisturbed magnetic field, since the others are subject to certain strong damping mechanisms. The two transverse modes propagating along the field are properly classified by their circular polarization direction. Because $v_A \ll c$, these waves are practically stationary from the point of view of a relativistic cosmic-ray particle. Therefore, we may picture the wave-particle interaction with the aid of the diagram in Figure 2. This stationary circularly polarized wave superposed on a static field $\mathbf{B}_0$ has a magnetic field $\mathbf{B}_1$ which exerts a force $(q/c)\,\mathbf{v} \times \mathbf{B}_1$ on a particle of velocity $\mathbf{v}$; this force has a nonzero time average if and only if the gyroperiod for the particle in the field $\mathbf{B}_0$ is equal to the time it takes the particle to travel one wavelength along the field line. That is, there is a resonance condition

$$kv_{\parallel} = \Omega = \frac{qB_0}{\gamma mc}$$

for strong interaction; particles of momentum p and pitch angle $\theta = \cos^{-1}\mu$ relative to $\mathbf{B}_0$ interact with those waves with wavenumber

$$k = \frac{qB_0}{cp_{\parallel}} = \frac{qB_0}{cp\mu}\,.$$

Thus a positively charged resonant particle, traveling upward with phase such that

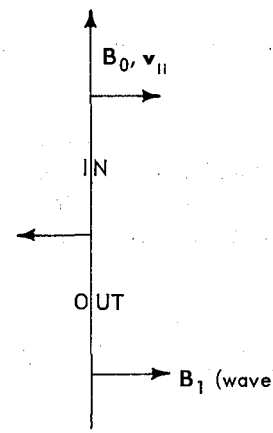

Figure 2–Diagram of stationary circularly polarized wave, the wave field spiraling in the sense of a proton with indicated $\mathbf{v}_{\parallel}$.

the component of its velocity perpendicular to $\mathbf{B}_0$ is into the paper at those points of Figure 2 where the arrows (i.e., $\mathbf{B}_1$) point to the right, is decelerated, but one with velocity out of the paper at the same points is accelerated. If all phases are equally likely, there is, to lowest order, no net change in the total momentum of all resonant particles taken together. But consider particles nearly in resonance: those going slightly too fast with "phase in" have their resonance improved, and so do those that are too slow and have "phase out." ("Fast and out" or "slow and in" particles become less resonant and have negligible effect.) If there are more fast particles than slow ones, there is a net deceleration of particles; therefore, the wave will gain momentum. (Remember that these statements concern acceleration parallel to B_0; in a static magnetic field, the energy of the particles can never change, so the process considered here is one of scattering, primarily. Energy changes are slower by a factor v_A/c.)

With a spectrum of waves present, a particular particle interacts with different waves from time to time, having $v_{\parallel}$ sometimes increased and sometimes decreased. This scattering in pitch angle tends to keep the distribution of cosmic-ray momenta isotropic; it can largely destroy the anisotropy that would be generated by a gradient in cosmic-ray density, and therefore keep the net streaming velocity low.

We now outline a quantitative calculation of the effects described above.*

First, the so-called quasi-linear theory of plasma fluctuations provides an equation for the behavior of the expectation value of the particle distribution function $f(\mathbf{r}, p, \mu, t)$ in the presence of a spectrum of waves of the type discussed above:

$$\frac{\partial f}{\partial t} + \mathbf{v} \cdot \nabla f = \frac{2\pi^2 e^2}{c} \frac{\partial}{\partial \mu} \left[\frac{M\left(\frac{qB_0}{cp\mu}\right)}{p^2} \frac{1-\mu^2}{|\mu|} \left(\frac{\partial f}{\partial \mu} + \frac{v_A}{c} p \frac{\partial f}{\partial p} \right) \right] .$$

*For more detail see D. Wentzel, *Astrophys. J.* 156, April 1969.

Here M is defined by requiring that the total energy density in the wave magnetic field be

$$\int_0^\infty M(k)\, dk \, .$$

Some terms of higher order in v_A/c have been omitted.

Second, an equation is written for the wave amplitudes:

$$\frac{1}{M(k)} \frac{\partial M(k)}{\partial t} = C_1 \frac{n_{cr}}{\sqrt{n_e}} \int d\mu p^2\, dp\, (1-\mu^2)\, \delta\left(p\mu - \frac{qB_0}{ck}\right)\left(\frac{\partial f}{\partial \mu} + \frac{v_A}{c}\, p\, \frac{\partial f}{\partial p}\right) - C_2 \frac{\sqrt{n_e}}{B_0^3}\, k^2\, M(k) \, .$$

Here C_1 and C_2 are calculable constants, n_e is the number density of the background plasma, and n_{cr} the number density of the cosmic rays, with f normalized to unity. The first term describes the reaction upon the waves when they scatter the particles; clearly if $\partial f/\partial \mu$ is sufficiently large and positive, this gives wave growth. The second term represents wave damping by the particular process that we believe is most important here: the nonlinear conversion of Alfvén waves into sound waves, which are then quickly damped.

Third, we hypothesize a cosmic-ray density gradient (ultimately maintained by a source and a sink which are not shown explicitly) that can be represented by a scale height which may be a function of energy, $L(p/mc)^g$. We also use observational knowledge to specify that the main part of the cosmic rays is described by the isotropic distribution function $f_i = \zeta p^{-\gamma}$ with $\gamma \simeq 4.5$. Then we ask for a simultaneous steady-state solution of these nonlinear equations:

$$\frac{\partial f}{\partial t} = 0 \, , \qquad \frac{\partial M}{\partial t} = 0 \, .$$

It is found to be

$$f = \zeta p^{-\gamma} \left[1 + \gamma \frac{v_A}{c} \mu + C_3 \left(\frac{B}{n_{cr} L} \right)^{1/2} \left(\frac{p}{mc} \right)^{(\gamma-3-g)/2} \mu^{(\gamma-3+g)/2} \right] ,$$

$$M = M_0 \left(k/k_0 \right)^{-(7-\gamma-g)/2} .$$

The interpretation of the second term within the brackets is that the cosmic rays may have streaming velocities up to $\gamma v_A/3 \simeq 1.5\ v_A \sim 50$ km/sec without causing instability and building up an appreciable wave spectrum; larger streaming velocities must be accompanied (and controlled) by waves. For permissible values of g, the anisotropy is an increasing function of energy.

This solution seems to confirm some of the ideas we have put forward about the physical processes. Cosmic rays of sufficiently high energy may flow readily from one place to another and have appreciable anisotropy. But the pressure of the cosmic rays is due mainly to those rays of energy below 10 GeV; and these are prevented (by waves they generate themselves) from streaming much faster than v_A. Hence, the rate of filling and rising of magnetic loops above the galactic disk is definitely limited. In fact, as B_0 becomes weaker, the instability and scattering become stronger and slow down the excess streaming more and more (perhaps until the wave energy becomes comparable to $B_0^2/8\pi$, at which point the calculation is invalid). Therefore, we may have an even stronger self-regulating mechanism than was described earlier.

It should be possible to investigate certain other interesting questions in much the same way. One example is energetic electrons; as they synchrotron-radiate, they tend to become anisotropic (although with no net streaming). Again, the waves so generated will limit the anisotropy. Preliminary calculations indicate that strong anisotropy may be found in the local cosmic-ray electrons when it becomes possible to extend our observations to energies of order 10^4 GeV. The same question is of some interest in connection with radio galaxies. Another problem along these lines is whether, and for how long, particles can become trapped in magnetic bottle configurations.

REFERENCES

1. Jokipii, J. R., and Parker, E. N., "Random Walk of Magnetic Lines of Force in Astrophysics," Phys. Rev. Letters 21(1):44-47, July 1, 1968.

2. Jokipii, J. R., and Parker, E. N., Astrophysics J. 155, March 1969.

Page Intentionally Left Blank

VI. RELATIVISTIC STOCHASTIC PROCESSES

J. R. Wayland
Department of Physics and Astronomy
University of Maryland
College Park, Maryland

INTRODUCTION

In high-energy astrophysics there are many phenomena which involve stochastic processes. One of the most often studied is that of cosmic-ray origin. To understand the concepts involved, we will develop the classical theory of random processes along the lines set forth by Wang and Uhlenbeck (Reference 1). We will then follow a parallel path to arrive at the relativistically correct formulation of the theory.

THE CLASSICAL THEORY OF STOCHASTIC PROCESSES

The process $x(t)$ is said to be random in time if the variable x does not depend in a definite way on the dependent variable time (t). This means simply that if you observe the process at different times, you find that the process is described by different functions. We can define the process $x(t)$ by the following set of probability distributions:

$\phi_1 (xt)\, dx$ = probability of finding x between x and $x + dx$ at time t; (1a)

$\phi_2 \left(x_1 t_1;\, x_2 t_2\right) dx_1\, dx_2$ = probability of finding x between x_1 and $x_1 + dx_1$ at time t_1, and between x_2 and $x_2 + dx_2$ at time t_2; (1b)

$\phi_3 \cdots$ (1c)

If we look at an xt plot of the trajectories of events, we can sketch the distribution at different times as in Figure 1. Because these are

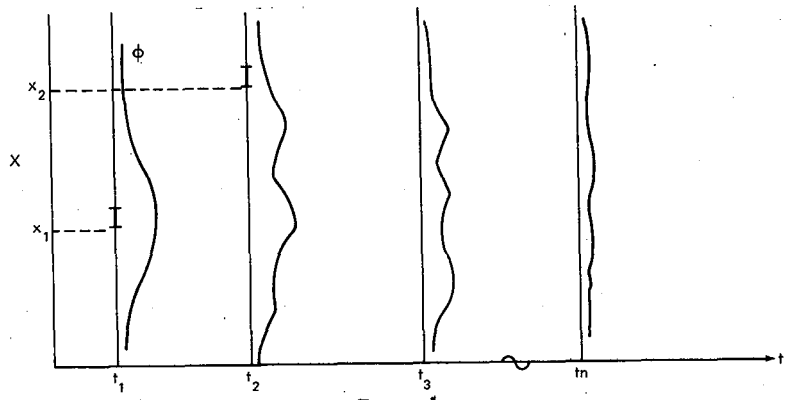

Figure 1.

probability distributions, it follows that

$$\phi_n \geq 0 \; ; \tag{2a}$$

$\phi_n \left(x_1 t_1; x_2 t_2 \cdots x_n t_n\right)$ is a function symmetric in the set of variables $x_1, x_2, \cdots, x_n$ but not necessarily in the set $x_1 t_1, \cdots, x_n t_n$; (2b)

$$\phi_k \left(x_1 t_1 \cdots x_k t_k\right) = \int \cdots \int dx_{k+1} \cdots dx_n \, \phi_n \left(x_1 t_1 \cdots x_n t_n\right) . \tag{2c}$$

The condition expressed by Equation 2b results from the requirement that ϕ_n is a joint probability. Equation 2c arises from the requirement that each ϕ_n must imply all previous ϕ_k when $k < n$.

If the cause of fluctuations is independent of time, the process is said to be stationary in time. Then in Figure 1, the distribution functions would all be the same at the times $t_1, t_2 \cdots$. The probability distributions in Equations 1 now become:

$\phi_1 (x) \, dx$ = probability of finding x in the range $(x, x + dx)$;

$\phi_2 \left(x_1 x_2 t\right) dx_1 \, dx_2$ = joint probability of finding a pair of values x within the ranges $(x_1, x_1 + dx_1)$ and $(x_2, x_2 + dx_2)$ at times that are an interval $t = t_2 - t_1$ apart;

etc.

We can assert from the foregoing equations that averaging over an ensemble will give us the time average.

We can use the conditions given in Equations 1 to classify random processes. A purely random process is one in which the successive values of x are not correlated; i.e.,

$$\phi_2 \left(x_1 t_1 ; x_2 t_2\right) = \phi_1 \left(x_1 t_1\right) \phi_1 \left(x_2 t_2\right), \text{ etc.}$$

Thus in terms of an xt plot, the distribution function at various values of x and t is completely independent of other values of x and t. Then the distribution function at each value of x and t will be ϕ_1 (xt). This is a meaningful concept as long as t is discrete; however, when t is continuous, x_1 and x_2 will be correlated for t sufficiently small.

By the conditional probability, $P_2 (x_1 \mid x_2, t)$, we mean the probability that given x_1 one finds x in the range $(x_2, x_2 + dx_2)$ after an interval of time t. Let us now consider stationary processes only. (In the notation used, a bar separates the variables that are given from those for which the probability is to be found.) We note the following properties:

$$\phi_2 \left(x_1 x_2 t\right) = \phi_1 \left(x_1\right) P_2 \left(x_1 \mid x_2, t\right) ; \tag{3a}$$

$$P_2 \left(x_1 \mid x_2, t\right) \geq 0 ; \tag{3b}$$

$$\int dx_2 P_2 \left(x_1 \mid x_2, t\right) = 1 ; \tag{3c}$$

$$\phi_1 \left(x_2\right) = \int \phi_1 \left(x_1\right) P_2 \left(x_1 \mid x_2, t\right) dx_1 . \tag{3d}$$

A Markov process is one for which the conditional probability that x lies in the interval $(x_n, x_n + dx_n)$ at time t_n, given that x is equal to

$x_1, x_2, \cdots, x_{n-1}$ at times $t_1, t_2, \cdots, t_{n-1}$ $(t_n > t_{n-1} > \cdots t_2 > t_1)$, depends only on the value of x at the previous time t_{n-1}; i.e.,

$$P_n\left(x_1\, t_1, \cdots x_{n-1}\, t_{n-1} \mid x_n\, t_n\right) = P_2\left(x_{n-1}\, t_{n-1} \mid x_n\, t_n\right) . \quad (4)$$

In other words, we are considering processes which "remember" practically nothing about what has happened in the past. In fact, the last event is just on the point of being "forgotten." However, these probabilities must still satisfy Equation 3d and also the condition

$$\lim_{t\to\infty} P_2\left(x_1 \mid x_2\, t\right) = \phi_1\left(x_2\right) . \quad (5)$$

This last requirement simply implies that there are no recurring chains.

Consider two events $(x_1, t = 0)$ and (x_2, t).

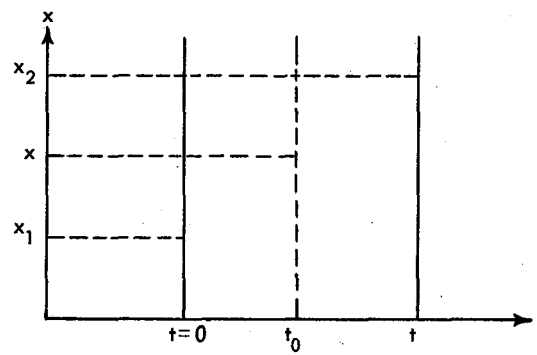

We can write the conditional probability that each will reach some intermediate state xt_0. Then the probability of $(x_1, t = 0) \to (x, t_0) \to (x_2, t)$ is just the product

$$P_2\left(x_1 \mid x, t_0\right) P_2\left(x \mid x_2, t - t_0\right) .$$

Integrating over all intermediate states x gives

$$P(x_1 \mid x_2, t) = \int dx\, P_2(x_1 \mid x, t_0)\, P_2(x \mid x_2, t - t_0) \; . \tag{6}$$

This is the Smoluchowski equation.

Let us now rewrite Equation 6 so that

$$P(x \mid y, t + \Delta t) = \int dz_2\, P(x \mid z_2, t)\, P(z_2 \mid y, \Delta t) \; . \tag{7}$$

We are interested in the moments of the spatial coordinate changes in a time Δt, which are defined by

$$a_n(z, \Delta t) = \int dy (y - z)^n P(z \mid y, \Delta t) \; .$$

The assumption that one usually makes at this point is that only the first and second moments are proportional to Δt. This allows us, in the limit as $\Delta t \to 0$, to consider only

$$A(z) = \lim_{\Delta t \to 0} \frac{a_1(z, \Delta t)}{\Delta t} \; , \tag{8a}$$

$$B(z) = \lim_{\Delta t \to 0} \frac{a_2(z, \Delta t)}{\Delta t} \; . \tag{8b}$$

In most of the problems we will consider, one can actually prove that this is the case. We will not give the details here, but from Equations

7 and 8 one can derive the Fokker-Planck equation (References 1 and 2):

$$\frac{\partial P}{\partial t} = -\frac{\partial}{\partial y}\left[A(y)\,P\right] + \frac{1}{2}\frac{\partial^2}{\partial y^2}\left[B(y)\,P\right], \tag{9a}$$

for one-dimensional problems; and

$$\frac{\partial P}{\partial t} = -\sum_i \frac{\partial}{\partial y_i}\left[A_i\,(y)\,P\right] + \frac{1}{2}\sum_{k,\ell}\frac{\partial^2}{\partial y_k\,\partial y_\ell}\left[B_{k\ell}\,(y)\,P\right] \tag{9b}$$

for n-dimensional problems.

THE RELATIVISTIC THEORY OF STOCHASTIC PROCESSES

To understand completely relativistic stochastic processes requires a sound grounding in the fundamentals of special relativity and relativistic statistical mechanics. We cannot possibly begin to cover the necessary background that this would involve in the short space that is available to us. We will instead draw a strong parallel to the above classical theory and compare the results of one to the other. We quote the results of the relativistic formulation without giving a detailed derivation. By taking this approach, we hope that the results will be more meaningful in a physical sense. For more complete discussion of the mathematical detail, see the recent work of R. Hakin (Reference 3).

Let us first define certain necessary quantities. We will consider a one-particle phase space, if you wish, a μ-space. To form a consistent, but not necessarily unique, set of definitions, we will take the metric tensor in Minkowski space-time as

$$\left.\begin{aligned} g^{oo} &= -g^{ii} = +1 \\ g^{\mu\nu} &= 0 \text{ for } \mu \neq \nu \\ c &= 1\,. \end{aligned}\right\} \left\{\begin{aligned} \mu,\ \nu &= 0,\ 1,\ 2,\ 3 \\ i &= 1,\ 2,\ 3 \end{aligned}\right. \tag{10}$$

We want to consider a particle whose motion is random in the μ-space

$$\mu = M^4 \times U^4\,, \tag{11}$$

where M^4 is the Minkowski space-time and U^4 is the four-velocity space. We are interested in an arbitrary coordinate system in μ-space; thus we will need to consider the system

$$\left(X^{\mu}, U^{\nu}\right) = X^{A} (A = 1, \cdots, 8) .$$

What we are actually concerned with are the trajectories in μ-space of a random point, and these are required to be timelike. However, in four-velocity space, the trajectories are spacelike. A seven-dimensional hypersurface in μ-space is spacelike when its normal is a timelike eight-vector. Let Σ^7 be a spacelike hypersurface imbedded in μ-space such that it cuts all possible timelike trajectories of the process in question in μ-space. Also let Δ be a Lebesque measurable subset of Σ^7. We want to define a probability

$$P\left(X^{A} \in \Delta \subset \Sigma^7 \subset \mu\right)$$

for all Δ. Then the P's are determined by the distributions $\phi_1\left(X^{A}\right)$ (analogous to the ϕ_1 (xt) in the classical case):

$$P\left(X^{A} \in \Delta \subset \Sigma^7 \subset \mu\right) = \int_{\Delta \subset \Sigma^7 \subset \mu} \eta^{B} \phi_1 \left(X^{A}\right) d\Sigma_{B} , \tag{12}$$

where $d\Sigma_B$ is the differential element of hyperspace, and the η^B is an eight-vector. The η^B are the "tangents" to the trajectories of the process. Analogous to the requirement of Equation 2a in the classical use, we here require

$$\phi_1 \left(X^{A}\right) \geq 0 ,$$

with the normalization

$$P\left(X^A \in \Sigma^7 \subset \mu\right) = \int_{\Sigma^7} \eta^B \phi_1 \left(X^A\right) d\Sigma_B = +1 \tag{13}$$

for all Δ.

We can now define the joint probability of finding X_1^A within $\Delta_1 \subset \Sigma_1^7$ and X_2^A within $\Delta_2 \subset \Sigma_2^7$ by

$$P\left[\left(X_1^A \in \Delta_1 \subset \Sigma_1^7\right) \cap \left(X_2^A \in \Delta_2 \subset \Sigma_2^7\right)\right]$$

$$\equiv \int_{\Delta_1 x \Delta_2 \subset \Sigma_1^7 x \Sigma_2^7 \subset \mu^2} \xi^{B_1 B_2} \phi_2 \left(X_1^A, X_2^A\right) d\Sigma_{B_1 B_2} \tag{14}$$

$$\left(A = 1 \cdots 8,\ B_i = 1 \cdots 16,\ i = 1, 2\right) ,$$

where $d\Sigma_{B_1 B_2}$ is the differential element of hypersurface corresponding to a 14-dimensional subsurface embedded in a 16-dimensional manifold, and $\xi^{B_1 B_2}$ serves the same purpose as η^B above. This corresponds roughly to condition 1b. Then from $\phi_2 \left(X_1^A, X_2^A\right)$ we can find all the probabilities

$$P\left[\left(X_1^A, X_2^A\right) \in \Delta \subset \Sigma^{14} \subset \mu^2\right] .$$

We have considered the cases of ϕ_1 and ϕ_2 separately. Now we can expand our definitions to the general case. This will parallel the classical definitions given by 1 and 2.

A relativistic stochastic process in μ-space will be determined completely when all the probabilities

$$P\left[\bigcap_{i=1}^{k} \left(X_i^A \in \Delta_i \subset \Sigma_i^7 \subset \mu\right)\right] ,$$

$k \in$ positive integer for all Σ_i^7 are given. Then, as before, we assume that all P's are given by the densities $\phi_k\left(X_1^A \cdots X_k^A\right)$. Again we must require that

$$\phi_k\left(X_1^A, \cdots, X_k^A\right) \geq 0 \; ; \tag{15a}$$

$\phi_k\left(X_1^A, \cdots X_k^A\right)$ is not necessarily a symmetric function in X_i^A; (15b)

$$\int_{\Sigma^{7k} C \mu^k} \xi^{B_1 \cdots B_k} \phi_k\left(X_1^A \cdots X_k^A\right) d\Sigma_{B_1 \cdots B_k} = 1 \tag{15c}$$

for all Σ^{7k} and $B_i = 1 \cdots 8k$, $i = 1 \cdots k$, $A = 1 \cdots 8$; and

$$\phi_k\left(X_1^A \cdots X_k^A\right) = \int_{\Sigma^{7(n-k)} C \mu^{(n-k)}} \xi^{B_1 \cdots B_{n-k}} \phi_n\left(X_1^A \cdots X_n^A\right) d\Sigma_{B_1 \cdots B_{n-k}} \tag{15d}$$

for all $\Sigma^{7(n-k)}$ and $n > k$. Here

$$\Sigma^{7(n-k)} C \mu^{(n-k)}$$

means a surface, $\Sigma^{7(n-k)}$, is embedded in a space spanned by $\left[X_{nA}, \cdots, X_{(n-k)A}\right]$.

The conditional probability is defined by

$$\phi_{n+1}\left(X_{0B}, X_{1B}, \cdots, X_{nB}\right) = P_n\left(X_{1B}, \cdots, X_{nB} \mid X_{0B}\right) \phi_n\left(X_{1B} \cdots X_{nB}\right) \tag{16}$$

(compare with Equation 3a). This is the probability density for reaching the state X_{0B} by passing through the states $X_{1B}, \cdots, X_{nB}$. (Note that we have reversed the order on the index.) Thus we have a partially

ordered sequence of states

$$X_{nB} < \cdots < X_{1B} < X_{0B} \; .$$

In the relativistic case a Markov process must satisfy

$$P_n\left(X_{1B}, \cdots, X_{nB} \mid X_{0B}\right) \equiv P_2\left(X_{1B} \mid X_{0B}\right) \tag{17}$$

(compare with Equation 4). Again we are led to a Smoluchowski equation. In the relativistic case, we find

$$P_2\left(X_{0B} \mid X_{1B}\right) = \int_{\Sigma} \eta^A\left(X_{2B}\right) P_2\left(X_{0B} \mid X_{2B}\right) \cdot P_2\left(X_{2B} \mid X_{1B}\right) d\Sigma_A\left(X_{2B}\right), \tag{18}$$

where $X_{0B} < X_{2B} < X_{1B}$ (compare Equation 6). This leads directly to the relativistic Fokker-Planck equation,

$$\frac{\partial}{\partial X^A}\left[-B^A\left(X_B\right) P_2 + \frac{1}{2}\frac{\partial}{\partial X^B} D^{AB}\left(X_B\right) P_2\right] = 0 \tag{19}$$

(compare to Equation 9). Here B^A and D^{AB} are the first and second moments in the limits of $\Delta t \to 0$.

Under more complete analysis, a number of interesting points about relativistic stochastic processes emerge, e.g.:

1. One can always think of a stochastic process in space as an idealization of an underlying dynamic problem if suitable assumptions about the scales of the variables are made.

2. A Markov process <u>may</u> be a consistent idealization if the invariant parameter characterizing the spatial extent of the system, λ, and the correlation time of the process, T, are related by $T \gg \lambda/c$.

3. Causality requirements in Minkowski space-time require that the Fokker-Planck equation (Equation 19) be applied to a system of particles; one cannot apply this form to a single particle.

4. A relativistic random process must have carefully specified tensorial properties, and one should probably also specify how it is observed and measured.

APPLICATION TO COSMIC RADIATION

Because of the difficulties encountered in trying to obtain an exact solution to the relativistic Fokker-Planck equation, we will consider the more often used non-relativistic Equation 9. When considering cosmic rays, one normally is concerned with how to obtain the very high energies observed. If we consider the case in which the variables are time, t, and energy, E, we find that

$$\frac{\partial n}{\partial t} = -\frac{\partial}{\partial E}\left(\frac{\langle \Delta E \rangle}{\Delta t} n\right) + \frac{1}{2}\frac{\partial^2}{\partial E^2}\left(\frac{\langle (\Delta E)^2 \rangle}{\Delta t} n\right), \tag{20}$$

where n is the particle density. The first term on the right-hand side describes the mean statistical energy change of cosmic-ray particles. The second term takes into account the statistical fluctuations in the energy change. Normally we can simplify Equation 20 by letting

$$\frac{\langle \Delta E \rangle}{\Delta t} = aE , \tag{21a}$$

and

$$\frac{\langle (\Delta E)^2 \rangle}{\Delta t} = 2bE^2 . \tag{21b}$$

Thus we must solve

$$\frac{\partial n}{\partial t} + an + aE\frac{\partial n}{\partial E} - 2bn - 4bE\frac{\partial n}{\partial E} - bE^2\frac{\partial^2 n}{\partial E^2} = 0 . \tag{22}$$

The form of the energy operator suggests a power-law solution. Therefore, we will apply a Mellin transformation with respect to the energy, E. This gives us

$$\frac{\partial g}{\partial t} - (s-1)\,ag - (s-1)(s-2)\,bg = 0 , \tag{23}$$

where

$$g(s) = \int_0^\infty E^{s-1}\, n(E)\, dE . \tag{24}$$

Then we have that

$$g = c \exp\left\{\left[(s-1)\,a + (s-1)(s-2)\,b\right] t\right\} . \tag{25}$$

The simplest injection one can assume is a delta function in energy as

$$q_0\, \delta\left(E - E_0\right)\, \delta\left(t - t_0\right) , \tag{26}$$

which in the transformed s space becomes

$$q_0\, p_0^{s-1}\, \delta\left(t - t_0\right) . \tag{27}$$

The solution for g above must be equal to (27) when $t = t_0$. Thus we find

$$g = q_0 p_0^{s-1} \exp\left\{\left[(s-1)a + (s-1)(s-2)b\right]\tau\right\}, \tag{28}$$

where $\tau = t - t_0$. The inverse Mellin transformation is given by

$$n(E, t) = \frac{1}{2\pi i} \int_{c-i\infty}^{c+i\infty} g(s, t) E^{-s} ds . \tag{29}$$

Dr. F. Jones has pointed out that this integral can be found analytically. The result is given by

$$n(E, t) = \frac{q_0}{E_0 \sqrt{4\pi b\tau}} \left(\frac{E_0}{E}\right)^{\gamma} \exp - (a-b)^2/4b\tau \tag{30}$$

where

$$\gamma = \frac{1}{4b\tau} \ln\left(\frac{E}{E_0}\right) + \frac{3b-a}{2b} .$$

Then we have a power law spectrum in which the exponent is a function of time. When $b\tau \ll 1$ the spectrum is very steep and is determined by the $\ln(E/E_0)$ term. If $b\tau \sim 1$ both terms are important and the resulting spectrum becomes steeper at higher energies. When $b\tau \gg 1$ the spectrum is determined by the $(3b - a)/2b$ term. If the observed spectrum is the result of $b\tau \gg 1$ type sources, then $a \approx -2.2b$ for $\gamma = 2.6$ (the observed value). We can only obtain a satisfactory fit to the experimental data for the integral spectrum when we assume a continuous deceleration (i.e., $a < 0$). This could be the result of the expansion of the source region. Note that we have a balancing of continuous acceleration against deceleration. While deceleration dominates, an acceleration process must be present. In the case of dominating deceleration, the primary cosmic-ray spectrum is entirely attributable to the consequences of statistical fluctuations.

Let us now consider how we can obtain the Fokker-Planck coefficients a and b. The collision probability is proportional to the relative velocity $\mathbf{v}_r$ of the scattering center (velocity $\mathbf{V}$), and the velocity of the particle (velocity $\mathbf{v}$); thus

$$\frac{v_r}{c} = \frac{\left(\beta^2 + B^2 - 2\beta B \cos\theta - \beta^2 B^2 \sin^2\theta\right)^{1/2}}{1 - \beta B \cos} , \tag{31}$$

where θ is the angle between $\mathbf{v}$ and $\mathbf{V}$, $\beta = cv$, and $B = Vc$. It is also proportional to the velocity distribution $f(\mathbf{V})$ of the scattering centers. The collision probability ψ is then given by

$$\psi \, d\mathbf{V} d\mu = \frac{v_r \, f(V) \, d\mathbf{V} d\mu}{\iint v_r \, f(V) \, dV d\mu} , \tag{32}$$

where $\mu = \cos\theta$. We will assume that μ is isotropically distributed.

From the foregoing, we will consider the case in which deceleration can dominate. Let us restrict ourselves, for the sake of illustration, to the case of magnetically turbulent scattering centers that are receding from each other. Please note that this is not the only possible case. The foregoing results are of a very general nature.

In the case of a spherical expansion from a common center, the scattering centers will recede from each other with a velocity $\lambda V_e/R$. Here V_e is the expansion velocity, λ is the mean free path between centers, and R is the radius of expansion. The average energy loss caused by expansion alone is $-\left(v V_e \lambda/c^2 R\right) E$. Let $k = \lambda V_e/vR$. If we consider Fermi acceleration, we can show that the fractional energy change per collision is given by

$$\frac{\Delta E}{E} = \Gamma^2 \left(1 + 2\beta B \cos\theta + B^2\right) - 1 . \tag{33}$$

We can expand Equations 31 and 33 in powers of B (keeping terms up to order B^2) and let $\beta \to 1$ (i.e., high-energy limit). Then using Equation 32, we can calculate a and b as defined in Equations 21a and 21b. Here we use

$$\langle(\Delta P)\rangle = \iint (\Delta P)^n \psi \, dV d\mu$$

and

$$\overline{B}^2 = \int B^2 f(\mathbf{V}) \, d\mathbf{V} .$$

Thus we find

$$\Delta t \, a \simeq 8/3 \overline{B}^2 - 2k + 2/3 \, k \overline{B}^2 , \tag{34a}$$

$$\Delta t \, b \simeq k^2 - 4k \overline{B}^2 + 4/3 \overline{B}^2 . \tag{34b}$$

We are interested in the case of $a = \alpha b$, where $\alpha < 0$ (i.e., a is negative). Then using Equation 34, we find

$$\overline{B} = \left[\frac{2 + \alpha B_e \frac{\ell}{R}}{\frac{4R}{3B_e \ell} (2 - \alpha) + 2(1 + 2\alpha)} \right]^{1/2} , \tag{35}$$

where $B_e = V_e/c$. Normally for a nova or supernova, $B_e \sim 10^{-2}$. We can make a very rough estimate of the number of scattering centers

by

$$N_{sc} = \text{number of scattering centers} \sim \frac{4/3\,\pi R^3}{4/3\,\pi \ell^3} = \left(\frac{R}{\ell}\right)^3 . \qquad (36)$$

We can, with the aid of Equation 31, obtain a plot of $\bar{B}$ vs R/ℓ as shown in Figure 2.

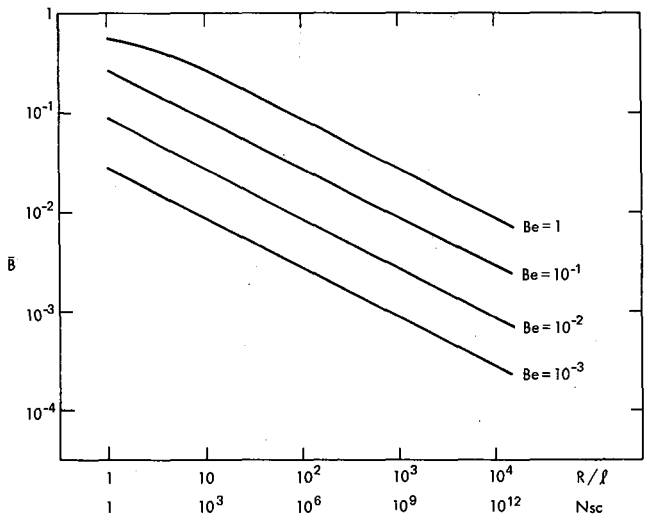

Figure 2.

CONCLUSIONS

We have obtained a relativistic Fokker-Planck Equation. Although we have solved a very particular form of this equation, we should point out that if one chooses a different set of coordinates, the resulting equation will be one of the many forms studied in recent years under the heading of relativistic stochastic processes.

REFERENCES

1. Wang, M. C., and Uhlenbeck, G. E., "On the Theory of Brownian Motion," Rev. Mod. Phys. 17(2-3):323-342, April-July, 1945.

2. Chandrasekhar, S., "Stochastic Problems in Physics and Astronomy," Rev. Mod. Phys. 15(1):2-89, January 1943.

3. Hakim, R., "Remarks on Relativistic Statistical Mechanics," J. Math. Phys. 8(6):1315-1344, June 1967 and 8: 1379, June 1967.

Page Intentionally Left Blank

VII. PROPAGATION OF SOLAR COSMIC RAYS IN THE INTERPLANETARY MAGNETIC FIELD

E. C. Roelof*
NASA Goddard Space Flight Center
Greenbelt, Maryland

The goal of the study of solar cosmic rays is the understanding of their production. At present, however, attention is focused on their propagation in the interplanetary plasma because their production spectrum is severely distorted by the time the particles arrive at the earth. The interplanetary magnetic field, carried out into space by the expanding corona (the "solar wind"), is the main source of this distortion, since its irregularities tend to randomize the trajectories of the particles. In this messy situation one must be grateful for the fact that the solar cosmic rays are so much more energetic than the solar wind particles (whose kinetic temperature is less than 10^6 °K, their average energy being about 100 eV) that their trajectories may be analyzed as individual particle orbits, neglecting cooperative effects in which they would modify the fields through which they pass.

The first step in understanding the propagation of solar cosmic rays is to understand the interplanetary magnetic field. Because of the huge conductivity of the tenuous interplanetary plasma (<10 particles/cm^3 at 1 AU), we can speak of the interplanetary magnetic field as being "convected" out from the sun because it is "frozen" into the plasma. This concept arises from considering the change of flux through any closed contour, L, moving with the plasma (at the plasma velocity $\vec{u}$). This change is due both to $(\partial/\partial t)\vec{B}$ and to the change in the area, since the shape of L will change if $\vec{u}$ is a function of position. The total time rate of change of the flux is thus

$$\frac{d}{dt}\Phi = \frac{d}{dt}\int_S d\vec{a}\cdot\vec{B}$$

$$= \int_S d\vec{a}\cdot\frac{\partial}{\partial t}\vec{B} + \frac{\delta}{\delta L}\int_S d\vec{a}\cdot\vec{B}\ ,$$

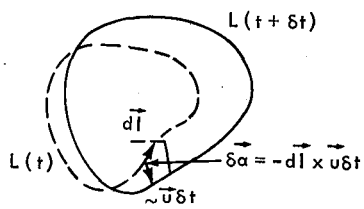

*NAS/NASA Postdoctoral Resident Research Associate

hence

$$\frac{d}{dt}\Phi = \int_S d\vec{a} \cdot (-c\nabla\times\vec{E}) + \oint_L (-d\vec{\ell}\times\vec{u}) \cdot \vec{B}$$

$$= -c\oint_L d\vec{\ell} \cdot \left(\vec{E} + \frac{1}{c}\vec{u}\times\vec{B}\right) .$$

Nonrelativistically, the electric field in the moving frame is $\vec{E}' = \vec{E} + \vec{u}/c\times\vec{B}$. If the plasma obeys Ohm's law, $\vec{J}' = \sigma'\vec{E}'$. Since conductivity is a property of the medium, $\sigma' = \sigma$; and since the plasma is neutral, $\vec{J}' = \vec{J} + \rho\vec{u} = \vec{J}$, resulting in the relation

$$\vec{J} = \sigma\left(\vec{E} + \frac{1}{c}\vec{u}\times\vec{B}\right) .$$

If the current is to remain finite while $\sigma\to\infty$, we must have $\vec{E} = -\vec{u}/c \times\vec{B}$. This is called a "polarization field" because it can be thought of as arising in the following way. The Lorentz force per unit charge on a particle moving <u>on the average</u> with the plasma is (since $\langle\vec{v}\rangle = \vec{u}$),

$$\langle\vec{F}/q\rangle = \langle\vec{v}/c\times\vec{B}\rangle = \vec{u}/c\times\vec{B} .$$

This force tends to separate positive and negative charges and polarize the plasma, inducing an electric field $\vec{E}_p$. The condition that there be finite current for infinite conductivity requires $\vec{E}_p \equiv -\vec{u}/c\times\vec{B}$. (Note that a particle not moving with the plasma responds only to its own Lorentz force $\vec{v}/c\times\vec{B}$, and to the polarization field $\vec{E}_p$, the sum of which is <u>not</u> zero on the average.)

The result of this modest excursion into plasma dynamics is that $d\Phi/dt = 0$. Thus field lines threading L at t_1 must also thread it at another time t_2. Obviously, great simplification of the "frozen-in"

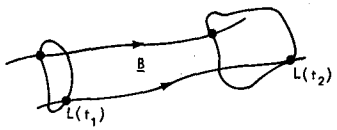

concept is that the magnetic field can be deduced from the plasma velocity field. The solar plasma corotates with the sun while it is close to the sun's surface. However, when u becomes comparable to Alfvén velocity $B/\sqrt{(4\pi\rho)}$, the Maxwell stresses cease to dominate the mechanical momentum; mechanical angular momentum is then conserved, and the plasma escapes radially at large distances from the sun. The solar wind accelerates rapidly to ~400 km/sec while the Alfvén velocity decreases so that the transition to radial flow occurs within ~0.1 AU.

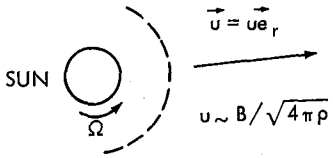

Problem: Assuming that the plasma flows radially out from the sun, where the field $B^0(\Theta)$ is $B(r_0, \Theta)$, and Θ is measured from the north ecliptic pole, show that the equation of the magnetic field lines is the Archimedean spiral $\phi = -\Omega r \sin\Theta/u$ and that the field at a distance r from the sun can be written

$$B(r, \Theta) = B^0(\Theta)\left(r_0/r\right)^2\left(\vec{e}_r - \frac{\Omega r \sin\Theta}{u} e_\phi\right)$$

(which satisfies $\nabla \cdot \vec{B} = 0$) where r_0 = the radius of the sun, Ω = the angular rate of rotation of the sun, and $\vec{e}_r$ and $\vec{e}_\phi$ are unit vectors in the radial and azimuthal directions, respectively.

Solution: The Archimedean spiral configuration of the IP field line is the locus of the plasma outflow (which is radial, $\Delta r = u\Delta t$) from a single area element on the rotating source (the plasma moves through a central angle $\Delta\phi = -\Omega\Delta t \sin\Theta$ relative to the area element in time Δt). Note: the field line must lie on the cone Θ = constant.

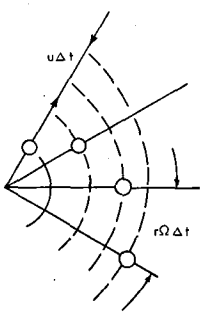

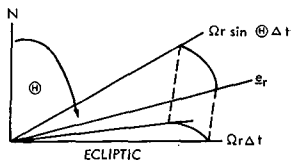

All points on the locus thus must satisfy

$$\frac{dr}{d\phi} = -\frac{u}{\Omega \sin\Theta} .$$

Integrating,

$$\phi = -\frac{\Omega r \sin\Theta}{u}$$

(choosing $r = 0$ when $\phi = 0$). By flux conservation through a moving surface when $\sigma \to \infty$, $d\Phi/dt = 0$; therefore $\vec{B}$ lies along the spiral, so that it must have the form

$$\vec{B}(r, \Theta) = \alpha(r, \Theta)\left(e_r + r \frac{d\phi}{dr}_{\text{spiral}} \vec{e}_\phi\right)$$

$$= \alpha\left(e_r - \frac{\Omega r \sin\Theta}{u} e_\phi\right) .$$

Clearly this contains no explicit ϕ-dependence, by azimuthal symmetry. For the field to be physical, Maxwell's equation $\nabla \cdot \vec{B} = 0$ must hold; hence,

$$0 = \frac{1}{r^2}\frac{\partial}{\partial r} r^2 B_r + \frac{1}{r \sin\Theta}\frac{\partial}{\partial\Theta} \sin\Theta B_\Theta + \frac{1}{r \sin\Theta}\frac{\partial}{\partial\phi} B_\phi ,$$

$$= \frac{1}{r^2}\frac{\partial}{\partial r} r^2 \alpha ; \quad \therefore \alpha = \frac{f(\theta)}{r^2} .$$

If $\vec{B}(\vec{r}_0, \Theta) = \vec{B}^0(\Theta)$, then

$$f(\Theta) = r_0^2 B_r^0(\Theta) = \frac{u r_0}{\Omega \sin\Theta} B_\phi^0(\Theta) .$$

Since

$$B_\phi^0 = -\frac{\Omega r_0 \sin\Theta}{u} B_r^0 ,$$

$$\Omega = 3 \times 10^{-1} \text{ sec}^{-1} ,$$

$$r_0 \simeq 700{,}000 \text{ km} ,$$

and

$$u \sim 400 \text{ km/sec} ,$$

we find that

$$B_\phi^0 \sim -0.005 B_r^0 ;$$

so

$$B^0(\Theta) \sim \sqrt{\left(B_r^0\right)^2 + \left(B_\phi^0\right)^2} \sim B_r^0(\Theta) ;$$

giving, finally,

$$B(r, \Theta) = B^0(\Theta)\left(\frac{r_0}{r}\right)^2 \left(\vec{e}_r - \frac{\Omega r \sin\Theta}{u} \vec{e}_\phi\right) .$$

By construction, $\nabla \cdot \vec{B} = 0$.

These field lines then corotate with the sun. It is now easy to see the effect of the polarization field for energetic particles spiraling along the lines. A steady electric field produces a drift velocity

$$\vec{v}_d = c\vec{E} \times \vec{B}/B^2 .$$

Substituting $\vec{E}_p$ gives

$$\vec{v}_d = c(-\vec{u}/c \times \vec{B}) \times \vec{B}/B^2 = \vec{u} - \hat{\vec{B}}(\hat{\vec{B}} \cdot \vec{u}) = \vec{u}_\perp ;$$

so the field tends to keep the spiraling particles on the corotating field lines by giving them a transverse velocity equal to the transverse velocity of the lines.

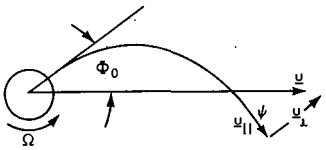

For a solar wind velocity of 400 km/sec, the field line passing through the earth ($r = 1.5 \times 10^8$ km) leaves the sun at a western longitude

$$\phi_0 = \frac{\Omega r}{u} = \frac{(3\times 10^{-6}/\text{sec})(1.5\times 10^8 \text{ km})}{4\times 10^2 \text{ km/sec}} = 1.13 = 65^\circ .$$

The Ω in the equations is 2π divided by the sidereal period. The sun's sidereal period is about 24 days, although the rotation period viewed from the earth is about 27 days because of the earth's orbital motion. The angle that the field makes with the earth-sun line is

$$\psi = \tan^{-1}\frac{\Omega r}{u} = \tan^{-1} 1.13 \sim 50^\circ .$$

The general field at the sun (r_0 = 700,000 km) is ~1 gauss; so this simple theory predicts that the field at earth is about 5×10^{-5} gauss.

All the foregoing theoretical predictions are borne out by direct and indirect physical measurements of the average properties of the field. However, there are considerable fluctuations about the average values. As we shall see later, these small fluctuations strongly effect charged particle motion.

Let us now consider the particle observations themselves. Even before there was any solid experimentally based theoretical knowledge of the interplanetary magnetic field, cosmic-ray physicists had concluded, from two different phenomena, that energetic particles undergo some diffusion-like transport in the interplanetary medium.

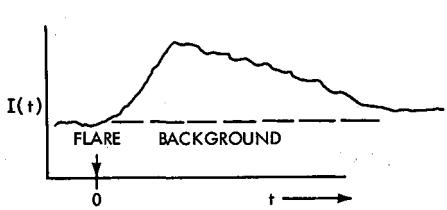

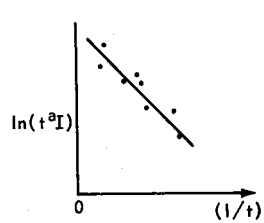

First, the time dependence of solar cosmic rays following large flares sometimes looked like a diffusion curve. The classical three-dimensional diffusion equation

$$\frac{\partial}{\partial t} N = D \nabla^2 N$$

has the solution

$$N(t) = \frac{N_0}{(4\pi Dt)^{3/2}} e^{-r^2/4Dt} .$$

Noting that $\ln\left(t^{3/2} I\right) = -\left(r^2/4D\right)(1/t) + \text{constant}$, one multiplied the counting rate $I(t)$ by $t^{3/2}$ and plotted this product versus $1/t$ (where $t = 0$ at the time of the flare). The result was often a good fit to a straight line. (Sometimes $t^a I$, where $1 < a < 3$, gives a better fit than $a = 3/2$.) Interpreting the slope as $-r^2/4D$ with $r = 1$ AU, the value of D was found to be on the order of 10^{22} cm^2/sec. This number seemed reasonable, since its use in the classical relation between the mean free path and the diffusion coefficient, $D = \lambda v/3$, yields $\lambda \sim 10^{12}$ cm = 0.06 AU. Even though the actual scattering process was not known, it was comforting to deduce that there were "many" scatterings between the sun and the earth so that the diffusion picture was self-consistent. However, it was clear that the process had to involve magnetic fields, since the mean free path for Coulomb interactions is $\left(\pi r_{Bohr}^2 n\right)^{-1} \sim 10^{16}/n$ centimeters which is many AU for reasonable values of the interplanetary proton density n.

The second phenomenon that supported the diffusion model was the modulation of galactic cosmic rays. Neutron-monitor counting

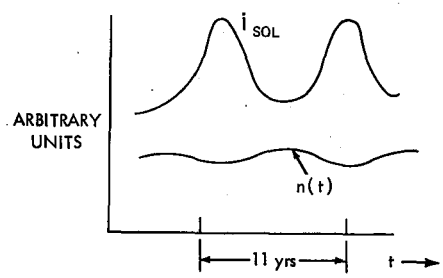

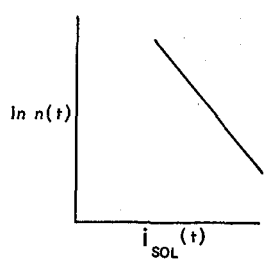

rates showed a long-term variation with an 11-year period which was just opposite that of indicators of solar activity (i_{sol} = sunspot number or corona green-line intensity, for example). This variation was explained on the basis of the convected magnetic irregularities. The galactic cosmic rays must "swim upstream" against the irregularities which tend to diffuse them. The net flux, then, is that due to the diffusion process ($-D\nabla n$) plus that due to simple convection at the velocity of the frozen-in field ($n\vec{u}$):

$$\vec{J} = -D\nabla n + n\vec{u} .$$

In a quasi-steady state, $\nabla \cdot \vec{J} \sim 0$. If we invoke spherical symmetry in the solar system so that D, n, and $\vec{u}$ are functions of r only, and also assume the direction of $\vec{u}$ to be radial, then $\nabla \times \vec{J} = 0$. Therefore $\vec{J}$ is a constant; since $\vec{J} = J\vec{e}_r$, the only constant value consistent with spherical symmetry is zero. This gives the equation for n:

$$\nabla n/n = \vec{u}/D ,$$

which may be integrated along any path (L) from $\vec{r}$ to $\vec{r}_0$ to give

$$n(\vec{r}) = n_0 \exp\left[-\int_{\vec{r}}^{\vec{r}_0} d\vec{\ell} \cdot \vec{u}/D\right] = n_0 \exp\left[-\int_{r}^{r_0} dr\ u/D\right] .$$

The modulating region must terminate at some distance r_0 at which $n = n_0$, the galactic intensity. In the approximation $u/D \sim$ constant, we can estimate the distance to the boundary if we assume D does not change much. From solar maximum to minimum, the average value of the solar wind decreases by about 100 km/sec while the neutron-monitor counting rates increase by 20 percent. From the equation

$$\frac{n_{min}}{n_{max}} - 1 \cong 1 - \exp \frac{\Delta r}{D}\left(u_{min} - u_{max}\right) \cong \frac{\Delta r}{D}\left(u_{max} - u_{min}\right)$$

we obtain $\Delta r \sim +(+0.2)\ (10^{22})/10^{7} \sim 2 \times 10^{14}$ cm ~ 10 AU, a number consistent with other estimates of the size of the solar cavity. The reader can find detailed discussions of all arguments up to this point, as well as many other theoretical concepts relating to cosmic rays, in Reference 1.

To make further progress towards the primary goal of understanding the nature of the solar cosmic rays at the sun, a microscopic description of particle motion in disordered magnetic fields is necessary. The calculations involve considerable arguments and the techniques of the theory of stochastic processes. However, a great deal of this may be circumvented by realizing that the velocity process in a spatially disordered magnetic field must be a random walk of the velocity vector on a sphere in velocity space. The contribution of the electric field $-(1/c)\vec{u} \times B$ to scattering is negligible compared to the Lorentz force $(1/c)\vec{v} \times B$ for $v \gg u$. (However, the electric field is important for long-term ($\sim$days) energy loss in the medium.) This justifies assuming that the magnitude of the velocity is constant.

The problem of a random walk on the surface of a sphere was solved beautifully by F. Perrin in 1928. He found the differential equation for the time-evolution of the distribution function in spherical polar coordinates (μ, φ, where $\mu = \cos\theta$) to be

$$\frac{\partial f}{\partial t} = \frac{1}{T}\left[\frac{\partial}{\partial \mu}\left(1-\mu^2\right)\frac{\partial f}{\partial \mu} + \frac{1}{1-\mu^2}\frac{\partial^2 f}{\partial \varphi^2}\right].$$

The operator on the right is the "transverse" part of the Laplacian in velocity space (i.e., that part not involving v). Its eigenfunctions are the well-known spherical harmonics, products of Legendre polynomials in μ and cissoids in φ. There is, reasonably, one parameter in the equation, the "relaxation time," T. Its role is easily seen from the Green's function solution

$$f_0(\mu, \varphi, t) = \sum_{\ell=0}^{\infty} \frac{2\ell+1}{4\pi} e^{-\ell(\ell+1)t/T} \sum_{m=-\ell}^{\ell} \frac{(\ell-m)!}{(\ell+m)!} P_\ell^m(\mu) P_\ell^m(\mu_0) e^{im(\varphi-\varphi_0)},$$

$$\lim_{t \to 0} f_0(\mu, \varphi, t) = \delta(\mu - \mu_0)\, \delta(\varphi - \varphi_0) .$$

For times $t \gg T$, an arbitrary initial velocity distribution on the sphere will have relaxed to near isotropy.

For magnetic scattering, a Fokker-Planck analysis leads to the Perrin equation if the mean field $\vec{B}_0$ vanishes. If $\vec{B}_0$ does not vanish, its presence introduces two new terms, yielding the equation

$$\frac{\partial f}{\partial t} = \Omega_0 \frac{\partial f}{\partial \varphi} + \frac{1}{T}\left[\frac{\partial}{\partial \mu}\left(1 - \mu^2\right)\frac{\partial f}{\partial \mu} + \frac{1}{1 - \mu^2}\frac{\partial^2 f}{\partial \varphi^2} + \zeta \frac{\partial^2 f}{\partial \varphi^2}\right] .$$

An explicit expression for T follows from the statistical analysis of particle orbits:

$$T = \frac{2}{\pi}\left(\frac{mc}{q}\right)^2 \frac{v}{P_\perp(k_0)} ,$$

$$k_0 = \frac{\Omega_0}{v} = \frac{q B_0}{mvc} ,$$

while

$$\zeta = \frac{P_\parallel(0) - P_\perp(k_0)}{P_\perp(k_0)} ,$$

where $P_\perp(k)$ and $P_\parallel(k)$ are one-dimensional (measured along the mean field) spatial power spectra of a random field component perpendicular and parallel to the mean field, respectively. Clearly the new terms vanish for $B_0 = 0$. This equation is valid only in the limit of small-angle scattering, which is equivalent to

$$\Omega \ell / v \ll 1 ,$$

where

$$\Omega = \frac{q}{mc}\sqrt{\overline{B^2}} ,$$

and ℓ is the "correlation length" of the random field. The terms "mean" and "random" are properly defined relative to the scale of the root-mean-square gyroradius, v/Ω; thus ℓ for low energy particles may be much shorter than ℓ for those of high energy, since the former smoothly follow irregularities of scale length much larger than their gyroradius, while the latter see these same irregularities as random perturbations. Thus ℓ really depends on energy for a given field configuration.

The physical consequences of the additional terms (which vanish when $B_0 = 0$) are (1) a simple tendency to gyrate in the mean field with frequency Ω_0, and (2) an enhanced azimuthal diffusion on the velocity sphere due to the mean field. Both terms can inhibit spatial diffusion across field lines, as we shall see.

Description of the process in velocity space is not enough—we need the phase space distribution function $W(\vec{r}, \vec{v}, t)$. Since the velocity scattering is small-angle, the change in position, $\Delta\vec{r}$, over a time interval $\Delta t \ll T$ (the appropriate time scale of the complete equation) is $\sim \vec{v}\Delta t$. Thus the full equation is obtained by replacing $\partial/\partial t$ with

$$\frac{\partial}{\partial t} + \vec{v} \cdot \frac{d}{d\vec{r}} .$$

If the mean field is constant (we shall see later why this restriction is important), the full equation is

$$\frac{\partial W}{\partial t} + \vec{v} \cdot \nabla W = \Omega_0 \frac{\partial W}{\partial \varphi} + \frac{1}{T}\left[\frac{\partial}{\partial \mu}\left(1-\mu^2\right)\frac{\partial W}{\partial \mu} + \left(\frac{1}{1-\mu^2} + \zeta\right)\frac{\partial^2 W}{\partial \varphi^2}\right],$$

where the components of $\vec{v}$ are $(v \sin\theta \cos\varphi,\ v \sin\theta \sin\varphi,\ v \cos\theta)$.

This equation is quite complicated, but fortunately we need only coarse information to discuss the general aspects of propagation.

Therefore degrade the equation to a diffusion process by assuming that W is nearly isotropic in velocity space; i.e., we take only the zero and first-order terms of a spherical harmonic expansion:

$$W \cong \frac{N}{4\pi} + \frac{3}{4\pi v}\left(\sqrt{1-\mu^2}\cos\varphi\, J_1 + \sqrt{1-\mu^2}\sin\varphi\, J_2 + \mu J_3\right),$$

where N and $\vec{J}$ are functions of $\vec{r}$, t, and only the magnitude of the velocity. Substitution in the equations, multiplication through by the orthogonal functions 1, $\sqrt{1-\mu^2}\cos\varphi$, $\sqrt{1-\mu^2}\sin\varphi$, and μ, and integration over $-1 \leq \mu \leq 1$ and $0 \leq \varphi \leq 2\pi$ gives the four equations (written in vector form):

$$\frac{\partial N}{\partial t} + \nabla \cdot \vec{J} = 0$$

$$\frac{\partial}{\partial t}\vec{J} + \frac{v^2}{3}\nabla N = -\frac{2}{T} + \frac{\zeta}{\Omega_0^2 T}\vec{\Omega}_0 \times \left(\vec{\Omega}_0 \times \vec{J}\right) - \vec{\Omega}_0 \times \vec{J}\,.$$

Consistent with the quasi-static diffusion approximation, we assume

$$\frac{\partial}{\partial t}\vec{J} \equiv 0$$

so the vector equation may be solved for $\vec{J}$.

$$\vec{J} \sim -\left(D_{\parallel}\nabla_{\parallel} N + D_{\perp}\nabla_{\perp} N\right) + T\vec{\Omega}_0 \times \nabla N\,,$$

where

$$D_{\parallel} = v^2 T/6\,, \qquad D_{\perp} = \frac{2(2+\zeta)}{(2+\zeta)^2 + \left(\Omega_0 T\right)^2} D_{\parallel}\,,$$

$$\nabla_{\parallel} = \hat{B}_0 \hat{B}_0 \cdot \nabla\,, \qquad \nabla_{\perp} = \nabla - \nabla_{\parallel}\,.$$

The last term is like a $\vec{J} \times \vec{B}$ term and (for $\vec{B}_0$ constant) contributes nothing to the diffusion process when J is substituted into the equation of continuity

$$\frac{\partial N}{\partial t} = D_\perp \nabla_\perp^2 N + D_\parallel \nabla_\parallel^2 N .$$

If $\vec{B}_0$ were not constant, the cross term would have introduced the well known curvature and gradient drifts. The constraining of the particles to field lines is quantitatively shown by the ratio $D_\perp/D_\parallel$, which varies as $(\Omega_0 T)^{-2}$ for $T \gg |2 + \zeta|$. As the relaxation time grows much larger than a gyro-period, the transverse scattering becomes negligible.

The parallel diffusion coefficient can now be expressed in terms of the transverse power spectrum of the field

$$D_\parallel = \frac{1}{3\pi}\left(\frac{mc}{q}\right)^2 \frac{v^3}{P_\perp(k_0)} ,$$

$$= \frac{v}{3\pi}\frac{R^2}{P_\perp(B_0/R)} , \qquad R = mvc/q .$$

This form suggests the introduction of a mean free path, λ, via the traditional kinetic theory relation $D = \lambda v/3$. We have also introduced the particle "rigidity," R, which determines the gyroradius, R/B. Note that $\lambda = R^2/P_\perp(B_0/R)$ is a function of particle rigidity, while $D_\parallel$ depends on velocity as well as rigidity. The observed power spectrum near 1 AU has roughly the form of a power law, k^{-m}, with m between 1 and 2. This predicts $\lambda \propto R^{(2-m)}$. Solar flare proton events above 20 MeV have been fit with rigidity-independent λ, while modulation of galactic cosmic rays appears to require $\lambda \propto R$. Thus, to within one power of R, the theory is consistent with observations. The measured values of P(k) also give the right order of magnitude for $D_\parallel$.

More information than just flux time histories has been obtained from experiments; in particular, the directional flux distribution has been measured (usually in the ecliptic plane). To interpret these observations, we must return to the full equation and, even more important, must allow $\vec{B}_0$ to be a function of position (e.g., the Archimedian spiral

field we previously discussed). In this case the axes in velocity space depend on position, since μ is measured from $\vec{B}_0$; therefore, if we wish an equation for $W(\vec{r}, \vec{v}, \mu, \varphi, t)$, we must take account of the implicit dependence of μ and φ on $\vec{r}$. Thus the total particle derivative with respect to $\vec{r}$ with $\vec{v}$ held constant involves the explicit determination of ∇W as well as the implicit terms:

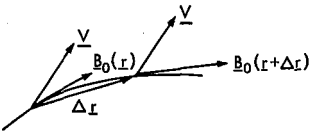

$$\frac{d}{d\vec{r}} W = \nabla W + \nabla\left(\hat{\vec{v}} \cdot \hat{\vec{B}}_0\right) \frac{\partial W}{\partial \mu} + \nabla\left(\vec{v} \cdot e_\perp \Big/ \sqrt{1 - \left(\hat{\vec{v}} \cdot \hat{\vec{B}}_0\right)^2}\right)\left(\frac{-1}{\sin\varphi}\right) \frac{\partial W}{\partial \varphi} ,$$

since $\mu = \hat{\vec{v}} \cdot \hat{\vec{B}}_0$ and $\hat{\vec{v}} \cdot \hat{\vec{e}}_\perp = \sqrt{1-\mu^2}\cos\varphi$, if φ is measured from some vector $\vec{e}_\perp$ normal to $\vec{B}_0$. The complete equation becomes, after using the identity $\nabla\left(\hat{\vec{v}} \cdot \hat{\vec{B}}_0\right) = (\hat{\vec{v}} \cdot \nabla)\hat{\vec{B}}_0 + \hat{\vec{v}} \times \left(\nabla \times \hat{\vec{B}}_0\right)$,

$$\frac{\partial W}{\partial t} + \vec{v} \cdot \nabla W = \Omega_0 \frac{\partial W}{\partial \varphi} + \frac{1}{T}\left[\frac{\partial}{\partial \mu}\left(1-\mu^2\right)\frac{\partial W}{\partial \mu} + \left(\frac{1}{1-\mu^2} + \zeta\right)\frac{\partial^2 W}{\partial \varphi^2}\right]$$

$$-\left(\vec{v} \cdot (\hat{\vec{v}} \cdot \nabla)\hat{\vec{B}}_0\right)\left[\frac{\partial W}{\partial \mu} - \frac{\cot\varphi}{1-\mu^2}\frac{\partial W}{\partial \varphi}\right] - \left(\vec{v}(\hat{\vec{v}} \cdot \nabla)e_\perp\right)\frac{1}{\sin\varphi\sqrt{1-\mu^2}}\frac{\partial W}{\partial \varphi} .$$

Rather than deal with this entire equation, we can simplify it for solar flare events, using the following argument. Applying the relation given earlier for T in terms of $D_\parallel$ and v, we can estimate that $T \sim 6\, D/v^2 \sim \beta^{-2}$ (minutes) where $\beta = v/c$. At 1 AU, $\Omega_0 \sim 1/2\ \mathrm{sec}^{-1}$, so $\Omega_0 T \sim 30\beta^{-2}$; thus $(\Omega_0 T)^2$ is a large number, so $D_\perp/D_\parallel \ll 1$ and nonrelativistic particles must follow field lines. This suggests that W must be independent of φ, for lines connecting to the flare region, and that the only spatial parameter is the distance out along the field line, x. Setting $\partial W/\partial\varphi = 0$ and averaging the complete equation over φ, we have an equation for the new function $w(x, v, \mu, t)$:

$$\frac{\partial w}{\partial t} + \mu v \frac{\partial W}{\partial x} = -\frac{v}{\partial L}\left(1-\mu^2\right)\frac{\partial w}{\partial \mu} + \frac{1}{T}\frac{\partial}{\partial \mu}\left(1-\mu^2\right)\frac{\partial w}{\partial \mu} ,$$

where $L = -B_0/\partial B_0/\partial x$. The new term arises from the manipulation

$$\frac{1}{2\pi}\int_0^{2\pi} d\varphi\, \hat{\vec{v}}\cdot(\hat{\vec{v}}\cdot\nabla)\hat{\vec{B}}_0 = \frac{1}{2}\left(1-\mu^2\right)\nabla\cdot\hat{\vec{B}}_0 + \frac{3}{2}\mu^2\hat{\vec{B}}_0\cdot\left(\hat{\vec{B}}_0\cdot\nabla\right)\hat{\vec{B}}_0 = \frac{v}{2L}\left(1-\mu^2\right),$$

since $\left(\hat{\vec{B}}_0\cdot\nabla\right)\hat{\vec{B}}_0$ is perpendicular to $\vec{B}_0$ and $\nabla\cdot\hat{\vec{B}}_0 = -\left(1/B_0\right)\partial B_0/\partial x$.

The physical significance of the new term becomes clear if we allow $T\to\infty$, in which case scattering becomes unimportant. Then we are left with a linear first-order partial differential equation which is immediately soluble in terms of the constants of integration of the characteristic equation

$$\frac{dx}{\mu v} = \frac{d\mu}{\frac{v}{2L}\left(1-\mu^2\right)}.$$

We can find $\mu(x)$ immediately by cross-multiplying and substituting

$$\frac{1}{L} = -\frac{1}{B_0}\frac{\partial B_0}{\partial x} :$$

$$2\mu\, d\mu + \left(1-\mu^2\right)\frac{1}{B_0}\,\partial B_0 = 0 ,$$

which integrates to $\left(1-\mu^2\right)/B_0$, constant. This is the well-known first adiabatic invariant (the magnetic moment M), so called because the product of the current and the area of a charge in helical motion is

$$M = q(\text{statcoul})\cdot(qB/2\pi mc)\left(\text{sec}^{-1}\right)\cdot\pi\left(mv_\perp c/qB\right)^2\left(\text{cm}^2\right)$$

$$= (c/q)\left(mv^2/2\right)\left(1-\mu^2\right)B .$$

Thus this term represents the tendency for the M of a particle to remain constant along a field line ($dM/dx = 0$), so that in a diverging field, (like the interplanetary field), the particle tends to "run out" along the field lines. Only the presence of velocity scattering ($T < \infty$) can prevent this strong collimation. For example, if the pitch angle $\theta = \pi/2$ for a particle at the sun ($B_0 \sim 1$ gauss), at 1 AU ($B_0 \sim 5 \times 10^{-5}$ gauss) the pitch angle would be

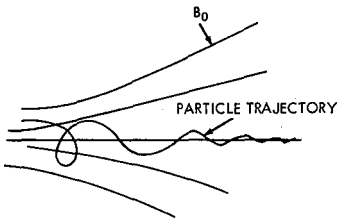

$$\theta \sim \sin\theta = \sqrt{B_{EARTH}/B_{SUN}} = 0.007 = 0.4°.$$

This competition between collimation and scattering is regulated by the single parameter $\alpha = vT/2L$, as may be seen by multiplying the transport equation through by T

$$T\frac{\partial w}{\partial t} + \mu\frac{\partial w}{\partial s} = -\alpha\left(1-\mu^2\right)\frac{\partial w}{\partial \mu} + \frac{\partial}{\partial \mu}\left(1-\mu^2\right)\frac{\partial w}{\partial \mu},$$

where $ds = dx/vT$. When $\alpha \to 0$, scattering clearly predominates and we have random transport; but when $\alpha \to \infty$ there is deterministic motion (M = constant).

<u>Problem:</u> Show that $e^{-2\alpha s}e^{\alpha\mu}$ is a solution and sketch the function.

<u>Solution:</u> Substitution leaves

$$(\mu - 2s)\frac{d\alpha}{ds} = 0,$$

so if α = constant (or if $s\,\partial\alpha/\partial s \sim 0$), this function is a solution to the steady state problem. This is indeed the dominant mode ($s > 1$) for steady outflow from the sun. The simplest assumption about propagation would be $s \sim x/vT$ ($T \cong$ constant); then $\alpha s \sim x/2L \sim 1$, independent of particle properties. Note, however, that the above

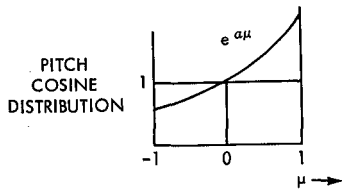

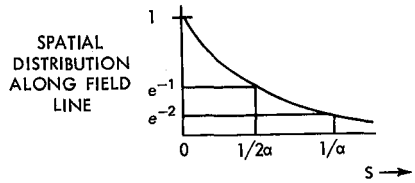

assumption is consistent with the condition on the solution ($s\ \partial\alpha/\partial s \cong 0$) only for $x \gg vT$, since $s\ \partial\alpha/\partial s = x\ \partial\alpha/\partial x \sim vT/x$.

To study time-dependent outflow, it is again simplest to degrade the equation with a weak anisotropy approximation.

<u>Problem</u>: Let

$$w = \frac{n(x, t)}{2} + \frac{3}{2v}\, j(x, t)\mu ,$$

and obtain the continuity and current equations by multiplying the w equation by 1 and $v\mu$ and integrating $-1 \leq \mu \leq 1$. In the quasi-stationary approximation, $\partial j/\partial t \equiv 0$, obtain the diffusion equation. What are these equations for $\vec{B} = B_0 \left(r_0/r\right)^2 \vec{e}_r$?

<u>Solution:</u>

$$\frac{\partial n}{\partial t} + \frac{\partial j}{\partial x} = -\frac{1}{L}\, j ,$$

$$\frac{\partial j}{\partial t} + \frac{v^2}{3}\frac{\partial n}{\partial x} = -\frac{2}{T}\, j .$$

Since $-1/L = (1/B)\ \partial B/\partial x$, the first equation can be written

$$\frac{\partial n}{\partial t} + B\frac{\partial}{\partial x}\, j/B = 0 .$$

In a curvilinear coordinate system defined by the field lines, such that one coordinate (x) is the distance along a line, it can be shown that for

a vector $\vec{j}$ which is always parallel to $\vec{B}$,

$$\nabla \cdot \vec{j} = B \frac{\partial}{\partial x} j/B .$$

This result depends on $\nabla \cdot \vec{B}$ vanishing. Combining the density and current equation in the diffusion approximation, we have

$$\frac{\partial n}{\partial t} = B \frac{\partial}{\partial x} \frac{1}{B} \left(\frac{v^2 T}{6} \right) \frac{\partial n}{\partial x} ,$$

where the (position-dependent) diffusion coefficient is identified in the operator $\nabla \cdot (D \nabla n)$. For a radial field we recover the familiar equations of isotropic diffusion

$$\frac{\partial n}{\partial t} + \frac{1}{r^2} \frac{\partial}{\partial r} r^2 j = 0 ,$$

$$\frac{\partial j}{\partial t} + \frac{v^2}{3} \frac{\partial n}{\partial r} = - \frac{2}{T} j ,$$

$$\frac{\partial n}{\partial t} = \frac{1}{r^2} \frac{\partial}{\partial r} \left(r^2 D \frac{\partial n}{\partial r} \right) .$$

Two aspects of propagation have not been considered here. First, electric fields have been neglected. This is justifiable for energetic solar cosmic rays since the characteristic time for appreciable energy loss is on the order of the duration of events (or longer); however, the effect on galactic cosmic rays, which can dwell in the interplanetary field for days, is of considerable importance. Second, the one-dimensional equations appropriate to the description of solar events

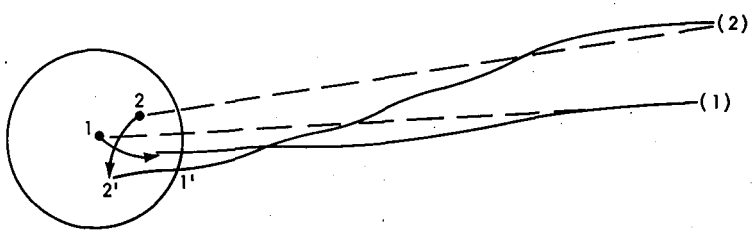

do not include any information on the relative positions of the field lines. The feet of the field lines undergo some disordered convection in the photosphere due to the turbulent velocity fields there. Thus field lines originating at positions 1 and 2 may later be at positions 1′ and 2′. If the solar wind has convected these fields out continually, it is clear that they will be quite tangled in interplanetary space. Another, and probably more important, mechanism leading to disordering of the spiral pattern operates in the Alfvén region, where the outgoing coronal plasma makes its transition from corotating to radial outflow. In fact, the transport of the field from the photosphere through the chromosphere and the corona to the Alfvén region is far from understood.

Now that we have covered the basic ideas in particle propagation, let us turn once more to the observations. The problem of galactic modulation is still unresolved and a discussion of its present status would be beyond the scope of this discussion. Suffice it to say that the diffusion-convection theory gives a generally acceptable explanation of modulation.

With respect to solar cosmic rays, we need only up-date the review by C. E. Fichtel and F. B. McDonald (Reference 2). (Note: The $\alpha + \beta$ in Equation 18, p. 391 of their paper should simply be α.) As solar (and experimental) activity increased after 1966, the last period covered in the review article, events became more frequent and more complex. The role of low-energy particles (protons <20 MeV, electrons >40 keV) has increased in importance, ironically, because they do not usually propagate in the manner of classical diffusion. They scatter considerably less, as is evidenced, for instance by the prompt arrival of 40 keV electrons about 30 minutes after the optical flare. This corresponds to almost direct spiraling out the field line, since $\beta \geq 0.4$ for these electrons, and line-of-sight transit is 8 minutes for light. Low energy particles also exhibit strong pitch-angle anisotropies, again showing that there is much less scattering than at higher energies. There is also a strong statistical tendency for 40 keV electrons to be present after flares on the western half of the sun's disc (i.e., longitudes between 30 and 90 degrees W), but not after flares on the eastern half. Thus low-energy particles serve as tracers of the interplanetary field lines. Moreover, they are often long-duration tracers, since they can be continually produced by the sun for a number of days. These ideas arose from the analysis of recurrent low-energy events in which enhanced fluxes appear on successive solar rotations about 27 days apart. One well documented nonrecurrent

event gave a composite sample of all the foregoing modes of propagation (Reference 5). By means of three satellites at different positions: IMP III, and OGO III near the earth, and Explorer XXXIII near the moon (Figure 1), the following picture of this complex event was deduced: The high energy protons (Figure 2a-II) arrived in a clean, classical diffusion mode after the flare at 0027 UT, July 7, 1966. However, 15 MeV protons (Figure 2a-III) show a hint of a second maximum a day after the flare. This tendency is clearer in the protons sensed by OGO III (Figure 2b), in which diffusion dominates at 32 MeV while the second-day maximum is practically all that is seen at 3 MeV. The low-energy electrons (Figure 2a-IV and V) show prompt arrival, but also a later maximum with an even sharper peak superimposed (about 0800 to 1200, July 8). The interpretation (Figure 3) is that there was prompt diffusive propagation of all components at early times, but

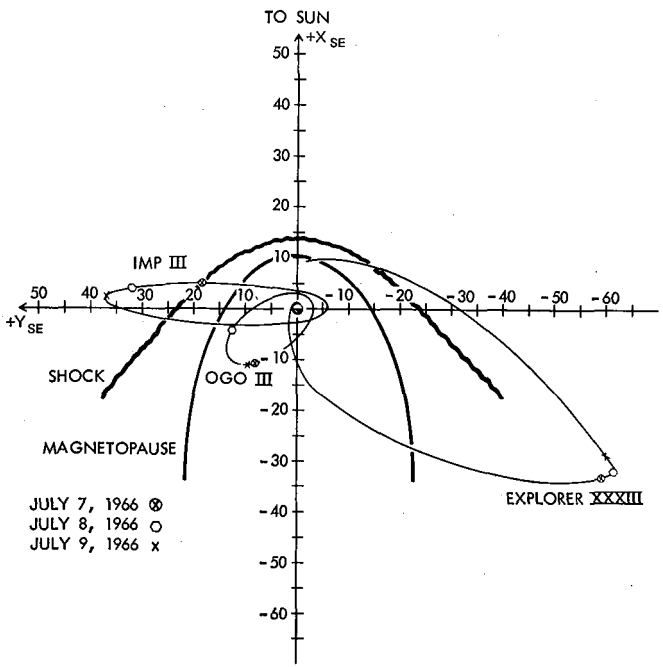

Figure 1. Locations of the IMP-III, Explorer XXXIII, and OGO III satellites during July 7 to 9, 1966 projected onto the ecliptic plane. OGO III is at high geomagnetic latitude (14 to 37 degrees) and therefore outside the magnetosphere during most of this period.

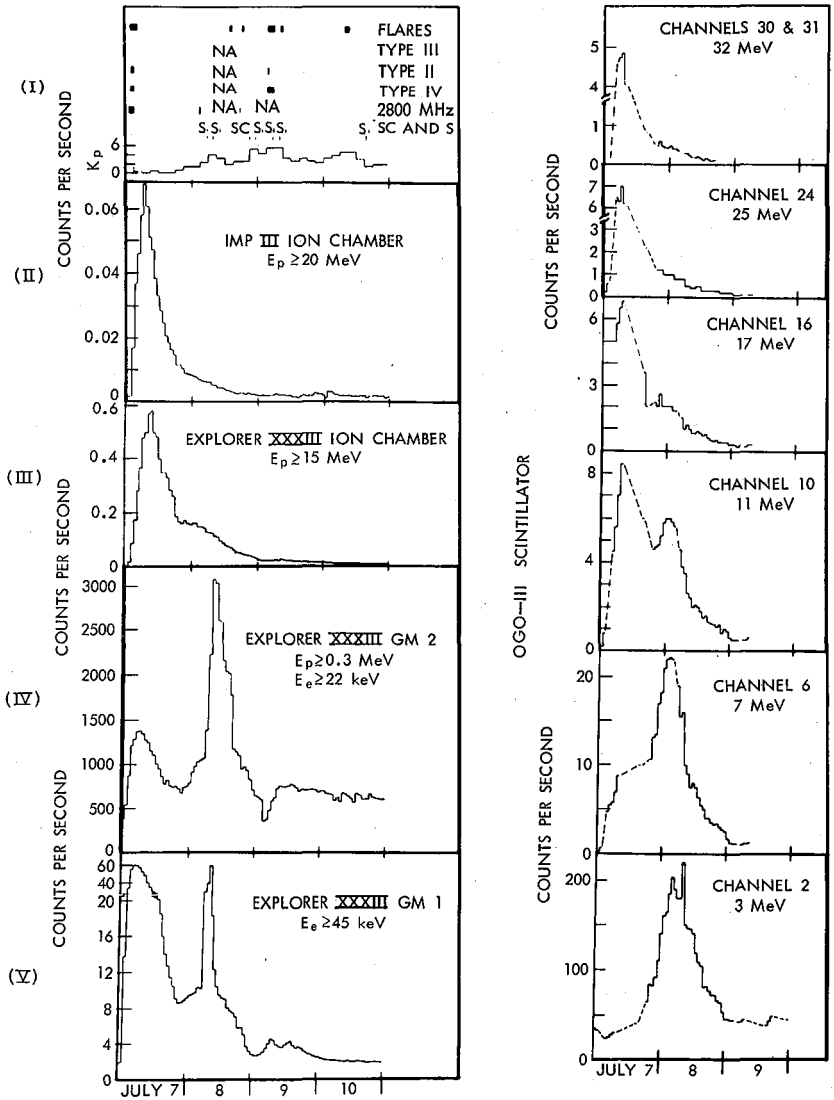

Figure 2. Part (a) shows: (1), the major solar flares and radio bursts, geomagnetic disturbances and K_p for the period July 7 to 9, 1966; (II), (III), (IV), and (V), the counting rates of particle detectors on IMP-III and Explorer XXXIII. Part (b) shows the count rates of six different energy channels of the OGO-III detector for the same time interval.

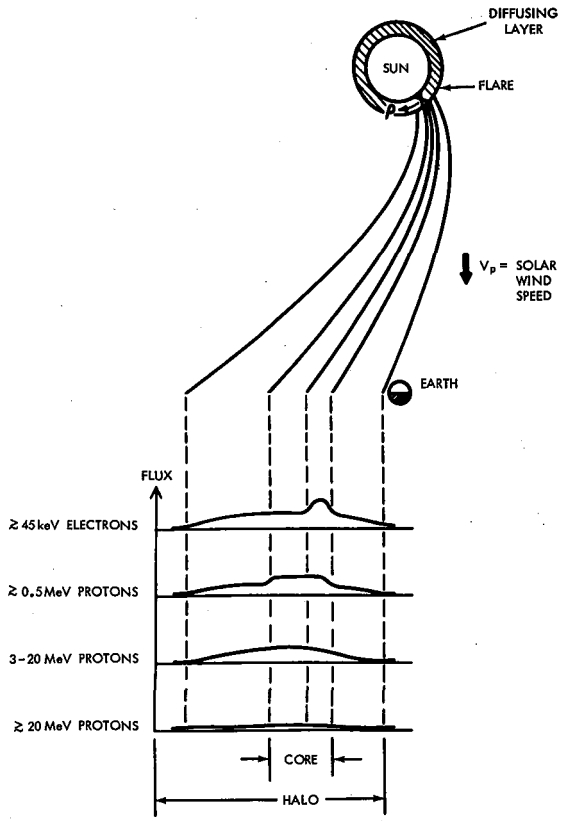

Figure 3. A schematic of the core and halo of the energetic particle fluxes on July 7. The core and halo are convected by the solar wind past the earth. The lower left graph indicates the spatial variation of the particle fluxes. The upper diagram shows the thin diffusing layer around the sun postulated by Reid in 1964 (Reference 3) and Axford in 1965 (Reference 4). ρ is the distance away from the flare measured in the diffusing layer.

that the sun continued to produce low-energy particles through July 8. Since the flare was at longitude 48 degrees W, the time for the flare region field lines to corotate to a position connecting to earth was about (60° - 48°)/(13° per day) ~ 1 day. These field lines were filled with electrons (≳40 keV) and protons (~10 MeV) so that the detectors actually recorded the spatial profile of the particle fluxes.

Problem: Using the contents of this paper, explain the propagation characteristics of the four groups of solar particles discussed.

Solution: For protons above 20 MeV we know there is diffusion with $D \sim 10^{22}$ cm^2/sec. Since $\beta > 0.2$ and the scale length is r/n for a field falling off as r^{-n}, the anisotropy parameter is

$$\alpha = \frac{vT}{2L} = \frac{3}{c}\frac{D}{\beta L} \leq \left(10^{-10}\right) \frac{10^{23}}{(0.2)\left(1.5 \times 10^{13}\right)} = 0.3 ,$$

so there is only weak velocity anisotropy, consistent with classical diffusion. Despite the fact that constraint to field lines is considerable since

$$\Omega_0 T = \frac{\Omega_0}{c^2}\frac{6D}{\beta^2} = \frac{(0.5)}{\left(9 \times 10^{20}\right)} \frac{\left(6 \times 10^{22}\right)}{\beta^2} = 30\beta^{-2} \gg 1 ,$$

the particles can still have a time history compatible with classical three-dimensional diffusion, because for $B \propto r^{-2}$ the one-dimensional diffusion equation is identical to the equation for isotropic classical diffusion

$$\frac{\partial n}{\partial t} = D \frac{1}{r^2}\frac{\partial}{\partial r}\left(r^2 D \frac{\partial n}{\partial r}\right) .$$

Furthermore, if $P_\perp(k) \propto k^{-2}$, then λ is independent of rigidity, as in classical transport theory. Thus energetic protons appear to diffuse classically.

Electrons of energy 3 to 12 MeV have a much smaller gyroradius than energetic protons: for example $R_{e(10\,\mathrm{MeV})} \sim 10^{-2} R_{p(20\,\mathrm{MeV})}$. However if, again, $P_\perp(k) \propto k^{-2}$, then

$$\frac{\lambda_e}{\lambda_p} = \frac{R_e^2}{P_\perp\left(B_0/R_e\right)} \frac{P_\perp\left(B_0/R_p\right)}{R_p^2} \sim 1 ,$$

and MeV electrons should diffuse like MeV protons. Since their values of β are of the same order, the electrons also would not have large pitch angle anisotropies.

On the other hand, as we go to lower-energy protons and electrons, less scattering and higher anisotropies are observed. Since the smaller velocities tend to decrease D and α, the only way D and α can increase is for T to increase. A strong anisotropy of $\alpha = 1$ (actually, $\alpha \sim 5$ has been observed for protons and electrons) gives $vT = 2L \sim 1$ AU so that the distance traveled in a relaxation time is comparable to our distance from the source. Clearly the diffusion approximation cannot be valid, although the one-dimensional equation (with steady-state solution $e^{-2\alpha s}\, e^{\alpha\mu}$) probably is still a reasonable description of this low-energy propagation.

We must end this discussion of the propagation of solar cosmic rays with a strong qualification. Another explanation of at least the early portions of high energy flare particle events is a very real possibility, although it is not incompatible with the ideas we have already presented. It is quite possible that flare particles spend a good part of their time after acceleration in the outer solar corona (Reference 2) before streaming out into interplanetary space (Reference 3). The time histories predicted by this "two-region" model are almost indistinguishable from those predicted by pure interplanetary diffusion. Only better measurements than we have now of velocity anisotropies throughout events can resolve the question because effective interplanetary diffusion implies small anisotropies ($\alpha < 1$) while the predominance of coronal storage with weak interplanetary scattering implies large anisotropies ($\alpha > 1$).

REFERENCES

1. Parker, E. N., Interplanetary Dynamical Processes, Interscience Publishers, New York, 1963.

2. Fichtel, C. F., and McDonald, F. B., "Energetic Particles from the Sun," Annual Review of Astron. and Astrophys., 5:391, 1967.

3. Reid, G. C., "A Diffusion Model for the Initial Phase of a Solar Proton Event," J. Geophys. Res., 69:26-59, 1964.

4. Axford, W. I., "Anisotropic Diffusion of Solar Cosmic Rays," Planetary and Space Science, 13:1301, 1965.

5. Lin, R. P., Kahler, S. W., and Roelof, E. C., "Solar flare injection and propagation of low-energy protons and electrons in the event of 7-9 July, 1966," Solar Physics, 4:338, 1968.

Page Intentionally Left Blank

VIII. INTERPLANETARY DUST

L. W. Bandermann
University of Hawaii
Honolulu, Hawaii

R. A. Schmidt has defined interplanetary dust as "microscopic particles occurring outside the limits of the earth's atmosphere." The particles are variously called cosmic dust, cosmic spherules, micrometeorites, micrometeoroids, nanometeorites, meteoric dust, meteoritic dust, primordial dust, zodiacal dust, interstellar dust and galactic dust (References 1 and 2). In Schmidt's definition, all reference to the physical properties and origin of the dust is avoided. An interplanetary dust particle is too small to be detected as a meteor when it enters the earth's atmosphere: the radius is less than 1 mm. But it can be detected by its impact on a satellite or space probe and, together with many other particles, it causes the zodiacal light. However, the "typical" zodiacal particle may be different from the particle typically detected by its impact on a micrometeoroid satellite (Reference 3).

Interplanetary dust has been a subject of interest for several centuries (Reference 4), and particularly in this age of space flights and interplanetary experiments—because dust is a hazard for such enterprises: the life time of delicate satellite instruments is limited because of erosion caused by interplanetary dust. To estimate the erosion rate we need to know the size distribution, mass per unit volume, and velocity distribution of the particles. These quantities have not yet been determined very accurately, but an upper limit to the space hazard has been obtained (References 5 and 6). A second reason for our interest in interplanetary dust is that it is a kind of "blanket" which blocks the diffuse star light from our view. Of particular interest in this connection is the total mass of dust in a column vertical to the ecliptic plane. Interplanetary dust is of further interest to us because it may be an important source of certain elements in the earth's crust. Interplanetary dust particles are an integral part of our solar system, and our knowledge of their physical properties, origin and evolution significantly increases our understanding of the solar system.

EXPERIMENTAL EVIDENCE ABOUT INTERPLANETARY DUST

The Zodiacal Light

There is a faint cone of light centered near the ecliptic plane and extending from the solar limb to the antisolar point (References 7 through 10). This is the zodiacal light which is sunlight scattered by dust particles between the sun and the earth and in regions beyond the earth's orbit. Near the antisolar point the zodiacal light brightness is slightly enhanced: This effect, called gegenschein has been variously attributed to (Reference 11):

1. An increase in particle concentration along the extended sun-earth line (a dust tail of the earth)

2. A localized dust cloud at a libration point on the extended sun-earth line (References 12 and 13)

3. An enhancement in the differential scattering cross section of dust particles near 180 degrees (glory) (References 14 through 18)

4. Continuum emission from a gas tail of the earth (analogous to a comet tail) (References 19 through 21) excited by the solar wind.

The third explanation is satisfactory, for the following reasons: (1) a dust tail of the earth requires a large geocentric dust cloud which we do not believe exists. (2) The dust concentration at a libration point required to explain the brightness of the gegenschein is dynamically impossible (References 22 and 23). Also, the center of the gegenschein should always lie exactly on the extended sun-earth line; this is not the case (Reference 24). The emission from a gas tail should be enhanced following a solar flare, but this is not observed (Reference 22).

It has been suggested that the zodiacal light—all or part of it—is caused by a geocentric dust cloud (References 25 and 26), but this is unlikely to be the case because:

1. The suggestion is based on the rates of particle detection by satellite-born acoustic sensors (References 27 through 29), and these rates are believed to be spurious (Reference 30).

2. No process has been discovered by which such a cloud is created (References 31 and 32).

3. The manner in which the zodiacal light brightness varies with ecliptic latitude is in conflict with the hypothesis (Reference 33).

The zodiacal light has been studied not only from the ground but also with rockets (Reference 34), balloons (References 8 and 35 through 37), and from orbiting spacecraft (References 36 through 39). In principle, it is possible to determine the average physical characteristics and the size spectrum and spatial distribution of zodiacal dust from the observed brightness (as function of elongation and ecliptic latitude), polarization, color, and spectral features of the zodiacal light. A single dust model which explains all the observations satisfactorily has not yet been found. The relatively large polarization of the zodiacal light (up to 25 percent) (Reference 40) presents a special problem: Although dust models have been constructed (References 41 through 44) which explain the polarization (in these models the average particle radius is less than 1 micron and the size distribution, given by a power law—$dN(s) = Cs^{-P}\,ds$, has a relatively large spectral index $p \geq 4$) such models are in conflict with results based on satellite impact measurements (Reference 45). The satellite data agree much better with a model in which the average particle radius is several microns, and $p \leq 3$. The polarization may also be caused by the peculiar physical shape of the particles. We know yet very little about the shape and the surface details of zodiacal dust; until recently, the theory of the zodiacal light had been based on the assumption that the particles are spherical. Now, calculations of scattering functions are made for non-spherical particles (References 44 through 49). Estimates of the bond albedo of zodiacal particles range from 0.005 to $\simeq$0.6 (References 7, 10, 16, and 50).

The concentration of zodiacal dust in the ecliptic plane at 1 AU is between one and several hundred particles per km^3, and the mass/volume between $\simeq 10^{-24}$ gm/cm^3 and $\simeq 10^{-21}$ gm/cm^3. It is assumed that the concentration varies with distance r from the sun as $r^{-\beta}$, and β is probably less than 3* (References 7, 10, 34, 35, 41, 42, 44, 45, and 51). The fact that the zodiacal light cone appears to be fairly narrow suggests that the dust particles are strongly concentrated toward a plane

*Powell et al. (Reference 47) have recently put forward the idea of distinct dust belts such as a Venus-Earth belt, a Mars-Earth belt, etc.

close to the ecliptic. However, the zodiacal light brightness depends on both the concentration and the scattering function of the particles; it is a quantity integrated along the line of sight and the strong concentration therefore, may be an illustion. After a study of the isophotes, some investigators (References 45 and 51) concluded that the average orbital inclination of the particle orbits may be as much as 30 degrees. This is contrary to the assumption of a thin dust layer. On the other hand, recent measurements (Reference 52) of the Doppler shift of Fraunhofer lines in the zodiacal light can be understood better in terms of small orbital inclinations (Reference 53). We do not know whether the dust is distributed symmetrically about the ecliptic plane, the invariable plane (off by 1.5 degrees), or the plane containing the solar rotational equator (off by 7 degrees). Evidence for each possibility has been cited (References 10, 54, 55, and 56). Symmetry properties of the dust distribution are directly related to the origin of dust or to the effects of perturbations on dust orbits.

Satellite Impact Experiments

Special sensors have detected the impact of interplanetary dust on satellites and space probes. The sensors are usually one of two types: microphone detectors (acoustic detectors, sounding boards) and penetration detectors (pressure cells, grids, wire cards, parallel plate condensors). In the first type, the particle is detected by its sound of impact; in the second, by its puncturing a thin film, grid, or plate. Neither detector gives any information other than that the particle has sufficient mass or velocity to overcome the detector threshold. Detectors are also being developed which measure the velocity or mass of an impacting particle (References 57 through 61).

The accurate calibration of acoustic and penetration detectors has proved difficult. In the United States, acoustic detectors are considered to be momentum-sensitive but are considered energy sensitive in the U.S.S.R. (Reference 60). Penetration detectors are energy sensitive, but there is no agreement concerning the proper functional relation between particle mass and velocity and detector threshold (References 62 and 63). In a micrometeoroid impact experiment one does not measure the dust concentration, but measures instead a kind of flux. An interpretation of the counting rate in terms of the distribution of particle radius and velocity requires some assumption about these distributions. These assumptions are usually based on studies of the zodiacal light.

Although our only knowledge about the impacting particles is that they overcome the detector threshold, the satellite experiments give us quite a bit of information about interplanetary dust. This is because we can determine how the counting rate varies with (1) satellite altitude (distance from the earth), (2) detector threshold, and (3) type of detector. The early acoustic rates obtained near the earth were much higher than expected on the basis of our present knowledge about zodiacal dust (References 27 through 29), and they were interpreted in terms of a very high dust concentration near the earth* (Reference 28). Attempts to explain why such a dust belt should exist have failed (References 25, 31, and 64 through 71). It was also discovered that the unexpectedly high counting rate near earth could be related to the threshold requirement of the detectors (References 45, 65, and 72). But even so, a very steep size distribution (and an unreasonably low geocentric velocity—which is the speed of dust relative to earth at 1 AU) would be required (References 31 and 45). Also, the variation of the acoustic rates with threshold was compatible only with a flat size spectrum ($p < 3$) (References 45 and 73). Eventually, the acoustic rates were identified with thermal noise in the detectors (References 30 and 75), and this put the dust belt to rest.

The penetration rates near the earth, and the acoustic and penetration rates far from the earth, agree fairly well with rates predicted for models of the zodiacal dust such as given in Reference 7 by van de Hulst ($p = 2.6$; $s \geq 1\mu$; mass/volume $= 3 \times 10^{-21}$ gm/cm^3 at 1 AU) and for a geocentric velocity of 5 to 15 km/sec (References 45, 73, 76, and 77).

In some cases the impact rate on the earth's morning side was different from that on the evening side, and there were seasonal variations as well (References 78 through 81). From such asymmetries one can derive valuable information about the sizes of interplanetary dust particles and their orbits (References 45, 73, and 82). Consider, for instance, dust particles which are partly supported by solar radiation pressure: their orbital velocity is smaller than the Keplerian velocity. Hence if they are in nearly the same orbit as the earth, the earth overtakes them and the influx of this dust into the atmosphere is greater on the morning side than on the evening side. The satellite impact rate, however, is not necessarily greater on the morning side since particle trajectories merge behind the earth. A systematic analysis of the satellite data with respect to time variations has not yet been undertaken, but the necessary theory has been developed (Reference 73).

*Although there was no convincing evidence from the altitude dependence of the impact rates (Reference 74).

Dust in the Atmosphere and in Sediments

Since the end of the last century, dust has been variously collected with balloons, airplanes, and rockets from the atmosphere and from ice and snow cores (References 3, 4, 83, 84 and 85). In the atmosphere, dust is collected on specially prepared surfaces which are exposed for a predetermined interval of time and altitude range. Prior to sending them aloft, the surfaces are carefully cleaned of laboratory dust and other contaminants. Some surfaces are purposely not exposed to the atmosphere and some others are kept in the laboratory; these serve as controls. Such experiments require the utmost cleanliness in the laboratory in order to avoid contamination. Nevertheless, in some experiments the control panels were found actually to contain more particles than the panels exposed in the atmosphere! (Reference 85). We do not yet possess reliable criteria by which to identify a particle as either extraterrestrial or terrestrial. But in recent very carefully conducted rocket collection experiments (Reference 87), nearly all particles were much like terrestrial dust. Some suggestions about the possible composition of interplanetary dust are based on the composition of meteorites which often contain anomalous amounts of nickel, cobalt, manganese, and sodium (References 85, 88, and 89). From the amount of dust collected and classified as extraterrestrial, the rate of accretion of such dust by the earth can be deduced. Estimates vary between 10 and 10^7 tons/day (Reference 1).

Interplanetary dust possibly contains considerable abundances of certain nuclides depleted in the earth's crust. Analyses of deep sea sediments indicated Al^{26} in relatively large quantities (References 86, 90, 91 and 92). In interplanetary dust, Al^{26} is produced by solar cosmic rays (10 MeV protons) from Mg^{26}, Al^{27}, and Si^{28}. By assuming equilibrium saturation of the dust particles with Al^{26} (this requires a sufficiently long exposure to the cosmic ray flux) and by making reasonable estimates of the relevant cross sections and of the cosmic ray flux, an Al^{26} equivalent dust accretion of some 10^3 tons/day by the earth was derived (Reference 93). Lately, however, it was suggested in Reference 94 that the Al^{26} may be entirely of terrestrial origin (from atmospheric argon). Furthermore, no anomalous amounts of Al^{26} were found in Greenland ice cores (References 95 and 96). The minute concentration of the nuclide in sediments and ice makes precise measurements of course difficult. The Al^{26} theory requires a stony dust composition; therefore, only a lower limit to the accretion rate can be obtained. Iridium and osmium are also depleted in the earth's crust.

From their abundance in deep sea sediments, a dust accretion of less than 10^3 tons/day (Reference 97) has been derived. From the abundance of Cl^{36}, an accretion of slightly more than 10^3 tons/day has been derived (Reference 98). Other estimates of the dust accretion rate are based on the abundance of He^3, Ar^{36}, Ne^{21}, and noble metals (References 85 and 99).

In moderate and high latitudes one often detects dust layers, called noctilucent clouds, in the upper atmosphere; they sometimes cover an area of several 10^6 km^2, and they are very thin ($\simeq$2 km) and have a well-defined altitude ($\simeq$80 km). The concentration of dust in these layers is between 10^{-2} and 1 per cm^3, and the particle radius is between 0.05 and 0.5, (References 100 through 102). Noctilucent clouds are also observed in the antarctica (Reference 103). The dust concentration cannot be explained in terms of straightforward sedimentation of dust (of interplanetary origin) in the upper atmosphere (Reference 104). Seasonal variations of the NLC and their peculiar structure, together with the fact that the particles are often coated with ice, indicate that the clouds are meteorologically conditioned (References 105 through 107).

Attempts are now being made to determine the dust content of the upper atmosphere directly by measuring the return signal of a laser beam. Dust layers have been found at altitudes from 60 to 90 km (References 108 through 110). The dust concentration is of the same order as that in noctilucent clouds. The extent of the laser back scattering is not known.

Evidence from Comets, Asteroids, Meteors and Meteorites

Some ideas about the properties of interplanetary dust can also be based on our knowledge of dust comets, asteroids, meteors and meteorites. Type II (dust) comets continually lose dust, and at a rate probably greatest near perihelion. Dust particles are also created in collisions between asteroids, and Poynting-Robertson drag (see below, DYNAMICS OF INTERPLANETARY DUST) moves them toward the Sun. Meteorites and meteors can be taken as evidence for the existence of much finer matter in the solar system. The size distribution of meteoric particles is steeper than the size distribution in some zodiacal dust models. Öpik (Reference 112) has suggested that both types of particles may have a common origin, but a non-uniformity in

the size distribution may arise because large particles are more easily disturbed by Jupiter than small particles. But such a non-uniformity may not actually exist (Reference 113). It has also been suggested that zodiacal dust has a different composition than meteoric particles (Reference 111), but there is no direct evidence on this point. Concerning composition and shape of interplanetary dust, little is really known. (1) The Al^{26} theory is based on an assumption that interplanetary dust is stony, and says nothing about other types of dust nor about the shape or structure of the stony dust. Some of the features of the zodiacal light have been successfully explained (2) with models of purely metallic dust and with models of purely dielectric dust, also with mixtures of dielectric and metallic particles. (3) From the satellite impact rates we cannot yet deduce much about the shape, density, and composition of the particles. (4) The composition, structure, and shape of particles collected in the atmosphere, deep sea sediments, and snow and ice cores are well known; but the extraterrestrial origin of these particles is unproven.

THE DYNAMICS OF INTERPLANETARY DUST

Several non-gravitational forces affect the orbits of interplanetary dust, and the evolution of an orbit depends on their relative importance. Some forces are steady over many orbital periods while others change rapidly. The physical properties of the dust particles also change with time.

Radiation Pressure and Poynting-Robertson Drag

A net force, P, is exerted on a dust particle by the solar electromagnetic radiation if the incident photon momentum is not all scattered in the forward direction. If E is the energy flux in erg/cm^2-sec, and c the speed of light, then

$$P = \pi s^2 Q_{pr} E/c \ , \tag{1}$$

where $\pi s^2 Q_{pr}$ is the radiation pressure cross section of the particle, and Q_{pr} depends on particle size, composition and shape; it can be larger than unity. For various types of spherical particles, Q_{pr} has been calculated from Mie theory (References 114 through 118). Since E is

proportional to r^{-2}, P does not secularly change any orbital parameter; however, the orbital velocity is by a factor $(1 - P/G)^{1/2}$ smaller than the Keplerian velocity where G is the gravitational force on the particle. P/G is proportional to (1/s), and very small particles cannot be in elliptic orbits. The value of s for which P = G, called radiation pressure limit, is approximately 0.2μ. A particle is in a parabolic orbit and it would leave the solar system, barring other effects, if its total energy is zero. This requires

$$P/G = 1 - r/(2a_0) , \tag{2}$$

where a_0 would be the semi-major axis of the orbit if P = 0, (Reference 119). The particle radius corresponding to (2) is roughly twice the radiation pressure limit.

The dust particle also experiences a retarding force (drag). Consequently, its total energy decreases with time and it tends to spiral toward the sun (References 120 and 121)—this is the Poynting-Robertson effect. (The orbit also precesses, but there are no other changes.) The semi-major axis a and the eccentricity e both decrease and are related by (Reference 122).

$$a\left(1 - e^2\right) e^{-4/5} = \text{constant} . \tag{3}$$

For a circular orbit (e = 0) the time T in which the orbital radius decreases from a_1 to a_2 is

$$T = 710\, s\, \delta\, a_1^2 \left(1 - a_2^2/a_1^2\right) Q_{pr}^{-1} \tag{4}$$

years, where s is the particle's radius in μ, δ its density in gm/cm^3, and a_1 and a_2 are in AU. For an initially nearly parabolic orbit with aphelion Q[AU] and perihelion q[AU], the total life time is

$$T = 2.3 \times 10^3\, s\, \delta\, Q^{1/2}\, q^{3/2}\, Q_{pr}^{-1} \tag{5}$$

years. The Poynting-Robertson drift velocity, da/dt, is proportional to s^{-1}; the particle mass is proportional to s^3; therefore, the net flow of dust toward the sun across a unit surface at r is proportional to the total surface area of dust in a unit volume at r. One can compute the rate at which interplanetary dust falls with the sun directly from the observed surface brightness of the zodiacal light, and therefore, assumptions about the particle size distribution are not necessary. The rate is approximately 1 ton/sec (Reference 123). There is some uncertainty about this number, as our knowledge of the dust distribution above the ecliptic plane is incomplete.

Planetary Perturbations

The effect of distant perturbations on dust orbits by the planets is insignificant because the life time of a particle is short compared with the time scale associated with such perturbations. However, during a close encounter with a planet, a large change in the particle's orbital velocity can occur. This change takes place instantly as compared with an orbital period. In the planetary frame of reference, the total energy of the particle is conserved; therefore, the planetocentric speed U of the particle before and after the encounter is the same. A second encounter with the planet, if it occurs, has the same value of U, and the effect of successive encounters is that orientation of the U-vector changes randomly. The particle's orbital semi-major axis, eccentricity and inclination are related by (Reference 111)

$$3 - r/a - 2\left[(a/r)\left(1 - e^2\right)\right]^{1/2} \cos i = \text{const.} \tag{6}$$

(Tisserand's criterion). The probability of an encounter at a planetocentric speed U and impact parameter d is, per orbital revolution (Reference 111),

$$P = (d/r)^2 \frac{U}{4\pi v_r \sin i}, \tag{7}$$

where v_r is the radial component of the heliocentric velocity of the particle. After N encounters, the net change in an orbital parameter is proportional to $N^{1/2}$. Since Poynting-Robertson drag removes the

particle relatively quickly from the region of space where an encounter with the planet is possible, N is relatively small; and therefore, the net change in any orbital parameter is small. Under certain conditions, however, a particle can be ejected from the solar system by a single encounter.

Corpuscular Radiation Pressure and Coulomb Drag

Interplanetary dust carries a surface charge which is a consequence of the absorption of solar UV photons and the accretion of ions and electrons from the solar wind. The charge is usually discussed in terms of an equilibrium potential V_0, and V_0 is a few volts, certainly not more than 10, perhaps even slightly negative. V_0 is nearly independent of particle radius and varies little with distance from the sun (References 124 through 128).

Solar wind ions and electrons which do not directly hit the dust particle nevertheless impart momentum to the dust particle because of their Coulomb interaction with the surface change—if the impact parameter is less than the shielding distance λ from the dust particle. Approximately, $\lambda = 0.5N_e^{-1/2}$, where N_e is the electron concentration in the solar wind. We account for physical impacts and Coulomb interaction by defining the total cross section σ. For the ith constituent of the solar wind (charge q_i) the cross section is given as follows (Reference 104): Let $V^* = V_0 q_i$; let K^* be the kinetic energy, T^* the mean thermal energy of the constituent, u its mean thermal velocity, and w the solar wind velocity. Then

$$\sigma/\pi s^2 = 1 + V^*/K^* + (V^*/K^*)^2 + \ln\left\{(K^*/V^*)(2\lambda/s)\right\} \quad \text{if} \quad K^* \gg T^*$$

$$= (2/3)(u/w)\left[1 + V^*/T^* + 2(V^*/T^*)^2 \ln\left\{(T^*/V^*)(2\lambda/s) - 0.58\right\}\right]$$

$$\text{if} \quad K^* \ll T^* \qquad (7)$$

The solar wind velocity is 300 to 500 km/sec (References 129 through 131), V_0 a few volts, and the solar wind temperature 10^4 to 10^6°K (Reference 132). We find $\sigma \simeq \pi s^2$. The total force on the dust particle is

therefore almost entirely due to impact of ions. It is much smaller than the solar radiation pressure. However, the corpuscular drag is comparable with Poynting-Robertson drag:

$$\frac{\text{solar wind drag}}{\text{Poynthing-Robertson drag}} \simeq 1.3 \times 10^{-9} F \ , \tag{8}$$

where F is the solar wind flux at 1 AU, 10^8 to 10^9 ions/cm^2-sec (Reference 104). The solar wind co-rotates with the sun to some extent (References 129 and 130), and therefore the drag on a dust particle is somewhat smaller than given by (8). It has been suggested that there may be a large number of very small dielectric dust particles in interplanetary space which are transparent enough that they do not contribute much to the zodiacal light (They are essentially "invisible."): these may be the noctilucent cloud particles. Such particles would experience very little Poynting-Robertson drag but they would always experience corpuscular drag and would therefore spiral into the sun much like under Poynting-Robertson drag—barring other effects, of course. If the solar wind were to co-rotate with the sun fully, then the corpuscular drag on the zodiacal particles would be strong enough to result in a pancake-shape zodiacal cloud (Reference 113). This is not observed.

Interaction with the Interplanetary Magnetic Field

The Lorentz force exerted on a dust particle due to the interaction of its surface charge with the interplanetary magnetic field is

$$L = V_0 s(\mathbf{v} + \mathbf{w}) \times \mathbf{B}/c \ , \tag{9}$$

where $\mathbf{v}$ is the particle's orbital velocity and $\mathbf{B}$ the field strength. The term involving $\mathbf{w}$ arises because the magnetic field is "forzen" into the solar wind and is carried along with it (Reference 132). Because of the sector structure of the field (Reference 133), the direction of L changes by 180 degrees many times during a single orbit of the particle. The change in an orbital parameter can therefore be described by a one-dimensional random walk (References 125 and 128). Of course, changes in the orbital parameters are inter-related; however, if we consider a large number of particles with initially similar orbital elements then we can calculate the r.m.s. change in any orbital element independently.

As an example, consider the inclination after a time T of initially circular orbits and having negligible inclinations: An r.m.s. value of 90 degrees can be expected in (Reference 104)

$$T = \frac{10^{10}\,\delta^2\,s^4\,a}{t\,V_0^2\,B^2\,w^2} \tag{10}$$

years, where δ is in gm/cm^3, s in μ, r in AU, V_0 in volts, B in gammas, w in km/sec, and t is the time (in years) which the particle spends in one sector of the magnetic field. For typical values $\delta = 3.5$, $s = 1$, $r = 1$, $t = 1/90$ (4 days), $V_0 = 5$, $B = 5$ (Reference 131), and $w = 500$, we find $T = 7 \times 10^4$ years. This is much longer than the Poynting-Robertson drift time da/dt given by (4). But we notice that T is proportional to s^4, whereas $da/dt \propto s^2$: clearly, the Lorentz force is very important for sub-micron size dust ($s < 1\mu$).

Sputtering, Evaporation, Collisions

The typical energy of solar wind ions is 1 keV (Reference 130); therefore they sputter atoms from the dust particle surface, and consequently the particle is gradually eroded. A recent estimate of the erosion rate is $ds/dt = 0.05\ r^{-2}$ Å/year (Reference 134), r in AU. The time scale associated with sputtering is much longer than the Poynting-Robertson time, and there are no significant dynamical effects associated with sputtering.

The temperature of an interplanetary dust particle, T(r), is not simply the black-body temperature. For dielectric particles (SiO_2), Over (Reference 135) finds

$$T(r) = 120\ r^{-1/2}\,°K; \qquad r \text{ in AU.} \tag{11a}$$

Whereas for metallic particles, Becklin and Westphal (Reference 136) find

$$T(r) = 418\ r^{-0.27}\,°K; \qquad r \text{ in AU.} \tag{11b}$$

According to the kinetic theory of gases, the rate of surface mass loss by evaporation is proportional to $P_v T^{-1/2}$ where P_v is the vapor pressure at a temperature T, and

$$\log_{10} P_v(T) = 13.66 - 22200/T \text{ for dielectrics (Reference 135)}$$

$$= 12.78 - 20040/T \text{ for metals (Reference 136).} \quad (12)$$

(For vapor pressure laws for Fe and Ni, see also Öpik (Reference 137). A dust particle at r shrinks at the rate

$$ds/dt = P_v \left[\frac{m}{2\pi kT}\right]^{1/2}, \quad (13)$$

where m is its molecular weight. A metallic particle at r = 1/50 AU (= 4.4 solar radii), $ds/dt \simeq 1\mu$ per orbital period. Within a distance of a few solar radii from the sun, there are no solid particles. Some peculiar dynamical effects are associated with thermal evaporation of dust (Reference 128): consider a particle with spirals toward the sun under Poynting-Robertson drag; because it evaporates rapidly near the sun, its drift speed da/dt increases. Also P/G increases; eventually the particle has too much velocity to remain in a circular orbit, then the semi-major axis and eccentricity increase. Eventually, the total energy becomes positive and the particle leaves the solar system. At the distance where the particles stop spiralling toward the sun and move out again, we expect an increase in the local dust concentration. Curiously enough, some enhanced infrared emission has been detected at about 5 solar radii and it is definitely thermal radiation by interplanetary dust (Reference 138).

Collisions between dust particles affect the size distribution of interplanetary dust and the distribution of their orbital elements. As a consequence, both distributions vary with distance from the sun. Sufficiently small collision fragments are expelled from the solar system by radiation pressure (cf. Eq. (2)). The total amount of dust lost from the zodiacal dust cloud in this manner is estimated to be 10 to 100 tons/sec (References 104, 123, and 139)—i.e. considerably more than evaporates near the sun. Collisions are particularly important for large zodiacal particles, and the chance that a sub-micron particle ever makes a collision is very small (Reference 104).

Because of collisions, and also because of the impact of solar wind ions, interplanetary dust particles rotate rapidly. We calculate the rate of rotation by assuming that the rotational vector performs a random walk due to ion impacts. Then the rotation rate after a time t is (Reference 104)

$$\nu(t) = 10^{-21} (Ft)^{1/2} w\left(\delta s^3\right) \sec^{-1} \tag{14}$$

(cgs units). A dynamical effect associated with the rotation of dust is the Yarkovsky-Radzievskii effect (Reference 111): A phase lag in the surface temperature exists between the morning and evening side of the particle and therefore the vapor pressure on these sides is not the same. The particle experiences a net force and is accelerated or decelerated in its orbit, depending on the sense of rotation.

THE ORIGIN OF INTERPLANETARY DUST

There are several possible sources of interplanetary dust: asteroidal collisions, fragmentation of comets, capture of interstellar dust, condensation of interplanetary gas, ejection of lunar surface material by meteoroid impact, and a primordial dust cloud residing in the outer regions of the solar system. Some of these may not be important. We particularly want to know which contribute most to maintaining the interplanetary dust cloud observable to us, and what the size and spatial distribution of dust from those sources would be. We also want to know if the present interplanetary dust cloud is a permanent feature of the solar system.

Asteroidal Collisions

In order to estimate the rate of production of zodiacal dust in asteroidal collisions, we need to know the rate of collisions as a function of asteroidal size, and the total mass and size distribution of debris resulting from a single collision. Although the collision probabilities for given asteroidal orbits are well known (References 110 and 111), the collision rate is not. This is because we do not know the distribution of asteroids with radii less than 1 km. There is no agreement as to whether the asteroid belt is an adequate dust source (References 35, 104, and 119). Concerning the size distribution of asteroidal dust it

has been found that if the distribution can be described by a power law $N(s) \propto s^{-p}$, then $p = 3.8$ (Reference 141). The debris drifts toward the sun under Poynting-Robertson drag; since the drift velocity is proportional to $(1/s)$, the effective size distribution of asteroidal dust has a spectral index $p = 2.8$ (in good agreement with the "flat" dust models deduced from zodiacal light observations) (References 7, 16, 46, 113, and 142). The velocity of ejecta is much smaller than the orbital velocity of the asteroids, and therefore the inclination of the dust orbits will be asteroidal (mean inclination: 9.5 degrees (Reference 143)). The spatial distribution of interplanetary dust of asteroidal origin, as determined by Poynting-Robertson drag, is such that the concentration is proportional to r^{-1} (References 104 and 139).

Dust from Comets

The relation of the rate of emission of dust by comets to the distance from the sun is not well known. For comet Arend-Roland an emission rate of 75 tons/sec at perihelion is estimated, but it has been pointed out that because of solar radiation pressure most dust particles of cometary origin do not remain in the solar system (Reference 119). The distribution of eccentricity and semi-major axis of cometary dust is therefore quite different from the distribution for the comets; however, the inclination of the orbits of cometary dust is much like the inclination of cometary orbits (mean: 15 degrees, for short period comets; long period comets have a random distribution of inclinations (Reference 143). If a single comet is responsible for the interplanetary dust cloud, then (because of Poynting-Robertson drag) the dust concentration should vary as (a) r^{-1} for $r < q$, where q is the comet's perihelion distance from the sun, and (b) $r^{-2.5}$ for $r > q$ (References 104 and 139). Probably many comets contribute to the zodiacal cloud, but the contributions may not be equally important.

Capture of Interstellar Dust

The mass/volume of interstellar dust near the solar system is $M_\infty \simeq 2 \times 10^{-26}$ gm/cm^3, and the solar motion relative to the nearby stars is about $v = 20$ km/sec (References 143 and 146). (This is also the solar motion with respect to interstellar Ca II clouds.) If we take 20 km/sec to be the solar motion relative to interstellar dust clouds,

then the dust mass/volume at a distance r from the sun is

$$M(r) = M_\infty \left(1 + \frac{2GM}{rv_\infty^2}\right)^{1/2}$$

$$\simeq 2 \times 10^{-26} \times \left(1 + \frac{4.5}{r}\right)^{1/2} \text{gm/cm}^3, \qquad r \text{ in AU}, \quad (15)$$

where M is the mass of the sun, R its radius. Clearly, a mere gravitational accumulation of dust near the sun does not account for the observed zodiacal dust cloud. It has been pointed out (Reference 145) that dust can be captured into an elliptic orbit via a single encounter with a planet (mainly Jupiter). The capture is permanent because Poynting-Robertson drag removes the particles from that region of space where a second encounter can occur which could result in the ejection of the particle from the solar system. (Even if ejection did occur, a particle would have already spent a very long time in the solar system.) The typical interstellar dust particle is much smaller than the typical zodiacal dust particle. For the two most seriously discussed interstellar dust models, the average radius is 0.16 and 0.3 (References 146 and 147)., and for these particles $P/G \simeq 2$. They can never be captured into elliptic orbits. But even if we neglect radiation pressure, we find the capture rate to be insufficient to explain the zodiacal cloud. An additional difficulty concerns the distribution of orbital inclinations of captured dust; the distribution is random. However, orbits which have a relatively small aphelion are more likely to have a small inclination (Reference 148). Such particles contribute most to the dust concentration in the inner solar system. Since they constitute only a very small fraction of the total amount of captured interstellar dust, it must be concluded that interstellar dust is <u>not</u> a major source of supply for the zodiacal cloud.

Lunar Ejecta; Condensation in situ; Primordial Remnants

The velocity at which debris is ejected from the site of impact of a meteoroid on the lunar surface is much smaller than the escape velocity from the moon's surface (2.2 km/sec); hence little debris escapes from the moon. Furthermore, the earth's orbital velocity is 30 km/sec, and therefore those particles which do escape are in earth-like

orbits and will eventually be accreted by the earth (and by the moon to a lesser degree). As a consequence, very little dust of lunar origin should be found beyond 1 AU, certainly much less than is observed.

Formation of solid particles by condensation of the interplanetary gas is probably not an important source of dust: The solar wind prevents condensation in the inner solar system (sputtering). Farther away from the sun the gas density is too low and the condensation time too long. Some interesting questions can be asked about the dynamics of condensation nuclei far from the sun: Because of their small size, radiation pressure and radiation drag are unimportant; corpuscular drag may be important but the Lorentz force on these particles is very large (cf. Eq. (10)), thus the particles may wander around randomly until they encounter a comet or other large body or enter the inner solar system where they are quickly eroded by sputtering.

The sun may be surrounded at large distances by a dust cloud much like the (hypothetical) comet cloud. There is no evidence for or against this hypothesis. If we consider only Poynting-Robertson drag, then a particle now at 1 AU was at a distance of $1.3 \times 10^3/(\delta s)^{1/2}$ AU some 4.5×10^9 years ago (cf. Eq. (4)).

REFERENCES

1. Schmidt, R. A., "Data Survey on Microscopic Extraterrestrial Particles," NASA Technical Note D-2719, 1965.

2. Krinov, E. L., "Nonterrestrial Dust on the Earth," Sky and Telescope 18:617-619, 1959.

3. Singer, S. F., and Bandermann, L. W., "Cosmic Dust—Intercomparison of Observations," Space Research 8:475-488, 1968.

4. Buddhue, J. D., "Meteoritic Dust," Univ. of New Mexico Publications in Meteoritics No. 2, 1950.

5. Whipple, F. L., "On Meteoroids and Penetration," J. Geophys. Res. 68:4929-4939, 1963.

6. Wall, J. K., in "The Zodiacal Light and the Interplanetary Medium," (J. L. Weinberg, ed.) NASA Special Publication 150, 1967, p. 343.

7. van de Hulst, H. C., "Zodiacal Light in the Solar Corona," Astrophys. J. 105:471-488, 1947.

8. Gillett, F. C., Stein, W. A., and Ney, E. P., "Observations of the Solar Corona from the Limb of the Sun to the Zodiacal Light, July 20, 1963," Astrophys. J. 140:202-305, 1964.

9. Smith, L. L., Roach, F. E., and Owen, R. W., "The Absolute Photometry of the Zodiacal Light," Planet. Space Sci. 13:207-217, 1965.

10. Blackwell, D. E., and Ingham, M. F., "Observations of the Zodiacal Light from a High Altitude Station. Part I. The Average Zodiacal Light," Mon. Not. R.A.S. 122:113, 1961.

11. Brandt, J. C., Astron. Soc. Pacific Leaflet No. 391, 1962.

12. Bahr, A., and Siedentopf, H., "Untersuchungen uber zodiakallight und Gegenschein nach Lichtelektrischen Messungen auf dem Jungfraujoch," Zeit. f. Astrophys. 32:19-50, 1953.

13. Moulton, F. R., Astron. J. 21:483, 1900.

14. Schwend, K., Dissertation, Munich, 1904.

15. Seeliger, H. V., Sitzgsber. Bayer. Akad. Wiss. Math.-Phys. 31, 265, 1902.

16. Siedentopf, H., "Zur Optischen Deutung des Gegenscheins," Ziet. f. Astrophys. 36:240-244, 1955.

17. Walter, H., "Theoretische Deutung des Gegenscheins durch Lichtstreuung an Spharischen Partikeln," Zeit. f. Astrophys. 46:9-16, 1958.

18. Tanabe, H., "Photoelectric Observations of the Gegenschein," Publ. Astron. Soc. Japan 17:339-366, 1965.

19. Fessenkov, B., "Gaseous Tail of the Earth," Astron. J. U.S.S.R. 27:89-96, 1950.

20. Saito, K., "The Gegenschein and Coronal Structure of the Sun," Publ. Astron. Soc. Japan 13:376-383, 1961.

21. Hope, E. R., in "The Earth's Exterior Atmosphere and the Counterglow," Sec. Ed. Defense Scientific Information Service DRB, Canada, T65R, 1954.

22. van de Hulst, H. C., "The Zodiacal Light," in Vistas in Astronomy, vol. 2, New York: Pergamon Press, 1956.

23. Haug, U., Dissertation, Tubingen, 1954.

24. Moiseyev, N. D., "Hypotehsis of Gilden-Moulton on Origin Counterglow, 6. Present State of the Problem on the Existence of Gilden-Moulton Accumulation," Russ. Astron. Zh. 15:226-231, 1938.

25. Peale, S. J., "Dust Belt of the Earth," J. Geophys. Res. 71:911-933, 1966.

26. Divari, N. B., "Contribution of the Dust Cloud Near the Earth to the Brightness of the Zodiacal Light and the F-Corona," Sov. Astron. J. 9:493-499, 1965.

27. Alexander, W. M., "Cosmic Dust," Sci. 138:1098-1099, 1962.

28. Whipple, F. L., "The Dust Cloud About the Earth," Nature 189: 127-128, 1961.

29. Dubin, M., and McCracken, C. W., "Measurements of Distributions of Interplanetary Dust," Astron. J. 67:248-256, 1962.

30. Nilsson, C. S., "Some Doubts About the Earth's Dust Cloud," Sci. 153:1242-1246, 1966.

31. Shapiro, I. I., Lautman, D. A., and Colombo, O., "The Earth's Dust Belt: Fact or Fiction. I. Forces Perturbing Dust Particle Motion," J. Geophys. Res. 71:5695-5704, 1966.

32. Ruskol, Y. L., "The Origin of the Concentration of Interplanetary Dust About the Earth," Planet. Space Sci. 11:311-316, 1963.

33. Peale, S. J., "Evidence Against a Geocentric Contribution to the Zodiacal Light," J. Geophys. Res. 73:3025-3033, 1968.

34. Wolstencroft, R. D., and Rose, L. J., "Observations of the Zodiacal Light from a Sounding Rocket," Astrophys. J. 147:271-292, 1967.

35. Gillett, F. C., "Zodiacal Light and Interplanetary Dust," Dissertation, Univ. of Minn., 1966.

36. Gillett, F. C., in "The Zodiacal Light and the Interplanetary Medium," J. L. Weinberg, ed., NASA Special Publication 150, 1967, p. 9.

37. Regener, V. H., and van de Noord, E. L., ibidem, p. 45.

38. Ney, E. P., and Huch, W. F., "Gemini V Experiments on Zodiacal Light and Gegenschein," Sci. 150:53-56, 1965.

39. Ney, E. P., "Night-Sky Phenomena Photographed from Gemini 9," Sky and Telescope 32(5):276-277, 1966.

40. Weinberg, J. L., Summary Report on The Zodiacal Light, No. 1, July 1964, No. 2, July 1967, Univ. of Hawaii Inst. of Geophysics.

41. Ingham, M. F., "Interplanetary Matter," Space Sci. Rev. 1:576-588, 1961-1962.

42. Giese, R. H., "Light Scattering by Small Particles and Models of Interplanetary Matter Derived from the Zodiacal Light," Space Sci. Rev. 1:589-611, 1961-1962.

43. Weinberg, J. L., "The Zodiacal Light at 53000 A," Ann. d'Astrophys. 27:718-738, 1964.

44. Little, S. J., O'Mara, B. J., and Aller, L. H., "Light Scattering by Small Particles in the Zodiacal Cloud," Astron. J. 70:346-352, 1965.

45. Singer, S. F., and Bandermann, L. W., in "The Zodiacal Light and the Interplanetary Medium," J. L. Weinberg, ed., NASA Special Publication 150, 1967.

46. Powell, R. S., et al., in "The Zodiacal Light and the Interplanetary Medium," J. L. Weinberg, ed., NASA Special Publication 150, 1967, p. 225.

47. Greenberg, J. M., ibidem, p. 215.

48. Donn, B., and Powell, R. S., New York: Pergamon Press, 1963.

49. Powell, R. S., et al., "Optical Scattering from Non-Spherical Randomly Aligned Polydisperse Particles," Planet. Space Sci. 15:1641-1652, 1967.

50. Elsasser, H., "Fraunhoferkorona und Zodiakollicht," Zeit. f. Astrophys. 37:114-124, 1955.

51. Zook, H. A., and Kessler, L. J., in "Interplanetary Dust: The Zodiacal Light and Meteoroid Measurements," Proc. OART-OSSA Meteoroid Environment Workship, NASA Headquarters, 1968, p. 351.

52. Reay, N. K., and Ring, J., "Radical Velocity Measurements on the Zodiacal Light Spectrum," Nature 219:710, 1968.

53. Bandermann, L. W., and Wolstencroft, R. D., "Interpretation of Doppler Shifts in the Zodiacal Light Spectrum," Nature 221:251-253, 1969.

54. Wolstencroft, R. D., "On the Location in Space of the Zodiacal Dust Particles," Planet. Space Sci. 15:1081-1089, 1967.

55. Hoffmeister, C., in "The Zodiacal Light and the Interplanetary Medium," J. L. Weinberg, ed., NASA Special Publication 150, 1967, p. 87.

56. Saito, K., and Huruhata, M., ibidem, p. 41.

57. Alexander, W. M., et al., Trans. Am. Geophys. Union 46, 133, 1965.

58. Berg, O. E., in "Interplanetary Dust: The Zodiacal Light and Meteoroid Measurements," Proc. OART-OSSA Meteoroid Environment Workship, NASA Headquarters, 1968, 1. 213.

59. Nilsson, C. S., and Alexander, W. M., "Measured Velocities of Interplanetary Dust Particles from OGO-1," Smiths. Contrib. Astrophys. 11:301-305, 1967.

60. Alexander, W. M. et al., "Review of Direct Measurements of Interplanetary Dust from Satellites and Probes," Space Res. 3:891-917, 1963.

61. LeGally, D. P., and Rosen, A., eds., in "Space Physics," J. Wiley and Sons, 1964.

62. Whipple, F. L., "On Meteoroids and Penetration," J. Geophys. Res. 68:4929-4939, 1963.

63. Alvarez, J. M., in "The Zodiacal Light and the Interplanetary Medium," J. L. Weinberg, ed., NASA Special Publication 150, 1967, p. 123.

64. Dole, S. H., "The Gravitational Concentration of Particles in Space Near the Earth," Planet. Space Sci. 9:541-553, 1962.

65. Singer, S. F., "Interplanetary Dust Near the Earth," Nature 192:321-323, 1961.

66. Shelton, R. D., Stern, H. E., and Hale, D. P., "Meteoroid Flux About Moving Satellites—Problems Associated With Measurement of Flux Count Rate Measured by Saturn Interpretation and Mathematical Basis for Meteoroid Focusing," NASA Technical Note D-2575, 1965.

67. Southworth, R. D., On S. H. Dole's Paper, "The Gravitational Concentration of Particles in Space Near the Earth," Planet. Space Sci. 11:499-502, 1963.

68. Beard, D. B., "Interplanetary Dust Distribution," Astrophys. J. 129:496-506, 1959.

69. Fremlin, J. H., "The Dust Cloud About the Earth," Nature 191: 31-32, 1961.

70. Hibbs, A. R., "The Distribution of Micrometeorites Near the Earth," J. Geophys. Res. 66:371-377, 1961.

71. McCracken, C. W., "Conditions of Encounter Between Dust and the Planets," Smiths. Contrib. Astrophys. 11:213-226, 1967.

72. Moroz, V. J., "The Dust Cloud About the Earth," Planet. Space Sci. 11:387-394, 1963.

73. Bandermann, L. W., and Singer, S. F., Reviews of Geophysics, Aug. 1969 (in press).

74. McCracken, C. W., Alexander, W. M., and Dubin, M., "Direct Measurement of Interplanetary Dust Particles in the Vicinity of the Earth," Nature 192:441-442, 1961.

75. Konstantinov, B. M., et al., NASA Technical Translation F-11, 753, 1968.

76. Alexander, W. M., et al., "Interplanetary Dust-Particle Flux Measurements Between 1.0 and 1.56 a. u. from Mariner 4 Cosmic-Dust Experiments," Smiths. Contrib. Astrophys. 11:227, 1967.

77. Gurtler, C. A., and Grew, G. W., "Meteoroid Hazard Near Moon," Sci. 161:462-464, 1967.

78. Clifton, S., and Naumann, R., NASA Technical Memorandum X-1316, 1966.

79. Dubin, M., "Meteoric Dust Measured from Explorer I," Ann. IGY 12(2):472-484, 1961.

80. McCracken, C. W., Alexander, W. M., and Dubin, M., "Direct Measurements of the Mass Distribution and Time Variations in the Flux of Small Dust Particles," Smiths. Contrib. Astrophys. 11:259-270, 1967.

81. Clifton, S., in "Interplanetary Dust: The Zodiacal Light and Meteoroid Measurements," Proc. OART-OSSA Meteoroid Environment Workship, NASA Headquarters, 1968, p. 287.

82. Singer, S. F., "Dust and Needles in the Magnetosphere," Trans. Am. Geophys. Union 44:29, 1963.

83. NASA Headquarters, "Interplanetary Dust: The Zodiacal Light and Meteoroid Measurements," Proc. OART-OSSA Meteoroid Environment Workship, 1968.

84. Hawkins, G. S., ed., "Meteor Orbits and Dust," Smiths. Contrib. Astrophys. 11:412p, 1967.

85. Parkin, D. W., and Tilles, D., "Influx Measurements of Extraterrestrial Material," Sci. 159:936-946, 1968.

86. Amin, B. S., Kharkar, D. P., and Lal, D., "Cosmogenic ^{10}Be and ^{26}Al in Marine Sediments," Deep Sea Res. 13:805-824, 1966.

87. Farlow, N. H., Blanchard, M. B., and Ferry, G. V., "Sampling with a Luster Sounding Rocket During a Leonid Meteor Shower," J. Geophys. Res. 71:5689-5693, 1966.

88. Castaing, R., and Fredrickson, K., Geochim. Cosmochim. Acta 14, 114, 1968.

89. Shedlovsky, J. P., and Paisley, S., "On the Meteoric Component of Stratospheric Aerosols," Tellus 18:499-503, 1966.

90. Lal. D., and Venkatavaradan, V. S., "Low-Energy Protons: Average Flux in Interplanetary Space During the Last 100,000 Years," Sci. 151:1381-1384, 1966.

91. Wasson, J., "Radioactivity in Interplanetary Dust," Icarus 2:54-87, 1963.

92. Wasson, J. T., Alder, B., and Oeschger, A., "Aluminum-26 in Pacific Sediment: Implication," Sci. 155:446-448, 1967.

93. Singer, S. F., "Zodiacal Dust and Deep Sea Sediments," Sci. 156:1080-1083, 1967.

94. Yokoyama, Y., "Terrestrial Origin of Aluminum-26 and Oceanic Sedimentation Rate," Nature 216:569-571, 1967.

95. McCorkell, R., Fireman, E. L., and Langway, C. C., Jr., "Aluminum-26 and Beryllium-10 in Greenland Ice," Sci. 158: 1690-1692, 1968.

96. Fireman, E. L., and Langway, C. C., Jr., "Search for Aluminum-26 in Dust from the Greenland Ice Sheet," Geochim. Cosmochim. Acta 29:21-27, 1965.

97. Barker, J. L., and Anders, E., Univ. of Chicago Enrico Fermi Inst. for Nuclear Studies, Report No. 67-93, 1967.

98. Schaeffer, O. A., Megrue, G. H., and Thompson, S. O., "Experiments to Test the Presence of Cosmogenic Nuclides in Ocean Sediments," Ann. N. Y. Acad. Sci. 119:347-350, 1964.

99. Baedecker, P. A., and Ehman, W. D., "The Distribution of Some Noble Metals in Meteorites and Natural Materials," Geochim. Cosmochim. Acta 29:329-342, 1965.

100. Fogle, B., Univ. of Alaska Geophys. Inst. Scientific Report No. UAG-R 177, 1966.

101. Fogle, B., Chapman, S., and Echols, C., Univ. of Alaska Geophys. Inst. Scientific Report No. UAG-R 162, 1965.

102. Fogle, B., and Echols, C., Univ. of Alaska Geophys. Inst. Scientific Report No. UAG-R 163, 1965.

103. Francis, R. J., Bennett, J. M., and Seedsman, D. L., "Noctilucent Clouds Observed in Antarctica," Nature 211:398, 1966.

104. Bandermann, L. W., Dissertation Univ. of Maryland, 1967.

105. Chapman, S., and Kendall, D. C., "Noctilucent Clouds and Thermospheric Dust: Their Diffusion and Light Distribution," Quart. J. Roy. Met. Soc. 91:115-131, 1965.

106. Webb, W. L., "Morphology of Noctilucent Clouds," J. Geophys. Res. 70:4463-4475, 1965.

107. "Investigations of Noctilucent Cloud Particles," U. S. Air Force, Cambridge Research Lab. Rept. AF CRL-65-122, 1965.

108. Poultney, S. K., Silverberg, E. C., and McCormick, P. D., Univ. of Maryland Tech. Report No. 815, 1968.

109. McCormick, P. D., et al., "Backscattering from the Upper Atmosphere (75-160 km) Detected by Optical Radar," Nature 209: 798-799, 1966.

110. Silverberg, E. C., and Poultney, S. K., Univ. of Maryland Tech. Report No. 765, 1967.

111. Opik, E. J., "Collision Probabilities with the Planets and the Distribution of Interplanetary Matter," Proc. Roy. Irish Acad. 54(12):165-199, 1951.

112. Kaiser, T. R., "Meteors and the Abundance of Interplanetary Matter," Space Sci. Rev. 1:554-575, 1961-1962.

113. Opik, E. J., "Interplanetary Dust and Terrestrial Accretion of Meteoric Matter," Irish Astron. J. 4:84-135, 1956.

114. van de Hulst, H. C., in "Light Scattering by Small Particles," J. Wiley and Sons, New York, 1957.

115. Giese, R. H., "Streuung Elektromagnetischer Wellen an Absorbierenden und Dielektrischen Klugelformigen Einzelteilchen und an Gemischen Soecher Teilchen," Zeit. f. Astrophys. 51: 119-147, 1961.

116. Irvine, W. M., "Light Scattering by Spherical Particles: Radiation Pressure, Asymmetry Factor, and Extinction Cross Section," J. Opt. Soc. Am. 55:16-21, 1965.

117. Kattawar, G. W., and Plass, G. N., "Electromagnetic Scattering from Absorbing Spheres," Appl. Optics 6:1377-1382, 1967.

118. Friedmann, C., and Schmidt, K. H., "Wirkungsfaktarea von Graphitteilchen," Wiss. Zeit. Friedrich Schiller Univ. Jena, Math. Nat. Reihe 1:173-178, 1966.

119. Harwit, M., "Origins of the Zodiacal Dust Cloud," J. Geophys. Res. 68:2171-2180.

120. Robertson, H. P., "Dynamical Effects of Radiation in the Solar System," Mon. Not. R.A.S. 97:423-438, 1937.

121. Poynting, J. H., "Radiation in the Solar System: Its Effect on Temperature and its Pressure on Small Bodies," Phil. Trans. Roy. Soc. A. 202:525-552, 1904.

122. Wyatt, S. P., Jr., and Whipple, F. L., "The Poynting-Robertson Effect on Meteor Orbits," Astrophys. J. 111:134-141, 1950.

123. Whipple, F. L., "A Comet Model. III. The Zodiacal Light," Astrophys. J. 121:750-770, 1955.

124. Rhee, J. W., in "The Zodiacal Light and the Interplanetary Medium," J. L. Weinberg, ed., NASA Special Publication 150, 1967, p. 291.

125. Parker, E. N., "The Perturbation of Interplanetary Dust Grains by the Solar Wind," Astrophys. J. 139:951-958, 1964.

126. Belton, M. J. S., Dissertation, Univ. of Calif., 1964.

127. Whipple, E. C., Jr., Dissertation, George Washington Univ., 1965.

128. Belton, M. J. S., in "The Zodiacal Light and the Interplanetary Medium," J. L. Weinberg, ed., NASA Special Publication 150, 1967, p. 301.

129. Brandt, J. C., "Interplanetary Gas. XIII. Gross Plasma Velocities from the Orientation of Ionic Comet Tails," Astrophys. J. 147:201-219, 1967.

130. Hundhausen, A. J., Bame, S. J., and Ness, N. F., "Solar Wind Thermal Anisotropies—Vela 3 and IMP 3," J. Geophys. Res. 72:5265-5274, 1967.

131. Ness, N. F., "Direct Measurements of Interplanetary Fields and Plasmas," NASA Technical Memorandum X-55-830, 1967.

132. Parker, E. N., "Dynamics of the Interplanetary Gas and Magnetic Fields," Astrophys. J. 128:664-676, 1958.

133. Wilcox, J. N., "Solar and Interplanetary Magnetic Fields," Sci. 152:161-166, 1966.

134. Wehner, G. K., and KenKnight, C. E., Litton Systems, Inc. Rept. No. 3107, 1967.

135. Over, J., "Vaporization of Solid Particles Near the Sun," Koninkl. Ned. Akad. Wetenschap. Proc. 51b:74-84, 1958.

136. Becklin, E. E., and Westphal., J. A., "Infrared Observations of Comet 1965f," Astrophys. J. 145:445-453, 1966.

137. Opik, E. J., "Physics of Meteor Flight in the Atmosphere," Interscience Publishers, Inc., New York, 1958.

138. MacQueen, R. M., Astrophys. J. 154:1059, 1968.

139. Southworth, R. B., "The Size Distribution of the Zodiacal Particles," Ann. N. Y. Acad. Sci. 119:54-67, 1964.

140. Wetherill, G. W., "Collisions in the Asteroid Belt," J. Geophys. Res. 72:2429-2444, 1967.

141. Dohnanyi, J. S., in "The Zodiacal Light and the Interplanetary Medium," J. L. Weinberg, ed., NASA Special Publication 150, 1967, p. 315.

142. Elsasser, H., "The Zodiacal Light," Planet. Space Sci. 11:1015-1933, 1963.

143. Allen, C. W., in "Astrophysical Quantities," Univ. of London, Athlone Press, London, 1963.

144. Blaauw, A., Bull. Astron. Neth. 11, 459, 1952.

145. Radzievskii, V. V., "Gravitational Capture of Cosmic Dust by the Sun and Planets and Evolution of the Circumterrestrial Cloud," Sov. Astron. AJ 11:128-136, 1967.

146. Wickramsinghe, N. C., and Krishna Swamy, K. S., Nature 192: 321, 1967.

147. Greenberg, J. M., in "Nebulae and Interstellar Matter," Univ. of Chicago Press (B. M. Middlehurst and L. H. Aller, eds.), 1968.

148. Newton, H. A., Mon. Not. Acad. Sci. 6:1, 1893.

NASA-Langley, 1968 —— 29